

POLYMETAMORPHISM AND DEFORMATION WITHIN THE BREVARD FAULT  
ZONE OUTSIDE OF ATLANTA, GEORGIA.

by

ADAM LEE BEDELL

(Under the Direction of Mike Roden)

ABSTRACT

The Brevard fault zone (BFZ) forms a striking, 375 km-long lineament that runs from eastern Alabama to Virginia. Boreholes drilled for the Chattahoochee Tunnel Project provided fresh, unweathered samples which were studied to develop tighter constraints on the metamorphic and deformational history of the BFZ.

Quartz mica schists and mica schists have experienced two prograde, Barrovian style, amphibolite grade metamorphic events ( $M_1$ ,  $M_2$ ) and a fluid enhanced metasomatic event ( $M_3$ ).  $M_1$  is defined by a relict metamorphic assemblage of garnet-staurolite. A second period of garnet growth and the development of muscovite-biotite define the  $S_2$  foliation and the  $M_2$  assemblage.  $M_3$  is indicated by the minerals calcite, chlorite and epidote which are commonly found in crosscutting veins. Three ductile deformational events ( $D_2$ ,  $D_3$ , and  $D_4$ ) produced a strong penetrative foliation, ( $S_2$ ), tight to close folds, ( $F_3$ ), and open to gentle folds, ( $F_4$ ); a later brittle event ( $D_5$ ) produced fractures and psuedotachylyte.

INDEX WORDS: Brevard, Fault zone, Georgia, Deformation, Metamorphism,  
Petrology, Shear zone, Petrography

POLYMETAMORPHISM AND DEFORMATION WITHIN THE BREVARD FAULT  
ZONE OUTSIDE OF ATLANTA, GEORGIA

by

ADAM LEE BEDELL

B.S., The University of Georgia, 1998

A Thesis Submitted to the Graduate Faculty of The University of Georgia in Partial  
Fulfillment of the Requirements for the Degree

MASTER OF SCIENCE

ATHENS, GEORGIA

2003

© 2003

Adam Lee Bedell

All Rights Reserved

POLYMETAMORPHISM AND DEFORMATION WITHIN THE BREVARD FAULT  
ZONE OUTSIDE OF ATLANTA, GEORGIA

by

ADAM LEE BEDELL

Approved:

Major Professor: Michael Roden

Committee: Alberto Patiño-Douce  
Sandra J. Wyld

Electronic Version Approved:

Maureen Grasso  
Dean of the Graduate School  
The University of Georgia  
May 2003

## ACKNOWLEDGMENTS

This project would not have been possible without the approval of Cobb County Water System. Its support of using drill core samples from the Chattahoochee Tunnel Project for the advancement of science and the understanding of such a complicated feature is greatly appreciated. I would also like to thank Jack Raymer, Mike Robinson, and Jeremy Reineke at Jordan, Jones, and Goulding, Inc., for continued employment, discussion of unpopular topics, and the chance to take a crane ride to work everyday supplemented with dangerous explosives. This project was supported by grants from Wheeler-Watts Allard and by a Geological Society of America grant from the Southeastern section.

This project would not have been completed if not for the direction of Mike Roden, Alberto Patiño-Douce, Sandra Wyld, and Beatrice Stephens. To my multiple families (geology department, natural and adopted, and Depalma's on the eastside), thank you for the encouragement and love given to help complete this achievement. I would especially like to thank my wife, Jenn, for putting up with all my B.S., so I could get my M.S..

Mike- Thanks for having the faith.

## TABLE OF CONTENTS

	Page
ACKNOWLEDGEMENTS .....	iv
SECTION	
1 INTRODUCTION, GEOLOGIC FRAMEWORK, AND PREVIOUS WORK .....	1
Metamorphism .....	3
Deformation .....	5
Timing of Deformation and Metamorphism .....	6
Present Study .....	8
2 SAMPLING AND ANALYTICAL METHODS .....	11
3 PETROGRAPHY .....	16
Introduction .....	16
Quartz Mica Schists .....	21
Mica Schists .....	27
Brittle Textures .....	34
4 MINERAL COMPOSITIONS .....	40
Psuedotachylyte Groundmass Composition .....	48
5 METAMORPHISM AND DEFORMATION .....	55
Metamorphism .....	55
Deformation .....	71

	Metamorphism and Deformation Correlation.....	77
6	DISCUSSION .....	86
	Metamorphism .....	87
	Deformation .....	88
7	CONCLUSION .....	93
	REFERENCES .....	95

## **INTRODUCTION, GEOLOGIC FRAMEWORK, AND**

### **PREVIOUS WORK**

Arthur Keith in 1905 was the first to describe the rocks outside Brevard, North Carolina. He named these rocks as the Brevard Schist and believed that with associated quartzite and limestone beds, a simple stratigraphic sequence was formed. He found these rocks lying unconformably on top of Precambrian rocks within a narrow syncline (Reed and Bryant 1964). The name Brevard now denotes a fault zone that extends over 375 km from Horseshoe Bend, Alabama to southern Virginia and parallels the northeast trending, Appalachian mountain chain (Figure 1.0). The width of the Brevard Fault Zone (BFZ) varies from 1-3 km along its strike (Medlin and Crawford 1973; Higgins 1966; Reed and Bryant 1964; Hatcher 1970). Depending on who is consulted, the BFZ has an inner and outer zone and the criteria determining the two is degree of mylonitization and alteration (J. Raymer and R. Kath, personal communication 2000). Which of these two zones delineate the BFZ along its strike also is debated. The Brevard Fault Zone has been extensively studied since first discovered in 1905. The earliest interpretations included antiforms and synforms and then, during the 1950's and 1960's with the advent of plate tectonics, new ideas surfaced. These ideas reflect evolving concepts in geology such as microtectonic observation including analysis of cataclastic lineations and micro shear sense indicators; e.g., muscovite fish.



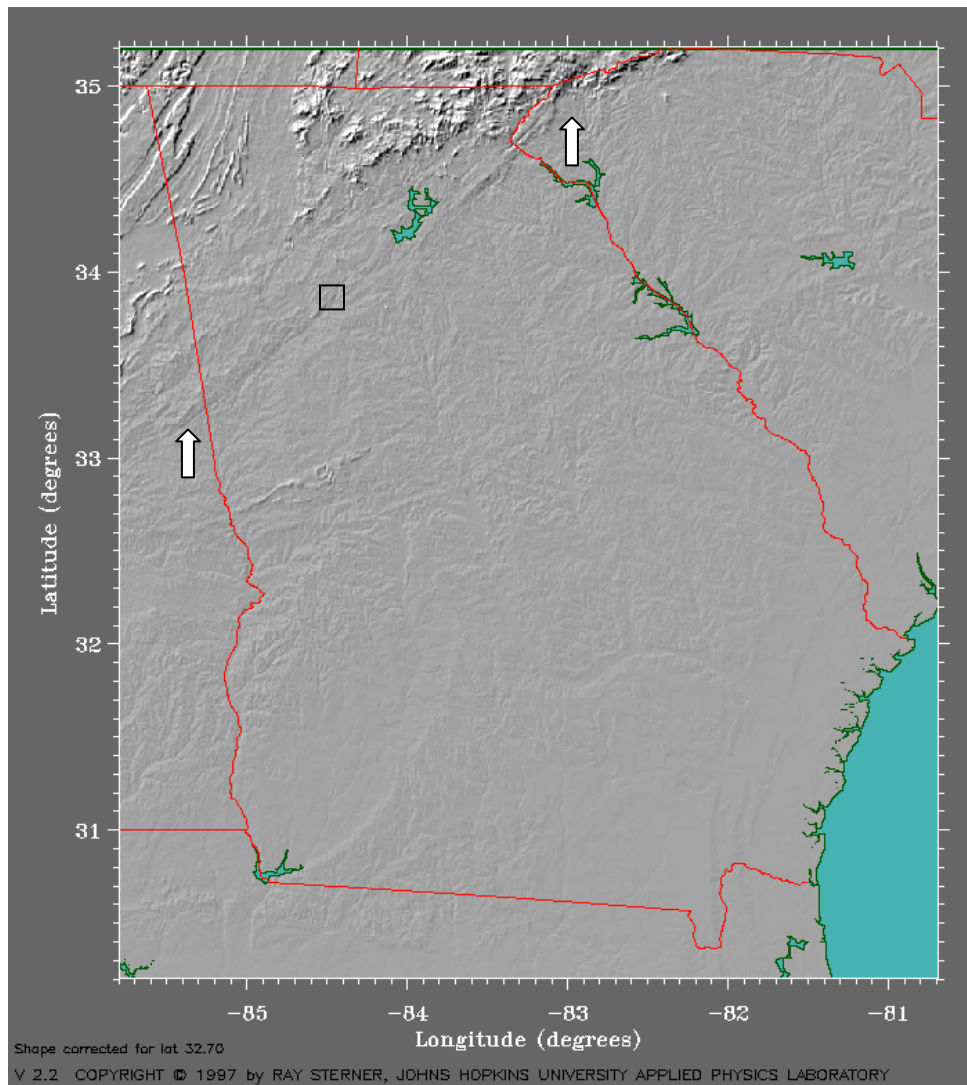


Figure 1.0. Shaded satellite relief image of Georgia. The Brevard fault zone forms a northeast trending lineament indicated by arrows. Small box indicates study area (After Sterner, 1997).

The BFZ has been interpreted over 42 times since first recognized (Bobyarchick 1999).

A brief list of interpretations includes:

Author	Year	Interpretation	Author	Year	Interpretation
Keith	1905	syncline	Carpenter and Dallmeyer	1974	reverse fault (unroofing)
Jonas	1932	thrust fault	Rankin	1975	transported suture
White	1950	normal fault	Hatcher	1978	reactivated Taconic root zone (thrust)
King	1955	dejective zone	Cooke and others	1979	Alleghanian splay thrust
Reed and Bryant	1964	dextral strike slip fault	Boyer and Elliot	1982	branch line merger
Higgins	1966	strike slip fault	Bobyarchick	1984	Alleghanian dextral strike slip
Hatcher	1969	back limb thrust fault	Vauchez	1987	low-angle dextral strike slip
Reed and others	1969	oblique sinistral strike slip fault	Bobyarchick	1988	Alleghanian dispersal fault
Roper and Dunn	1970	sheared isoclinal syncline	Vauchez and others	1993	Acadian to Alleghanian dextral strike slip
Reed and others	1970	sinistral strike slip and root zone			
Hurst	1970	trough fault			
Odom and Fullagar	1973	Taconic suture and root zone			
Medlin and Crawford	1973	fold zone overprinted by cataclasis			

-Modified from Bobyarchick, 1999.

## Metamorphism

Metamorphic facies within the BFZ range from greenschist to amphibolite grade across the Brevard and have been pieced together from Alabama to Virginia (Reed & Bryant 1964; Higgins 1966; Crawford and Medlin 1973; Hatcher 1970). There is continuing debate on whether there are two distinct, metamorphic events, or one long protracted event, affecting the Brevard Fault Zone (Hatcher 1999; Hatcher 1988; Hatcher 1978; Hatcher and Odom 1980; Roper and Justice 1973; Roper and Dunn 1973; Vauchez 1988). Ages of possible metamorphic events are controversial: the earliest event may have occurred during the mid- Ordovician during the Taconic orogeny (Reed & Bryant

1964; Roper & Dunn 1973; Odom & Fullagar 1973; Sinha et. al. 1988). Other ages range from the middle to late Paleozoic (Edelman et. al. 1987).

Roper and Dunn (1973) identified two main metamorphic episodes ( $M_1$  and  $M_2$ ) based upon plagioclase compositions, pre-tectonic garnets, and mylonitic foliations. Plagioclase feldspar compositions ( $An_{32}$ - $An_{28}$ ), and garnet pre-tectonic porphyroblasts characterize  $M_1$  amphibolite grade metamorphism.  $M_2$  attained upper greenschist to greenschist-amphibolite grade metamorphism. Characterizing  $M_2$  are garnet porphyroblasts that contain very few to no inclusions and cut the  $S_1$  foliation. By displacing the  $S_1$  foliation, Roper and Dunn interpreted this as indicating a coeval evolution between  $M_2$  and  $D_2$ . Medlin and Crawford (1973) reported two generations of garnets present within the Brevard in eastern Alabama and western Georgia. One generation appearing sheared and the other un-sheared, suggesting garnet growth after cataclasis. Other scientists have found more evidence for a second metamorphic event. Sinha et al. (1988) describes a fluid enhanced event with an assemblage of muscovite-sphene-albite-epidote- and quartz. They explain the addition of fluid to drive this reaction by overthrusting during the Alleghanian of relatively hot allochthons over autochthonous sediments of the North American margin.

The students of the Brevard all agree on one basic metamorphic interpretation: The Brevard Zone thermal peak reached amphibolite grade metamorphism and was followed later by retrograde metamorphism (Roper and Dunn 1973; Crawford and Medlin 1973; Russell et al. 1985; Hatcher 1978; Higgins 1966; Bobyarchick 1999).

## **Deformation**

The deformational history of the BFZ is quite complex due to its involvement in multiple orogenies (Liu and Hatcher 1988; Lewis 1980; Hatcher 1988; Hatcher 1978; Roper and Dunn 1973; Edelman et al. 1987; Roper and Justice 1973). Movement must be younger than mid-Ordovician. The Taconic orogeny begins at 450-480 Ma and is the first orogeny affecting the southern Appalachians following the Grenville orogeny and the rifting of Rodinia (Rodgers 1982; Hatcher 1989). Movement along the Brevard can not occur later than 245 Ma due to crosscutting undeformed Triassic age dikes (Bobyarchick 1999; Reed & Bryant 1964; Higgins 1966). Structural and microtectonic analysis suggests early ductile deformational histories followed by later brittle phases (Reed & Bryant 1964; Higgins 1966; Vauchez 1987; Evans and Mosher 1986).

Reed and Bryant (1964) were the first geologists to attempt to discern the nature of movement along the BFZ and to recognize the zone as a fault zone. Cataclastic lineations (mineral stretching) within the Grandfather Mountain window were observed to be parallel to those within the Blue Ridge thrust sheet and plunge down along SE dipping cleavage planes (Reed and Bryant 1964). The southeastward dipping cleavage planes are parallel to axial traces of shear folds in Precambrian volcanic and sedimentary rocks. They also noticed that individual bed offsets are parallel to the cataclastic lineation. They interpreted these lineations as lying in the direction of tectonic transport resulting from right lateral strike-slip movement. Later brittle deformation including dip-slip movement has been suggested based on the occurrence of a subset of lineations that rotate from regional strike into the line of strike of the BFZ (Higgins 1966; Evans and Mosher 1986). Roper and Dunn (1973) identified two main ductile deformational

episodes. Rocks of the Brevard-Poor Mountain sequence in northwestern South Carolina were isoclinally folded,  $F_1$ , during the first deformation event,  $D_1$ . These folds were sheared out at the end of the  $F_1$  event (Roper and Dunn 1973). This deformation was accompanied by  $M_1$  metamorphism, which reached amphibolite grade and recrystallized the rocks into an axial trace schistosity,  $S_1$ . The second deformation event,  $D_2$ , produced an axial trace cleavage expressed as schistosity,  $S_2$ .  $D_2$  produced nearly overturned to isoclinal folds,  $F_2$  (Roper and Dunn 1973).

### **Timing of Deformation and Metamorphism**

Deformational and metamorphic events range in style, grade, and number within the BFZ (Higgins 1966; Reed & Bryant 1964; Hatcher 1978). The majority of studies concerning the Brevard Fault Zone scrutinize gneisses and granites sheared by movement along the fault. Vauchez (1987) investigated movement along the Brevard Fault Zone using kinematic indicators such as stretching lineations and the Palmetto & Ben Hill Granites, which crystallization has been dated at 325 Ma. He found that these granites were sheared only once, which he postulated to be at  $\sim 310$  Ma, which would correspond to the Alleghanian orogeny.

Hatcher (1988) suggested that an Ordovician event could be partially responsible for the observed features within the BFZ, but interpretation was difficult due to overprinting. Sinha et al. (1988) conducted Rb-Sr whole rock analyses on the Henderson gneiss and U-Pb analyses on zircons and monazites from the Henderson gneiss in North Carolina. Their Rb-Sr data from retrograded zones from within the gneiss with U-Pb ages is, in their opinion, the only evidence for two discrete events. They suggest a prograde event at 450 Ma, which, with the first deformation event, develops the mylonitic

fabric. Temperatures during this event were high enough to recrystallize zircons and were within the amphibolite facies (Sinha et al. 1988). Rb-Sr data for the most retrograded gneiss samples indicate a 273 Ma second retrograde event.

Higgins et al. (1997) investigated the age of the Austell gneiss, which lies to the northwest of the Brevard Zone outside of Atlanta, Georgia. Geochronology using U-Pb techniques on zircons and Rb-Sr whole rock methods were applied. Ages of 430 Ma were determined for the igneous precursor to the gneiss. Geochemical evidence from the Austell gneiss indicates that this igneous protolith formed by partial melting of crustal rocks. These results suggest that the U-Pb date could indicate that a thermal event affected the area between Early Silurian and Late Devonian (Higgins et al. 1997). Both Sinha et al. (1988) and Higgins et al. (1997) correlate their 430-450 Ma dates with ductile deformation within the Brevard Fault Zone. But in such a complex fault system as the BFZ, one cannot neglect the overprinting effects that the Acadian or the Alleghanian orogenies may have had on the rocks of the BFZ.

In summary, the BFZ records early ductile deformation due to the Taconic orogeny as well as later ductile and brittle deformation and metamorphism related most likely to the Alleghanian orogeny (Hatcher 1988; Higgins et al. 1988). The Taconic orogeny is thought to be the main thermal event during the Ordovician in the southeast (Roper and Dunn 1973; Hatcher 1988; Higgins et al. 1997). Roper and Dunn (1973) correlate their  $D_1F_1$  event with the Taconic and their  $D_2F_2$  event with the Acadian orogeny. The  $D_2F_2$  event reported may be associated with Alleghanian deformation rather than Acadian.

## **Present Study**

The purpose of this thesis is to investigate the deformational and metamorphic history of the Brevard Fault Zone, outside of Atlanta, Georgia. In 1998, Cobb County Water System contracted Jordan, Jones, and Goulding to expand the waste water treatment capacity for the eastern section of the county. Jordan, Jones, and Goulding concluded a tunnel option would have the lowest environmental impact and contracted QORE Property Sciences (formerly Atlanta Testing and Engineering) and Boart Longyear for hard rock coring. Drill cores along the proposed tunnel alignment were studied for the subsurface geotechnical investigation. Drill core samples from the Chattahoochee Tunnel Project outside of Atlanta, Georgia, allowed a fresh look at the Brevard fault zone. Samples were taken from cores drilled within the interior of the BFZ. Boreholes were approximately located within the button schist unit from Higgins (1966) and from the mylonitic button schist and mylonitic biotite gneiss units of Kath and Crawford (2001). Depths of samples range from 8 to 60 m below the ground surface (Figures 1.1 and 1.2). Previous studies have all used surface outcrops.

By carefully interpreting the information gleaned from the petrology and textures of very fresh rocks from the middle of the fault zone, I attempted to develop new constraints on the polymetamorphic and deformational history of the BFZ.

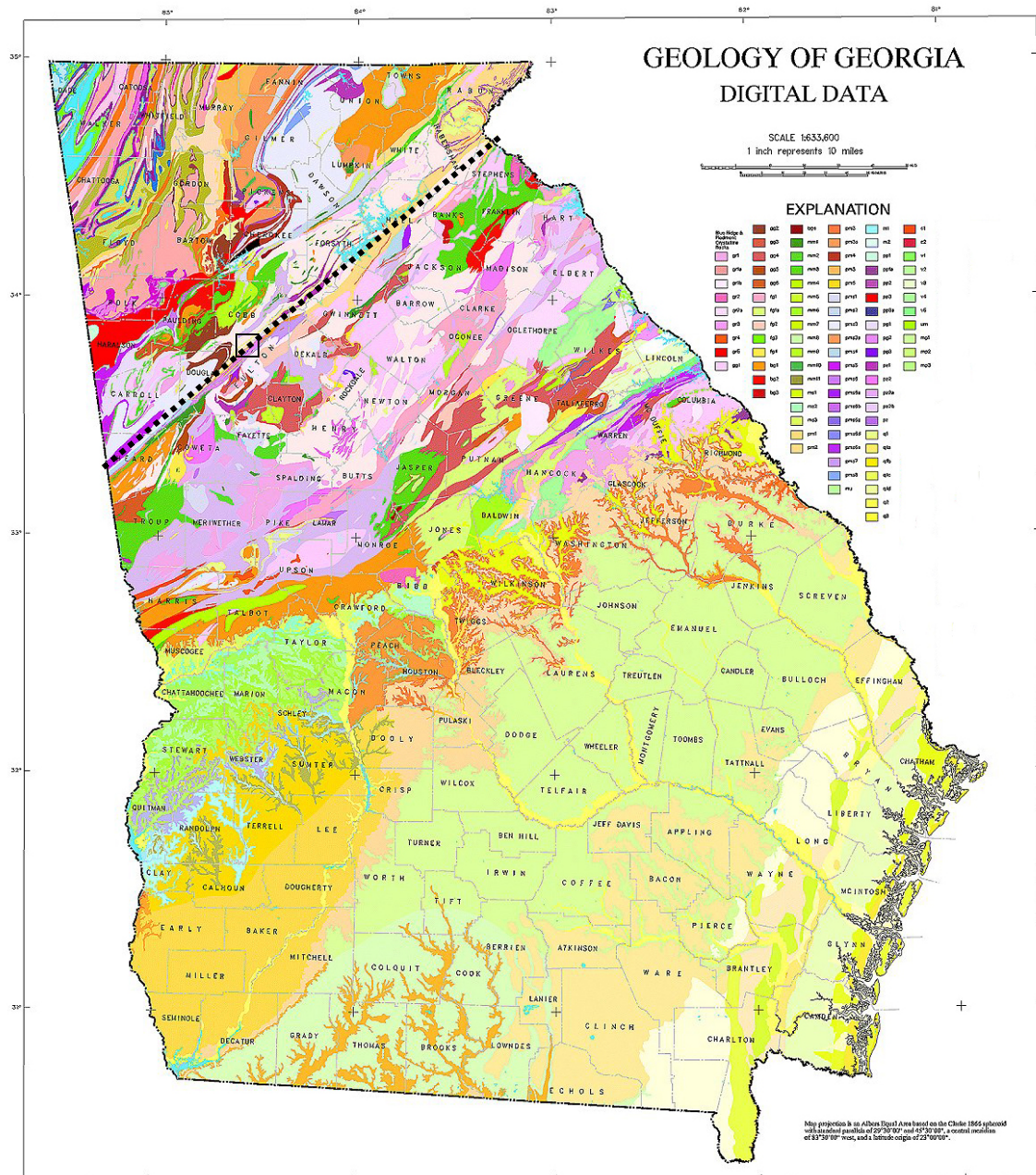


Figure 1.1. Geologic map of Georgia depicting the Brevard zone (dotted line). From Alden 2001. The Brevard Zone roughly delineates the boundary between the Blue Ridge and Piedmont geologic provinces. Box represents study area. Study area begins in unit pms7, button mica schist; passes through unit bg1, biotite gneiss; and ends within unit pms1, mica schist. To the south of this zone is described as gr1b, a porphyritic granite.



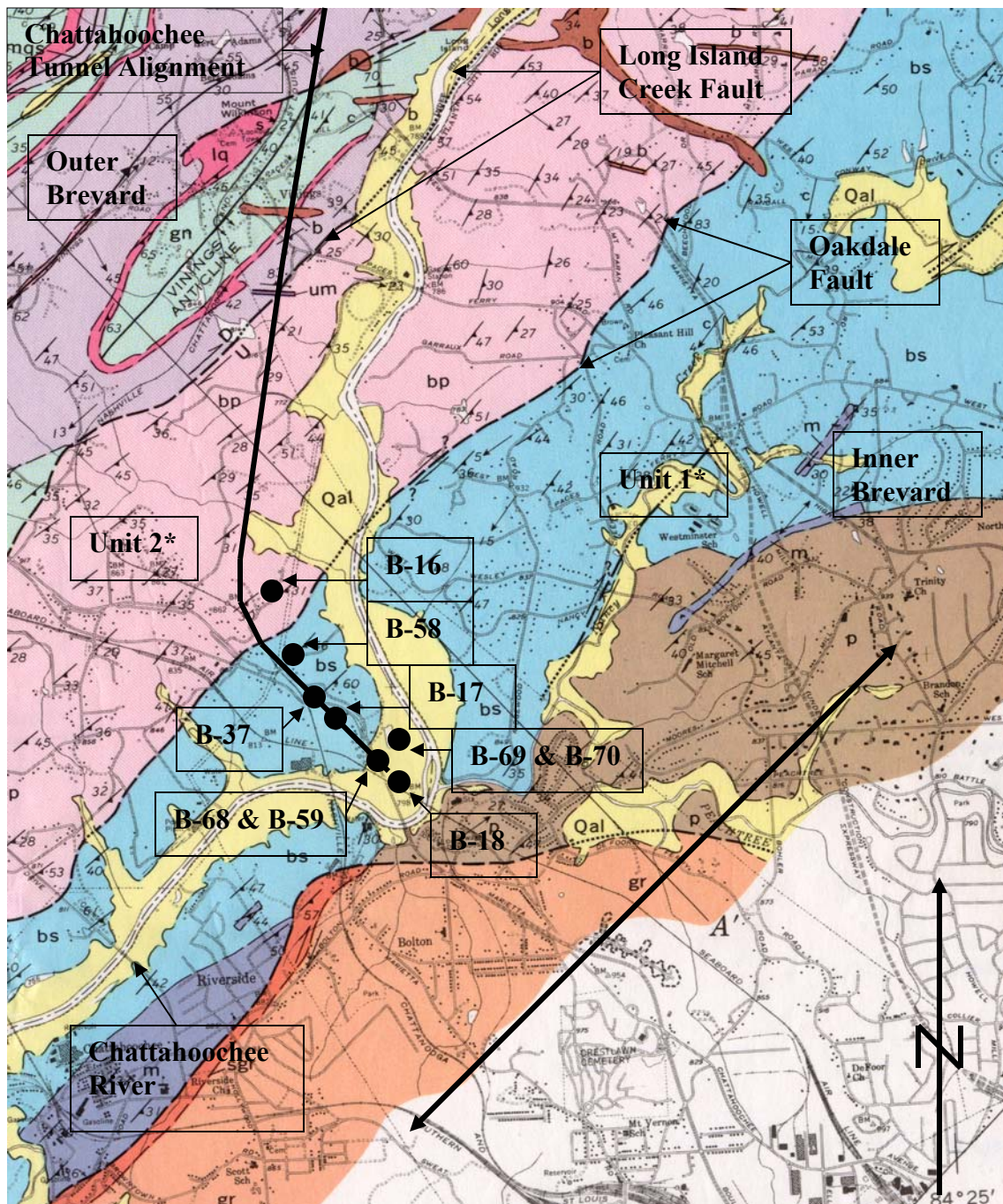

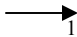

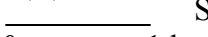


Figure 1.2. Geologic map shows strike of the BFZ (double arrow), location of sampled boreholes, Chattahoochee Tunnel alignment, and units from Higgins (1966) and Kath and Crawford (2001). Blue unit labeled bs is Higgins's button schist. bp is an epidote-biotite-plagioclase gneiss which is referred to as the Long Island Creek gneiss. Unit 1\* and Unit 2\* are from Kath and Crawford (2001). After Higgins (1966). 1:48,000.

Legend (from Higgins 1966)		Color	Unit
	Strike and dip of foliation	Yellow	Qal
	Bearing and plunge of mineral lineation or rodding	Blue	bs button schist
	Overturned anticline	Pink	bp biotite gneiss
	Scale	Brown	p phyllonite
		Orange	gr granitic rocks

## **SAMPLING AND ANALYTICAL METHODS**

The Chattahoochee Tunnel Project yielded over 3,660 m of core along the tunnel alignment for tunneling analysis. Tunnel alignment is approximately perpendicular to the strike of the BFZ and I chose samples from the southernmost 370 m of the tunnel because the deformation is most intense here (Figure 1.2). Boreholes were selected for this study on the basis of location relative to the BFZ. Drill cores were then sampled at 8 m intervals to obtain a representative sampling of drill core lithologies. By sampling at 8 m intervals, sixty-two drill core samples were obtained for a more thorough petrographic analysis. The boreholes contain phyllonite and quartz mica schist units that are located within the innermost section of the Brevard fault zone (BFZ). These rocks correlate on the surface with Unit 1 and Unit 2 from Kath and Crawford (2001) which they describe as mylonitic button schist, mylonitic biotite gneiss, and a medium to coarse grained sphene-epidote-biotite-quartz-feldspar gneiss. On Higgins (1966) base map (Figure 1.2) my samples are from his button schist unit (bs) and an epidote-biotite-plagioclase gneiss (bp) unit. My samples are very well foliated with contorted laminations and are typical of rocks in the BFZ that have undergone the most intense deformation and metamorphism (Figure 2.0).

Drill core sections were cut parallel to foliation and then normal to the stretching lineation and marked in the up direction to obtain a section (Figures 2.1 and 2.2).



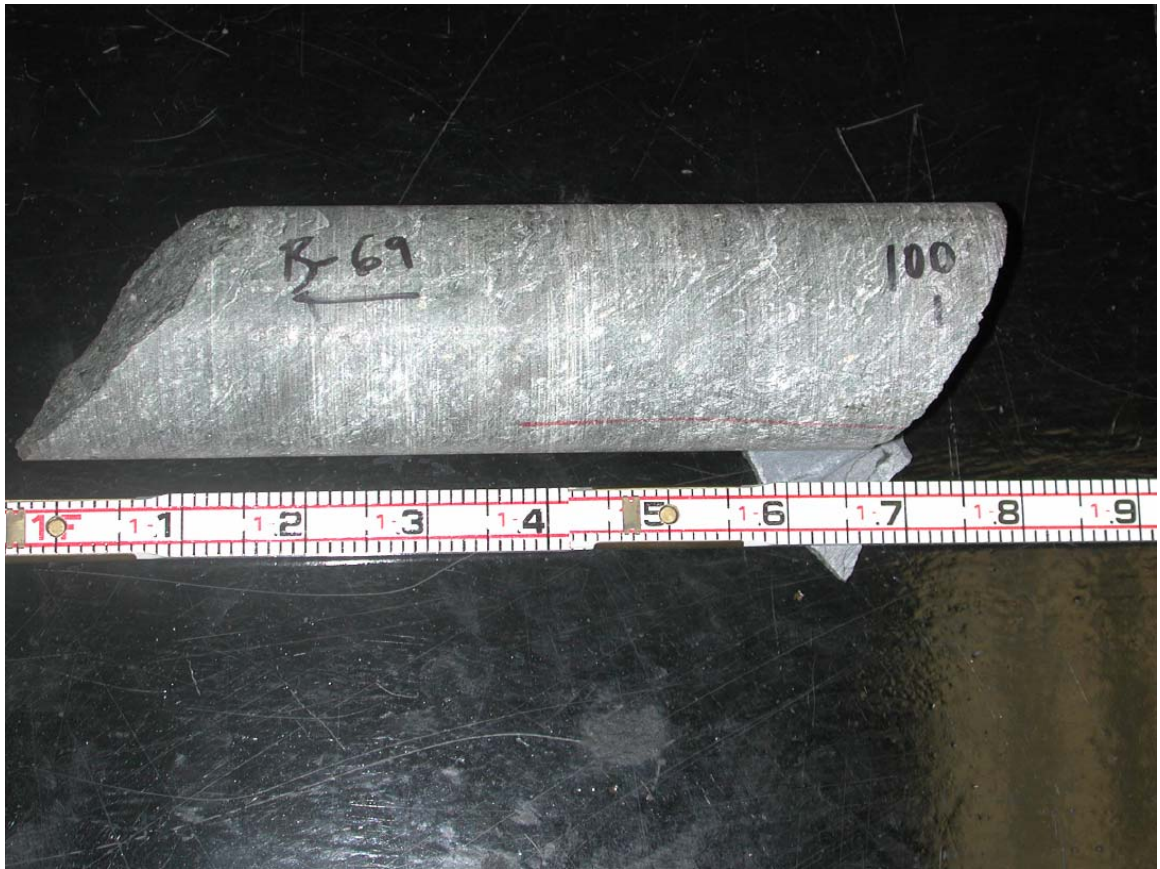


Figure 2.0. Representative intact core from 100ft. (30.5 m) below ground surface. Core measures 0.8 ft. (0.24 m).



Figure 2.1. Representative drill core cut in half; perpendicular to foliation.

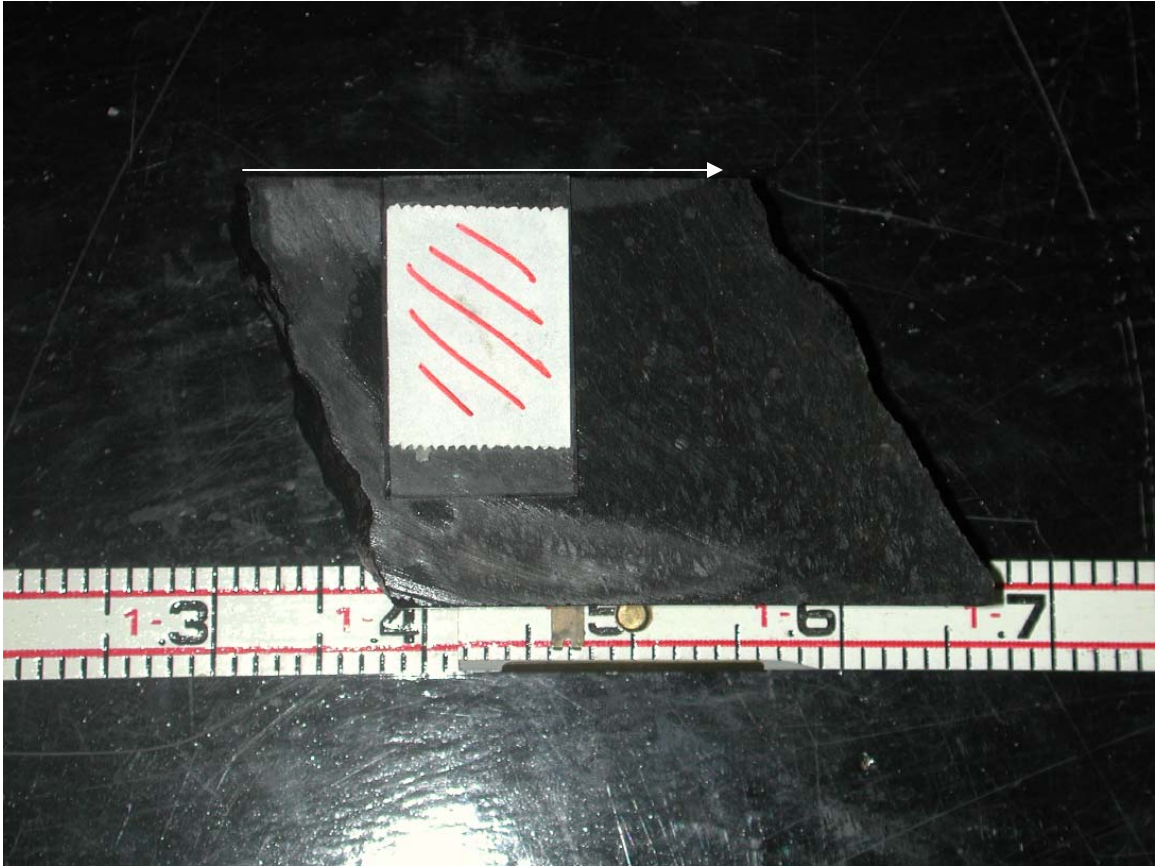


Figure 2.2. Representative drill core showing approximate location of thin section. Arrow indicates up direction.

Petrographic study focused on analysis of the following features in drill core thin sections:

- Mineralogy
- Modal percentages
- Mineralogical textures (mineral overprinting, grain rotation, and recrystallization)
- Microstructure analysis (foliations, styles and numbers folding events, axial trace orientations, and brittle features)

Following petrographic analysis, samples were selected for microprobe analysis.

Samples selected for microprobe analysis were chosen to characterize the peak metamorphic assemblage as well as to ascertain the possibility of documenting different metamorphic episodes. A JEOL 833 electron microprobe at the University of Georgia was used for the analyses. Typical operating conditions were 15kV accelerating voltage and electron beam currents ranging from 5 to 15 nA. During feldspar analyses, the beam was defocused to a 10 micron diameter area. X-ray intensities were converted to weight percent oxides using a Bence-Albee correction scheme and X-ray intensities for natural mineral standards. Mineral compositions are reported for plagioclase, garnet, biotite, muscovite, staurolite, and psuedotachylyte in Tables 4.1 through 4.6. The borehole location of thin section samples was also taken into account to assure spatial variation within the BFZ.

## **PETROGRAPHY**

### **Introduction**

Rocks within the Brevard Fault Zone (BFZ) have been described as button schists, phyllonites, phyllites, and mylonites. Names have been applied depending on localities studied and personal interpretations. For example, Higgins (1966) described button schists in Atlanta, Georgia, containing magnetite-graphite-biotite-quartz-muscovite. Muscovite within these samples displays a "fish-scale" texture within the foliation plane that causes a button texture to develop upon weathering. Phyllonitic schists in the Grandfather Mountain area in North Carolina were described by Reed and Bryant (1964). These units contain chlorite-quartz-sericite and contain porphyroclasts of muscovite fishes within the foliation plane. Crawford and Medlin (1973) described rocks within the BFZ in eastern Alabama and western Georgia as graphitic schists and various other schists containing muscovite-garnet-biotite-quartz-feldspar and commonly containing a button texture. The rocks of the Brevard Zone and Poor Mountain area in western South Carolina were described by Hatcher (1970) as graphitic button phyllites and he also states that the button texture is not unique to Brevard rocks in Georgia.

The BFZ near Atlanta, Georgia is shown in Figure 3.1 and can be delineated into an inner and outer zone based upon rock textures in thin section as well as hand sample. Textures such as obliterated plagioclase twin planes, secondary foliations, and tight-similar folds characterize the inner BFZ. To the north, this zone is bounded by the

Oakdale fault, which forms the southern boundary of a transition zone between rocks of the inner Brevard zone and the Long Island Creek gneiss, which comprises the outer zone of the BFZ. This transition zone is a ductile shear zone characterized by biotite-quartz-muscovite-orthoclase augen gneiss with orthoclase augens that range in diameter from 2 cm to 18 cm. This zone is approximately 90 m in width and separates the inner Brevard lithologies from those of the outer Brevard including the Long Island Creek gneiss (Higgins et al. 1998). The Long Island Creek gneiss is a medium grained, granitic gneiss that displays some effects of mylonitization such as recrystallized quartz and muscovite fishes. To the south of the tunnel, Higgins (1966) mapped two additional units; a phyllonite unit, p, and a granitic unit, gr. Phyllonites described are green- gray green rocks that appear waxy in hand sample and have the mineralogy quartz-mica-chlorite-feldspar. Feldspar occurs as porphyroclasts and quartz is very fine grained. The granitic unit is described as the Palmetto granite, which forms a boundary on the southern side of the Brevard zone. The granite is poorly foliated, coarse grained with large feldspar phenocrysts. As the contact with the Brevard becomes closer, the Palmetto granite becomes more strongly foliated and grades into the phyllonite unit (Higgins 1966).

Kath and Crawford (2001) described the different lithologies located along the Chattahoochee Tunnel alignment outside of Atlanta, Georgia (Figure 1.2). Unit 1 is described as a mylonitic button schist and mylonitic biotite gneiss. The mylonitic button schist is composed of fine grained sericite-muscovite-quartz-feldspar with coarse muscovite forming “eyes” and displays a well developed shear foliation (Kath and Crawford 2001). The mylonitic biotite gneiss is very fine grained, and contains biotite-quartz-feldspar and also displays a very well developed shear foliation (Kath and



Crawford 2001). Unit 2 is correlative to Higgins (1966) unit bp and the Long Island Creek gneiss and is composed of medium to coarse grained sphene-epidote-biotite-quartz-feldspar gneiss. This unit is strongly sheared close to the contact with unit 1 (Kath and Crawford, 2001). The drill cores I studied sampled rocks below the surface outcrops of units 1 and 2 of Kath and Crawford.

Rocks within my thesis area are all from the inner Brevard and are quartz mica schists and mica schists. Quartz mica schists (Figure 3.1) are quartz rich, fine-grained rocks, moderately jointed, and break into angular fragments due to their high quartz content. Mica schists are medium to coarse-grained rocks (Figure 3.1) that display deformational features such as recrystallized quartz, folds, and other ductile textures (Marshak and Mitra 1988). In the area studied, both units are interlayered on scales of cm to m, but quartz mica schists are dominant in the south and mica schists are more prevalent in the north. Within the tunnel, foliation in both units strikes N 35° E and dips 44° to the southeast.

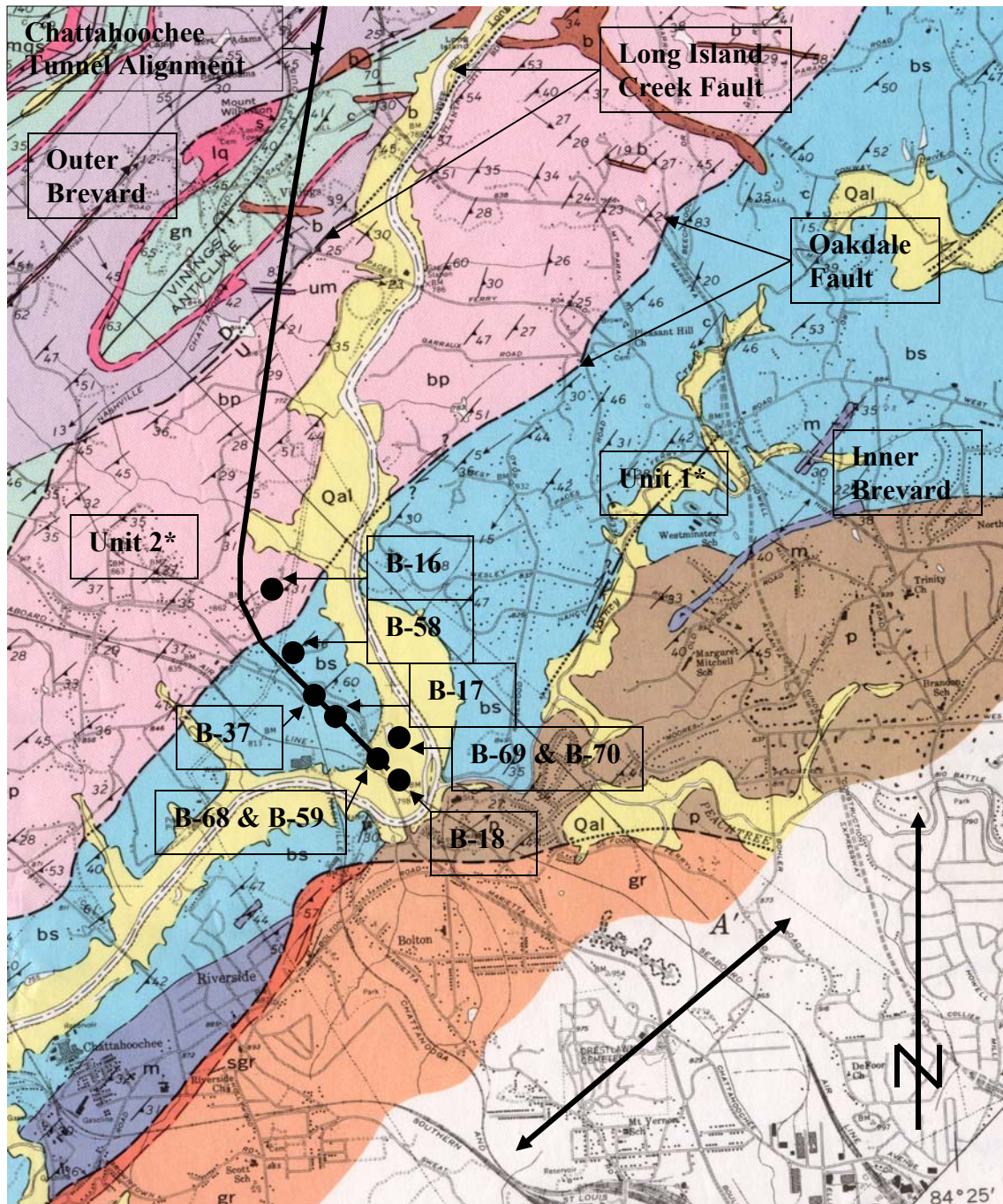


Figure 3.0. Modified geologic map from Higgins (1966) shows borehole locations along the southern portion of the Chattahoochee Tunnel. Circles represent boreholes where samples were collected. B-16 is the most northern borehole sampled. Double arrow indicates overall strike of the Brevard Fault Zone; from lower left to upper right. bs is the button schist unit, bp is the epidote-biotite-plagioclase gneiss unit, p is the phyllonite unit, and gr is the sheared Palmetto granite from Higgins (1966). Unit 1 and Unit 2 are lithologic units from Kath and Crawford, 2001. Scale and symbols as in Figure 1.2.





Figure 3.1. Interlayering between quartz mica schist (A) and mica schist (B). Taken from Chattahoochee Tunnel, south end, 53 m below ground surface (bgs).

## Quartz Mica Schists

Quartz mica schists are typically fine grained (0.2 to 1.5 mm diameter), quartz-rich rocks and have assemblages of quartz, plagioclase, muscovite, biotite, +/- garnet, +/- epidote, and +/-tourmaline. A typical mode is 44 % quartz, 9.7 % plagioclase, 12 % muscovite, and 27.6 % biotite, with minor garnet, tourmaline, chlorite, and epidote (Table 3). Quartz elongation axes and long dimensions of muscovite and biotite grains define the foliation while quartz veins and folded muscovite lenses define folds (Figure 3.3). Quartz occurs within the matrix as well as in deformed veins and ribbons. Matrix quartz is fine grained (0.2 mm), displays undulose extinction, and has long axes aligned parallel to the foliation. Vein quartz is typically folded in open-gentle, similar, to close-tight, similar folds. Vein quartz commonly displays undulose extinction with long axes of grains aligned parallel to the axial trace of folds. Both the long axes of recrystallized vein quartz and the axial trace of folds (when present) intersect the primary foliation by an acute angle of approximately  $15^{\circ}$ . More rarely quartz veins are not folded but long axes of grains still define an acute angle of  $\sim 15^{\circ}$  with primary foliation (Figure 3.4).

Plagioclase feldspar occurs as anhedral, porphyroclasts that range in diameter from 0.2 mm to 1.5 mm. Some still retain twin planes while more commonly twins were obliterated during deformation (Passchier and Trouw 1998). Muscovite occurs as large single “fishes” (Higgins 1966; Crawford and Medlin 1973; Reed and Bryant 1964) that range in length from 0.5 mm to 1.5 mm. Most grains have been bent, kinked, and/or sheared. Brown biotite ranges in size from 0.1 mm to 0.4 mm and long axes of grains are roughly parallel to foliation. Long axes of biotite grains are also commonly parallel to fold axes (Figure 3.5). Biotite is locally concentrated and appears both roughly

aligned with foliation and also parallel to axial traces of folds. Biotite also commonly occurs as small (0.1 mm) single grain inclusions within garnet porphyroblasts.

Garnet occurs as sparse porphyroblasts with diameters ranging from 0.5 to 1.0 mm. The grains are subhedral to euhedral, commonly contain quartz and biotite inclusions, and are fractured. Inclusions are more abundant towards the rim of porphyroblasts. Muscovite commonly wraps around garnet porphyroblasts. Green tourmaline occurs as 0.1 to 0.3 mm diameter, euhedral grains that commonly cross-cut the foliation (Figure 3.5). Tourmaline's c-axis consistently lies within the foliation plane, parallel to the stretching lineation. Tourmaline commonly is optically zoned with dark green cores and lighter green rims. Epidote occurs as small, ~0.2 mm, euhedral grains which cross-cut other fabrics present. Local concentrations of chlorite grains (0.05mm) are restricted to fractures and veins and do not appear to replace garnet or biotite.

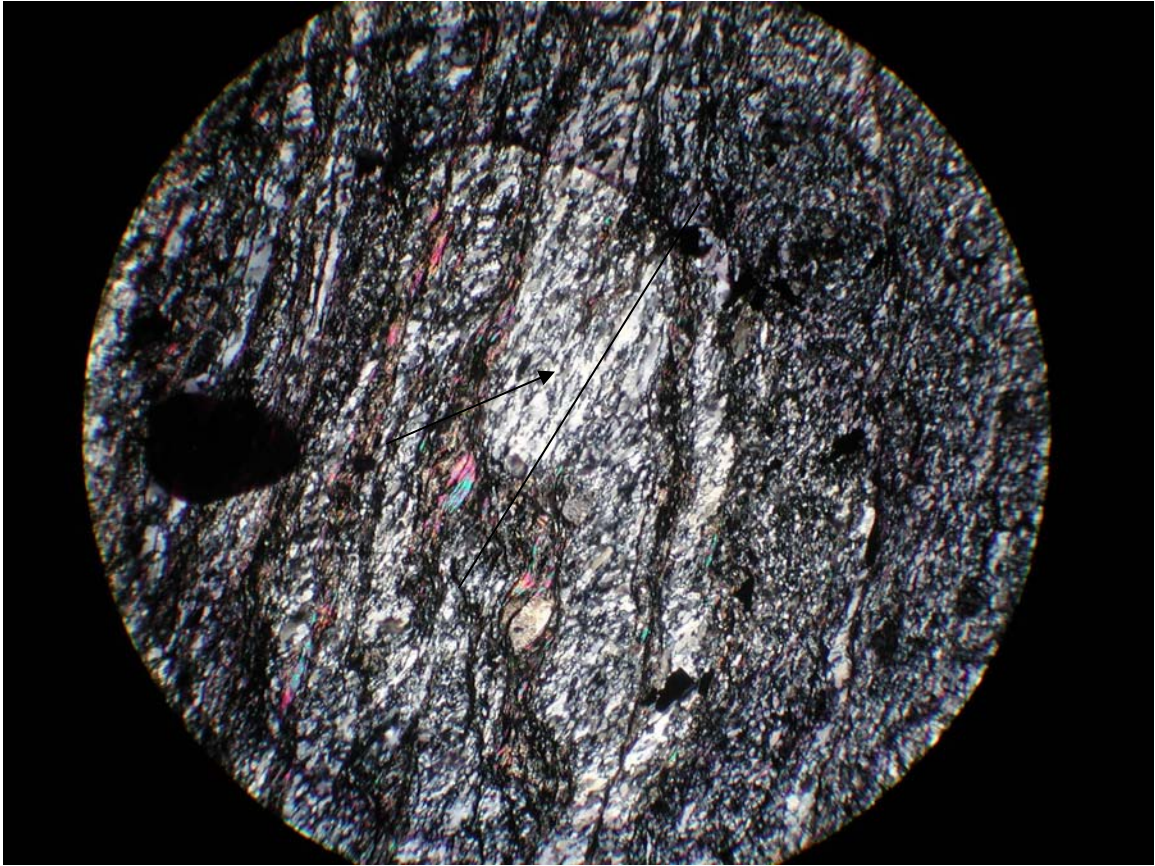


Figure 3.2. Photomicrograph of a quartz vein (arrow) within typical quartz mica schist that has been tightly folded. Quartz neoblasts within the vein have been dynamically recrystallized into an orientation parallel to the axial trace of the fold (line). Field of view is 5.5 mm. Crossed nicols. Quartz mica schist; sample ATT-14; borehole B-18; 38m bgs.



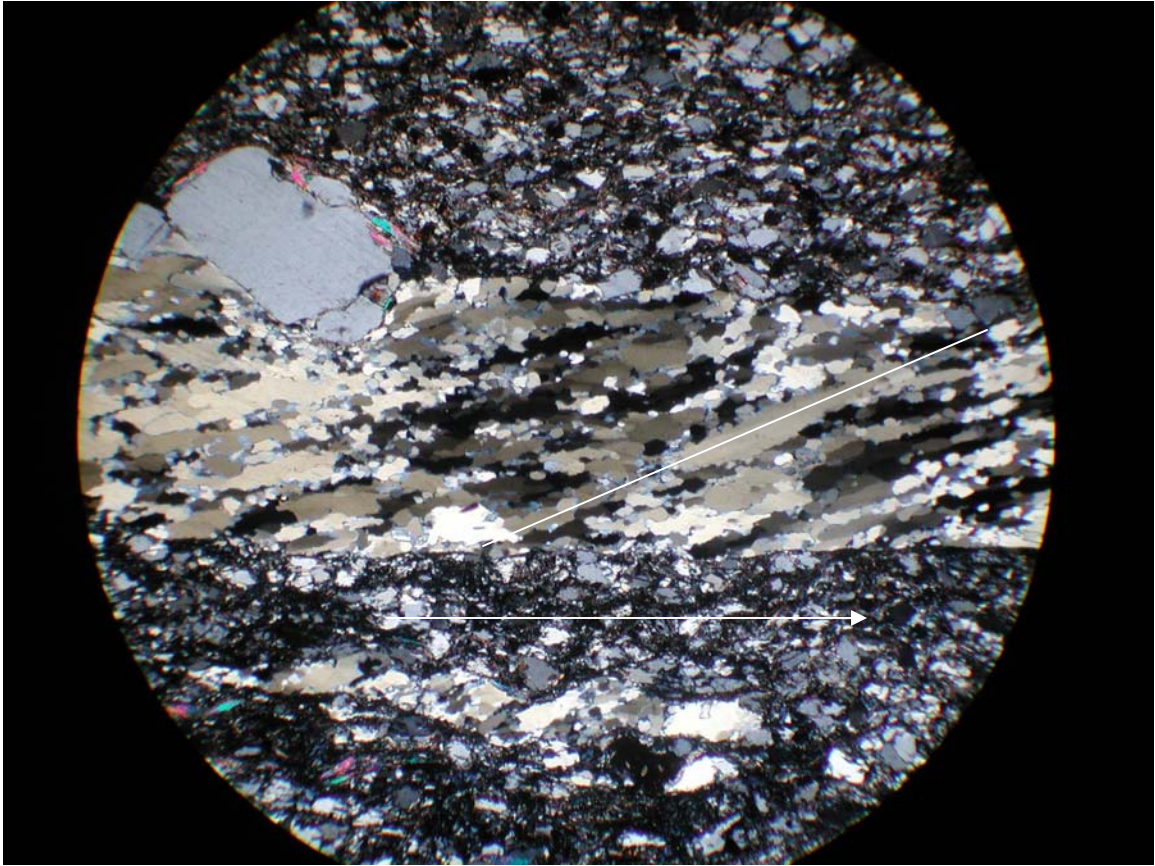


Figure 3.3. A quartz vein in quartz mica schist that appears relatively undeformed. Muscovite and biotite define foliation (from left to right) as well as boundary edges of the quartz vein (arrow). Neoblasts within the vein have been dynamically recrystallized in an orientation (line) that intersects foliation at  $\sim 15^\circ$ . Crossed nicols. Field of view is 2.0 mm. Quartz mica schist; sample ATT-11; borehole B-18; 15.7 m bgs.

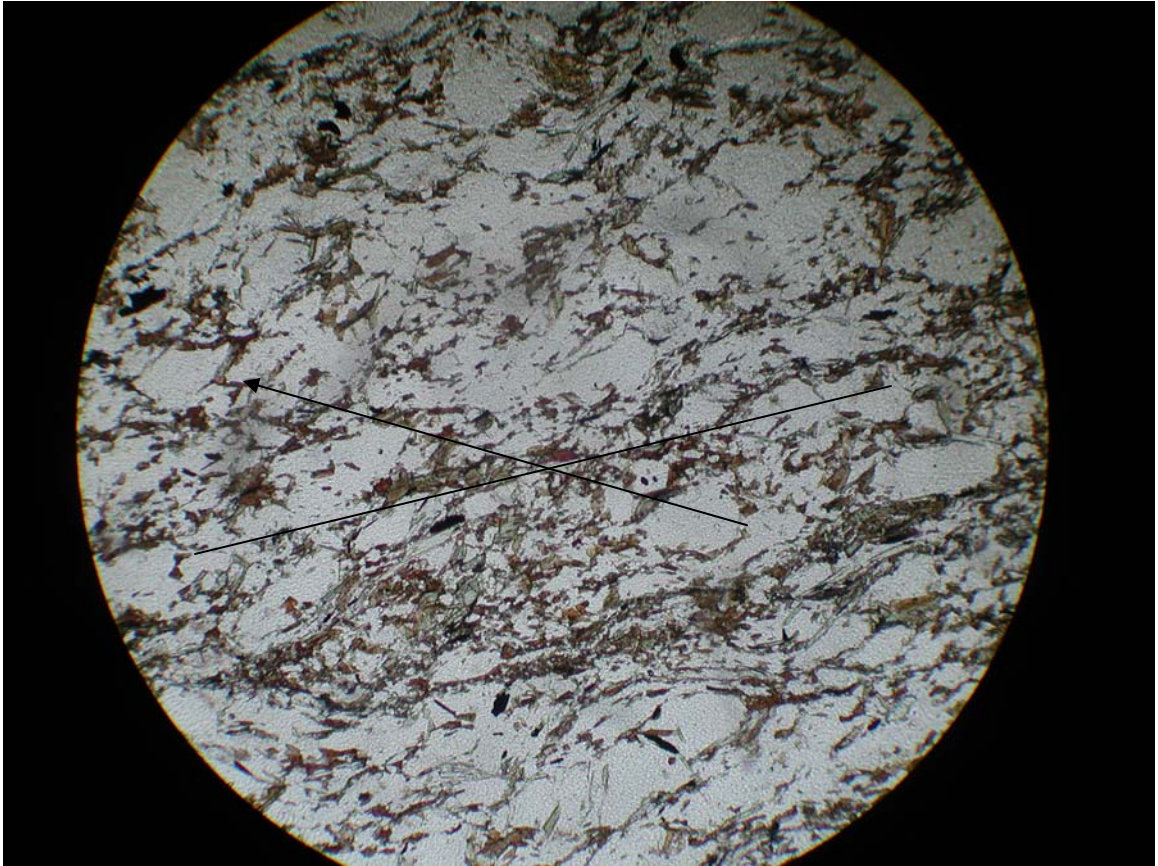


Figure 3.4. Biotite aligned parallel to foliation (line). Biotite defining foliation has been gently folded. Long axes of biotite also define an acute angle of  $\sim 15^\circ$  to foliation indicated by arrow. Uncrossed nicols. Field of view is 2.0 mm. Quartz mica schist; sample ATT-17; borehole B-68; 38.1 m bgs.



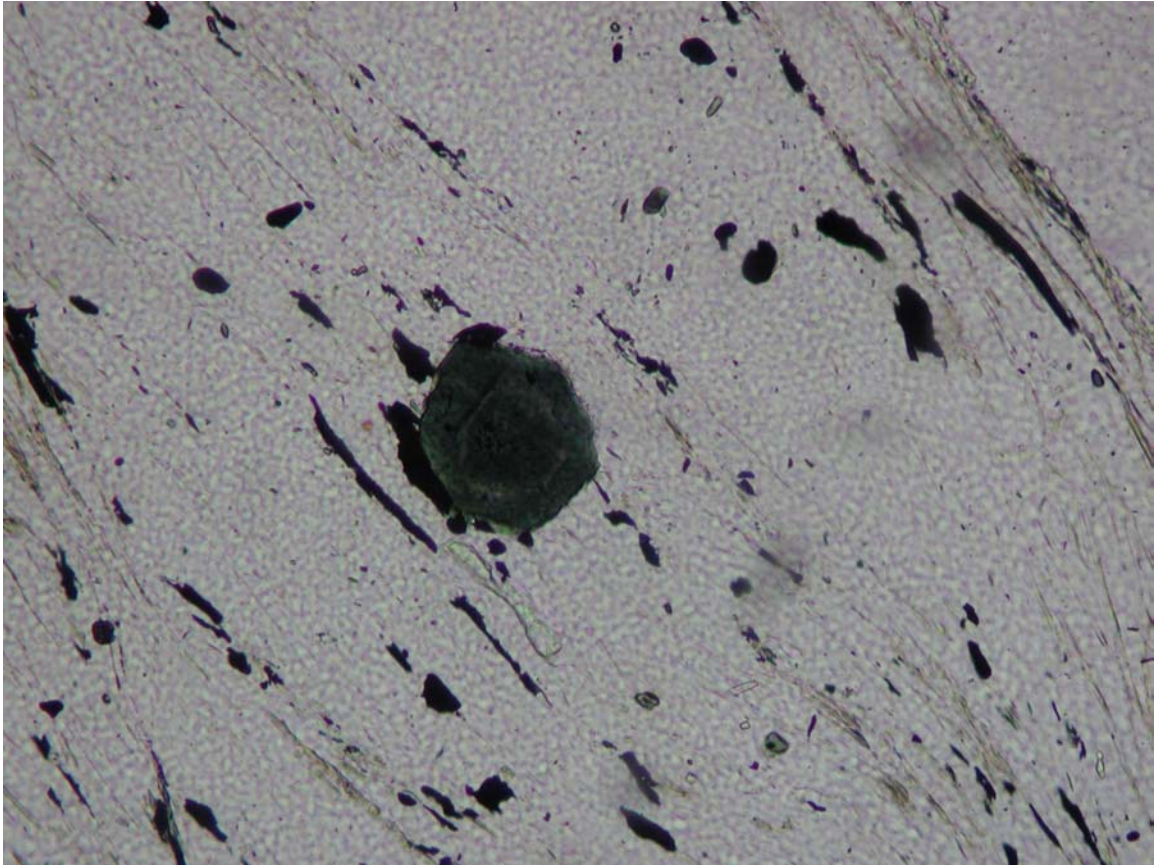


Figure 3.5. Optically zoned tourmaline porphyroblast cross-cutting muscovite. Uncrossed nicols. Field of view 2.0 mm. Quartz mica schist; sample ATT-55; borehole B-58; 53.3 m bgs.

## **Mica Schists**

Mica schists are light gray in color and are strongly foliated, medium to coarse grained (0.2 mm to 6 mm) rocks with typical assemblages of muscovite, biotite, quartz, plagioclase feldspar, +/- garnet, +/- staurolite, and +/- tourmaline, with accessory calcite, epidote, and chlorite. A typical mode is 31.4% muscovite, 26.4% biotite, 27.7% quartz, 5.9% plagioclase, 4.3% garnet, and 4 % staurolite, with minor tourmaline, epidote, calcite, and chlorite (Table 3).

Muscovite occurs as large mat-like fishes and defines the foliation (Figure 3.7). Grains range from 0.5 mm to 1.5 mm in length and are commonly folded. Muscovite, also defines a secondary foliation (Figure 3.8). The mica schists also commonly have smaller (0.2 mm) muscovites that cross-cut primary muscovites and have long axes parallel to axial traces of folds. Brown biotites are typically 0.5 mm in length and do not precisely follow the primary foliation and are oriented in more of an axial trace fashion to folds. Quartz occurs as a matrix phase and as veins. Veins are commonly folded and vein quartz exhibits no undulose extinction or other strain characteristics.

Plagioclase feldspar occurs as anhedral porphyroclasts that range in diameter from 0.2 to 1.0 mm. Some still retain twin planes while more commonly twins are obliterated. Garnet occurs as porphyroblasts with diameters ranging from 0.3 to 2.5 mm and displays variable morphologies defined by grain size, fracture and inclusion density, and proximate fabric disturbance. Some garnets are large (up to 2.5 mm diameter) subhedral porphyroblasts that contain numerous fractures and commonly exhibit sinusoidal inclusion trails of quartz and ilmenite suggesting grain rotation during formation (Figure

3.8). These larger garnets commonly possess irregular grain boundaries and are commonly embayed. Muscovite wraps around these porphyroblasts. Smaller garnets (0.2 to 0.4 mm) are euhedral and contain no fractures or inclusion trails. Biotite and muscovite plates terminate without bending at the crystal face of these smaller garnets (Figure 3.9).

Staurolite typically occurs as small (0.5 mm) subhedral, pale yellow porphyroblasts that contain quartz and opaque inclusion trails suggesting that these minerals also rotated during crystal growth. Tourmaline occurs as 0.4 mm, euhedral grains that are commonly optically zoned with dark green cores and light green rims. The c-axis of porphyroblasts consistently lies within the primary foliation plane and commonly cross-cuts folded muscovites (Figure 3.10). Epidote occurs as single grains (0.3 mm) that cross-cut other fabrics. Calcite and chlorite occur within cross cutting fractures suggesting that these minerals formed after peak metamorphism.

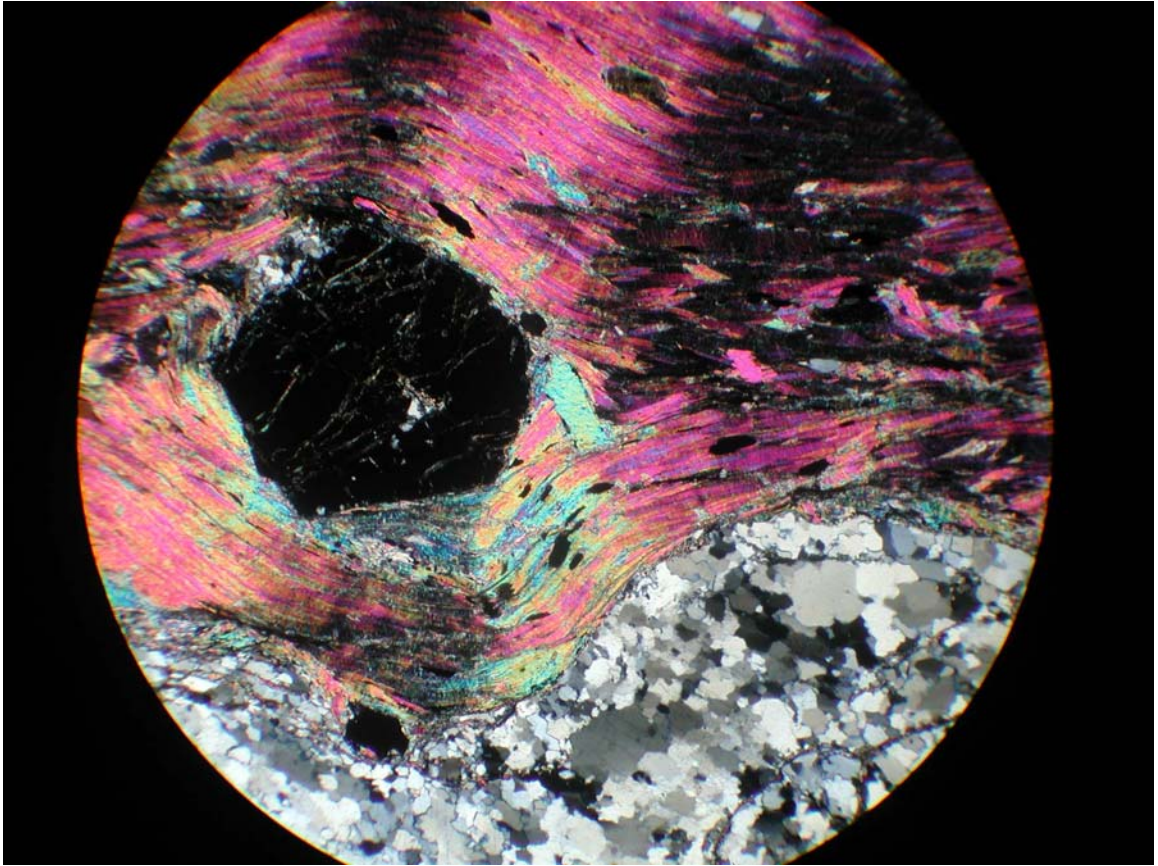


Figure 3.6. Muscovite defines foliation and wraps around garnet porphyroblast. Field of view is 5.5 mm. Mica schist; sample ATT-21; borehole B-59; 38.1 m bgs.



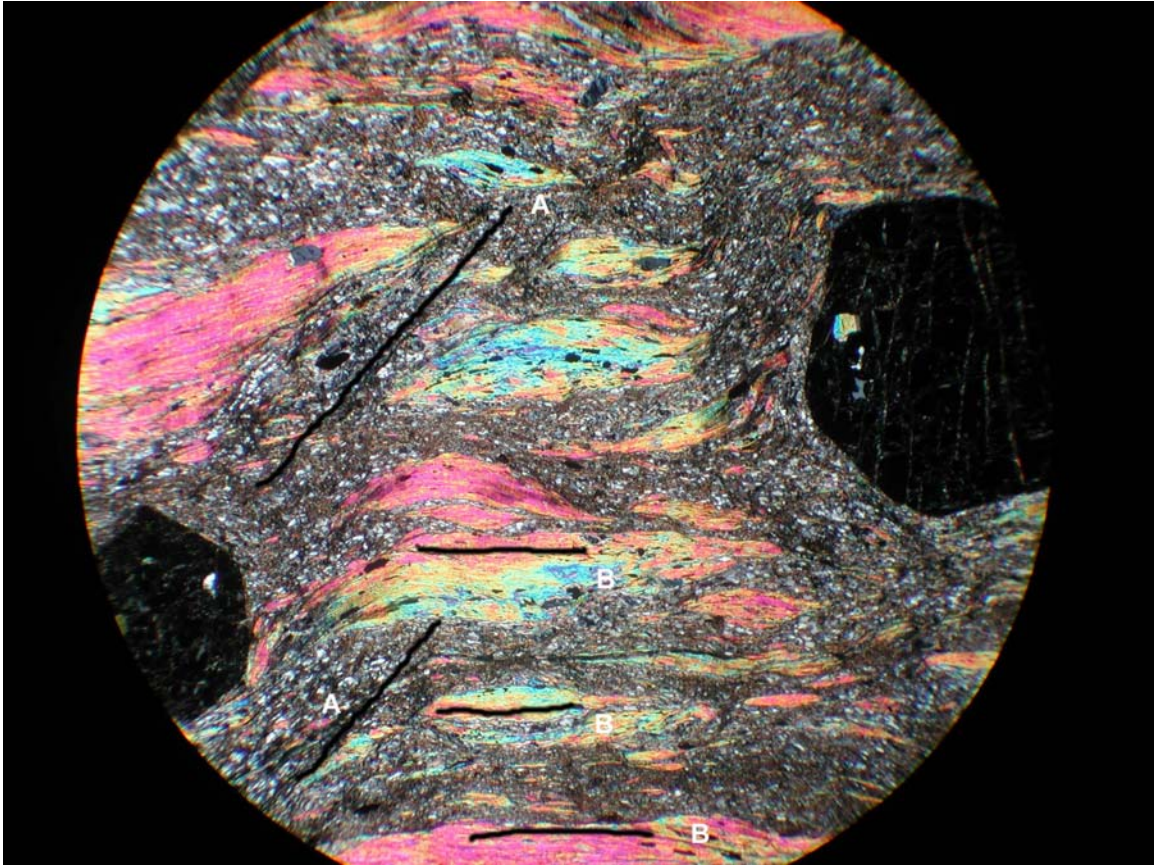


Figure 3.7. Muscovite defines primary foliation (B) and a secondary foliation, (A). Crossed nicols. Field of view is 5.5 mm. Mica Schist; sample ATT-18, borehole B-68; 45.8 m bgs.

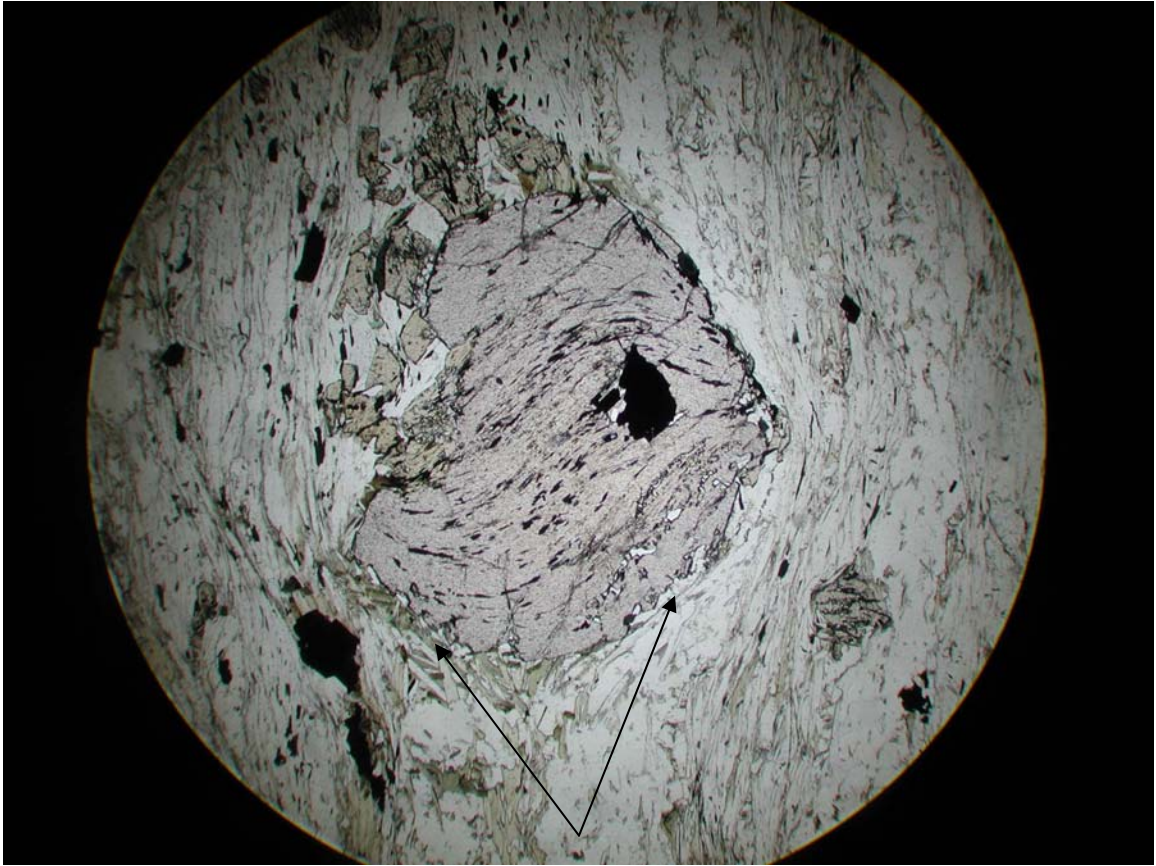


Figure 3.8. Fractured, subhedral garnet containing sinusoidal inclusion trails of quartz and ilmenite. Muscovite and biotite wrap around garnet. Arrows emphasize irregular grain boundaries. Uncrossed nicols. Field of view is 5.5 mm. Mica schist; sample ATT-52; borehole B-58; 30.5 m bgs.



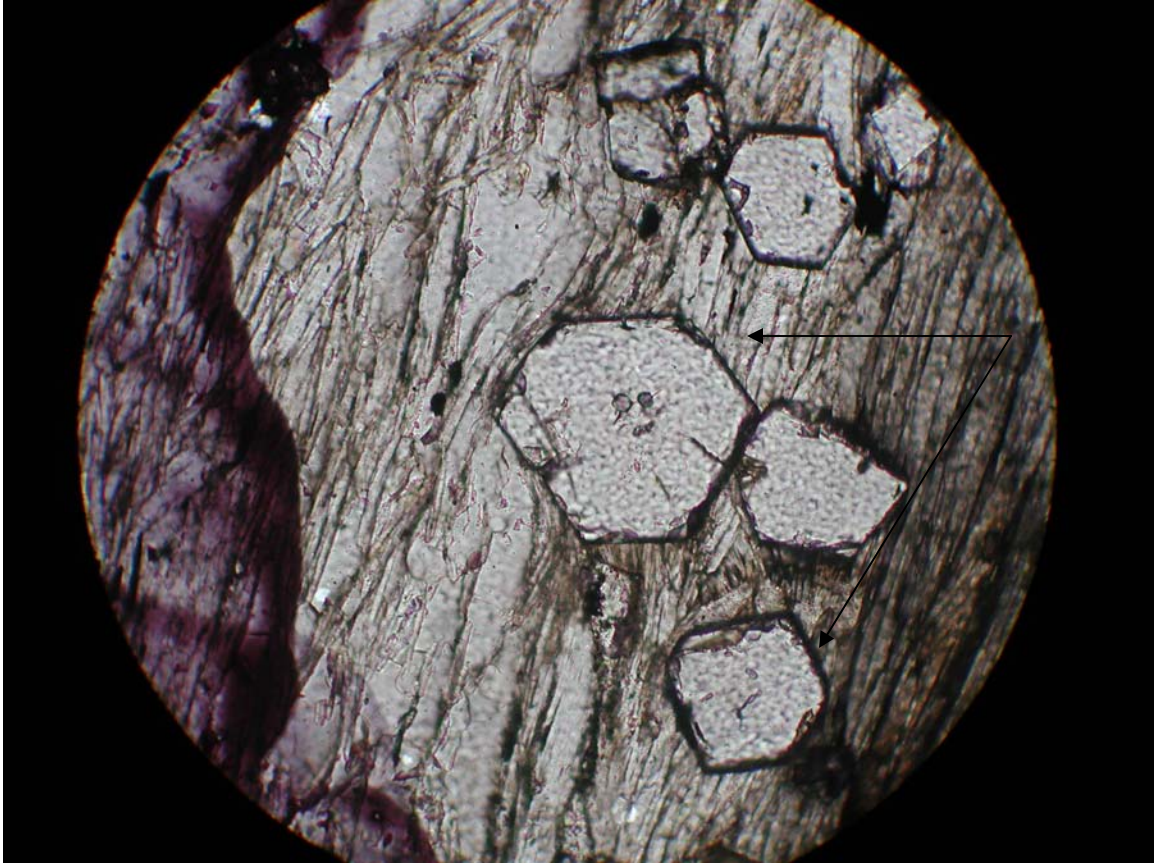


Figure 3.9. Small garnets lack inclusions and fractures. Note that muscovite terminates at the crystal face. Arrows emphasize straight, euhedral grain boundaries. Field of view is 2.0 mm. Uncrossed nicols. Mica schist; sample ATT-37; borehole B-17; 15.2 m bgs.

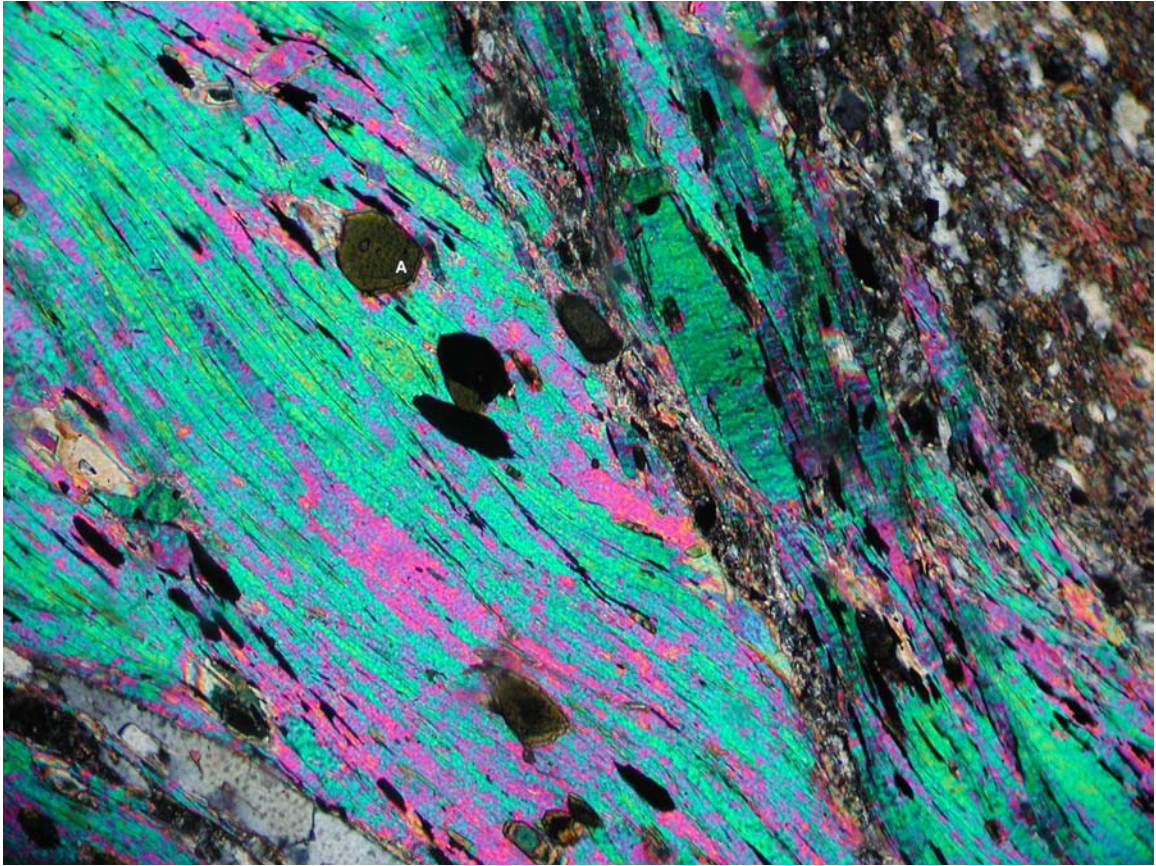


Figure 3.10. A. Tourmaline porphyroblast whose c-axis is parallel to the  $S_1$  plane and cross-cuts muscovite that define the primary foliation. Crossed nicols. Field of view is 2.0 mm. Mica schist; sample ATT-19; borehole B-68; 53.4 m bgs.



## **Brittle Textures**

Quartz mica schists and mica schists both contain brittle features, but these features are more common within quartz mica schists. Brittle features include possible psuedotachylytes in BFZ samples ATT-9 and ATT-10 (Figure 3.11) and vein filled fractures.

Psuedotachylytes are the result of localized melting of a host rock due to heat generated from frictional sliding along a brittle fault plane (Passchier and Trouw 1998). The inferred psuedotachylytes are light to medium green in color, up to 5.0 mm in thickness, and have a very fine-grained matrix containing small (~0.05 mm diameter) fragments of quartz and plagioclase. Layering within psuedotachylyte is common and may be folded; this layering is interpreted to form during fluid flow within the melt (Norwick 2001; Passchier and Trouw 1998). Inferred psuedotachylytes present in samples ATT-9 and ATT-10 are banded and possess sharp contacts between their matrix and the host rock. Contacts between psuedotachylytes and host rock are typically sharp unlike cataclasites (Passchier and Trouw 1998). Psuedotachylytes typically contain a homogenous matrix that has a chemical composition comparable to the host rock while the matrix of a cataclasite or breccia contains fragments of variable grain size and composition. Electron microprobe analysis of inferred psuedotachylytes in samples ATT-9 and ATT-10 confirms the presence of quartz and feldspar but no micas within the matrix of the psuedotachylyte. Identifiable micas are typically absent from the psuedotachylytes probably due to high temperatures generated during formation (Passchier and Trouw 1998). The presence of flow bands, sharp contacts between psuedotachylyte vein and host rock, the lack of micas in the matrix, and the homogenous

appearance of the matrix suggest that the flow-banded veins that I observed in samples ATT-9 and ATT-10 are psuedotachylytes and not cataclasites or breccias.

Brittle fractures are commonly filled with chlorite, calcite, and quartz and can be up to 1 mm wide (Figures 3.12 and 3.13). Psuedotachylytes and brittle fractures cross-cut all ductile fabrics.

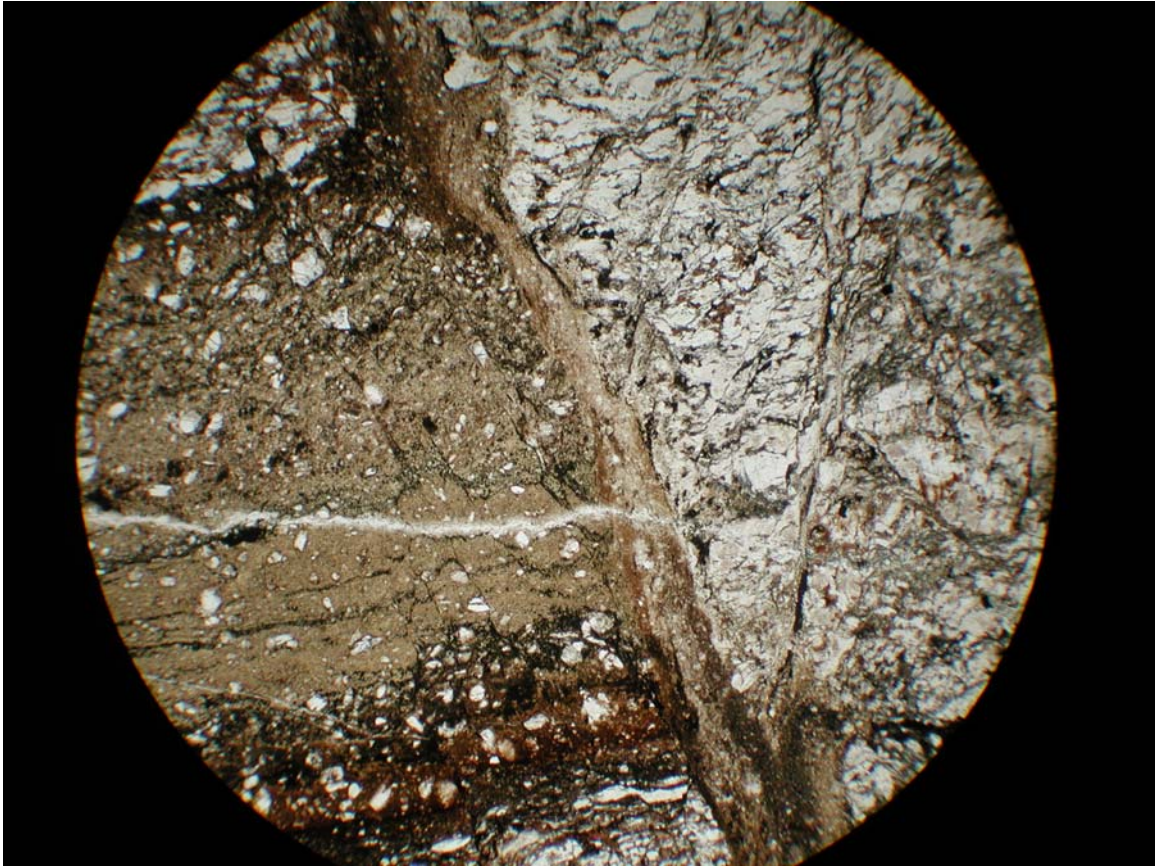


Figure 3.11. Photomicrograph of inferred psuedotachylyte in quartz mica schist. Clasts are quartz and plagioclase feldspar. Psuedotachylyte vein has green core with darker brown rim. Psuedotachylyte is cut by another brittle fracture. Uncrossed nicols. Field of view is 5.5 mm. Quartz mica schist; sample ATT-9, borehole B-68; 56.3 m bgs.

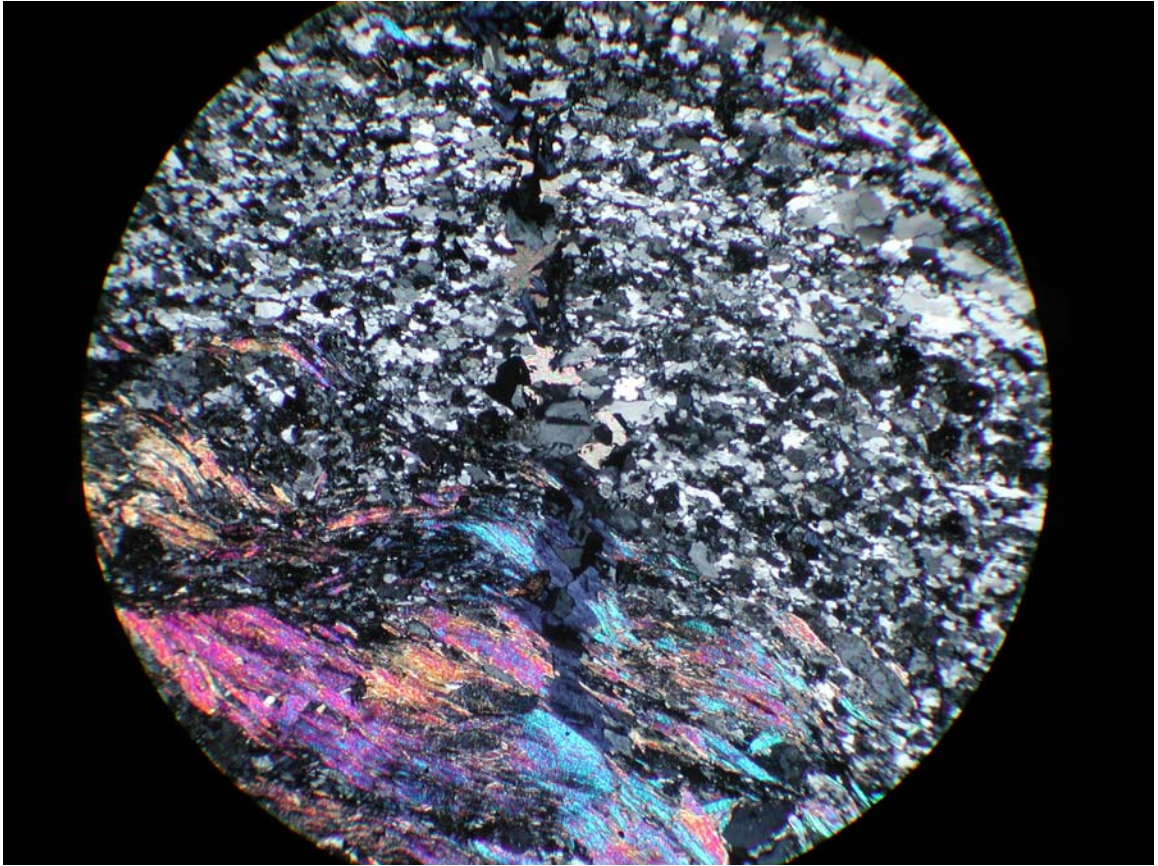


Figure 3.12. Brittle fracture runs down through the middle of the sample section. Fracture contains chlorite and calcite. Crossed nicols. Field of view is 5.5 mm. Mica schist; sample ATT-26; borehole B-59; 60.4 m bgs.



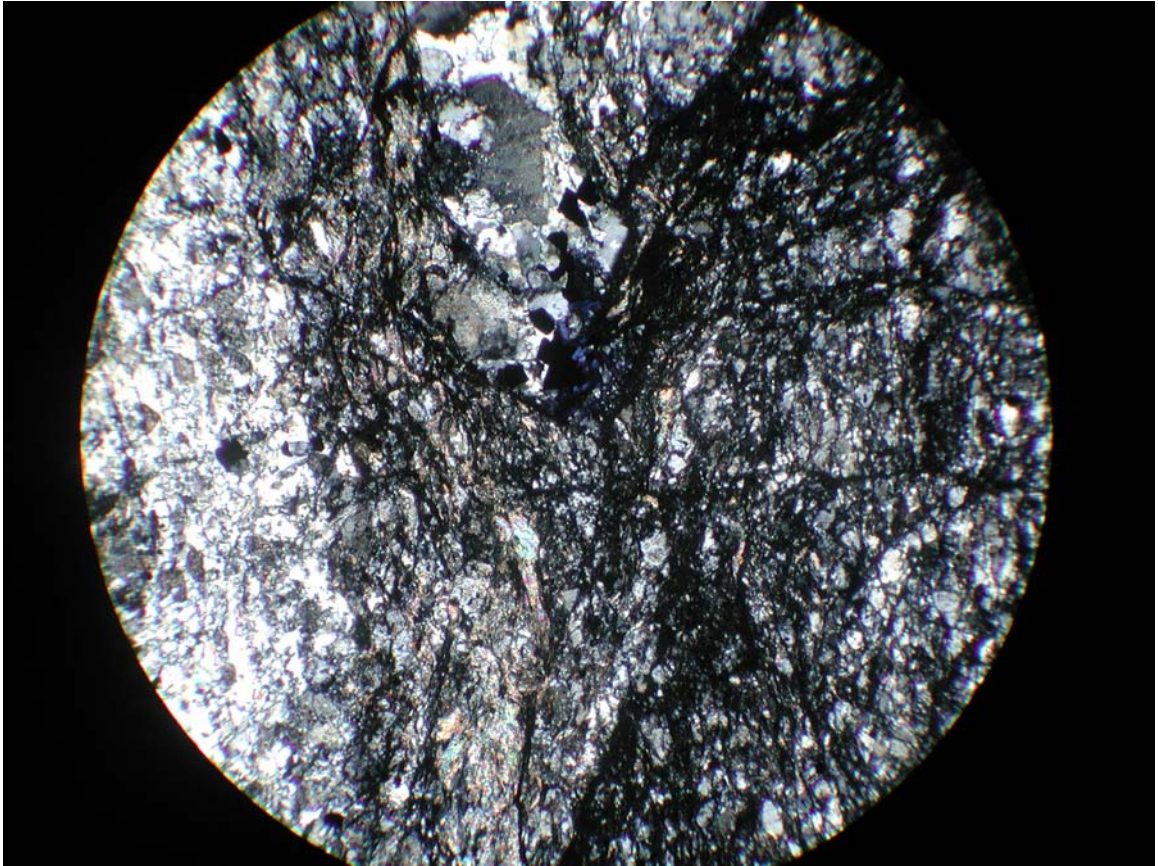


Figure 3.13. Fracture network. Fractures are filled with chlorite and rock fragments. Crossed nicols. Field of view is 5.5 mm. Quartz mica schist; sample ATT-28; borehole B-69; 23.2 m bgs.

**Table 3.0****Modes of Representative Mica schists (MS) and Quartz mica schists (QMS)**

<b>Sample #</b>	<b>ATT-25</b>	<b>ATT-37</b>	<b>ATT-48</b>	<b>ATT-17</b>	<b>ATT-28</b>	<b>ATT-35</b>
<b>Rock Type</b>	<b>MS</b>	<b>MS</b>	<b>MS</b>	<b>QMS</b>	<b>QMS</b>	<b>QMS</b>
<b>Points (n)</b>	<b>n=300</b>	<b>n=300</b>	<b>n=300</b>	<b>n=300</b>	<b>n=300</b>	<b>n=300</b>
<b>Muscovite</b>	<b>29.3</b>	<b>33.3</b>	<b>31.7</b>	<b>15.7</b>	<b>16</b>	<b>4.33</b>
<b>Biotite</b>	<b>33.7</b>	<b>24.3</b>	<b>21.3</b>	<b>28</b>	<b>16.3</b>	<b>38.3</b>
<b>Plagioclase</b>	<b>9.66</b>	<b>4.66</b>	<b>3.33</b>	<b>6.66</b>	<b>8.66</b>	<b>13.7</b>
<b>Quartz</b>	<b>18.3</b>	<b>26</b>	<b>38.7</b>	<b>44</b>	<b>49.3</b>	<b>38.7</b>
<b>Opaque</b>	<b>4.66</b>	<b>1.66</b>	<b>2</b>	<b>0.33</b>	<b>4</b>	<b>1.66</b>
<b>Epidote</b>	<b>0</b>	<b>0</b>	<b>1</b>	<b>0.33</b>	<b>0.33</b>	<b>0</b>
<b>Chlorite</b>	<b>2</b>	<b>0</b>	<b>1.33</b>	<b>5</b>	<b>5.33</b>	<b>3.33</b>
<b>Garnet</b>	<b>2.33</b>	<b>10</b>	<b>0.66</b>	<b>0</b>	<b>0</b>	<b>0</b>

<b>Minerals</b>	<b>Mean Modes</b>	
	<b>Mica schist</b>	<b>Quartz mica schist</b>
<b>Muscovite</b>	<b>31.4</b>	<b>12</b>
<b>Biotite</b>	<b>26.4</b>	<b>27.6</b>
<b>Plagioclase</b>	<b>5.9</b>	<b>9.7</b>
<b>Quartz</b>	<b>27.7</b>	<b>44</b>
<b>Opaque</b>	<b>2.8</b>	<b>2</b>
<b>Epidote</b>	<b>0.3</b>	<b>0.3</b>
<b>Chlorite</b>	<b>1.1</b>	<b>1.1</b>
<b>Garnet</b>	<b>4.3</b>	<b>0</b>

## MINERAL COMPOSITIONS

Mineralogy of both quartz mica schists and mica schists reflect greenschist to amphibolite grade, Barrovian style metamorphism. Samples chosen for electron microprobe analyses were selected to characterize the peak metamorphic assemblage of garnet-biotite-staurolite.

Other phases analyzed were plagioclase and muscovite to characterize the overall mineralogy of the samples. Sample locations and depths vary and range from the inner Brevard Zone towards the Oakdale Fault (Figure 4.1).

**Plagioclase feldspars** occur as anhedral porphyroclasts that muscovite and biotite wrap around and also as a matrix constituent. Porphyroclasts are relatively homogenous with compositions in the range An<sub>20-30</sub> (Table 4.1). Plagioclase grains showed little compositional variability between cores and rims; larger porphyroclasts and smaller grains within the groundmass also had similar compositions.

**Garnet** appears as large, fractured, and inclusion-rich porphyroblasts (“first generation garnet” to be justified later) as well as small, unfractured, and inclusion-free porphyroblasts (“second generation garnet” also to be justified later). Both morphological types of garnet grains were analyzed in traverses to fully document zoning, if present, and to distinguish any chemical differences between garnets with different morphologies.

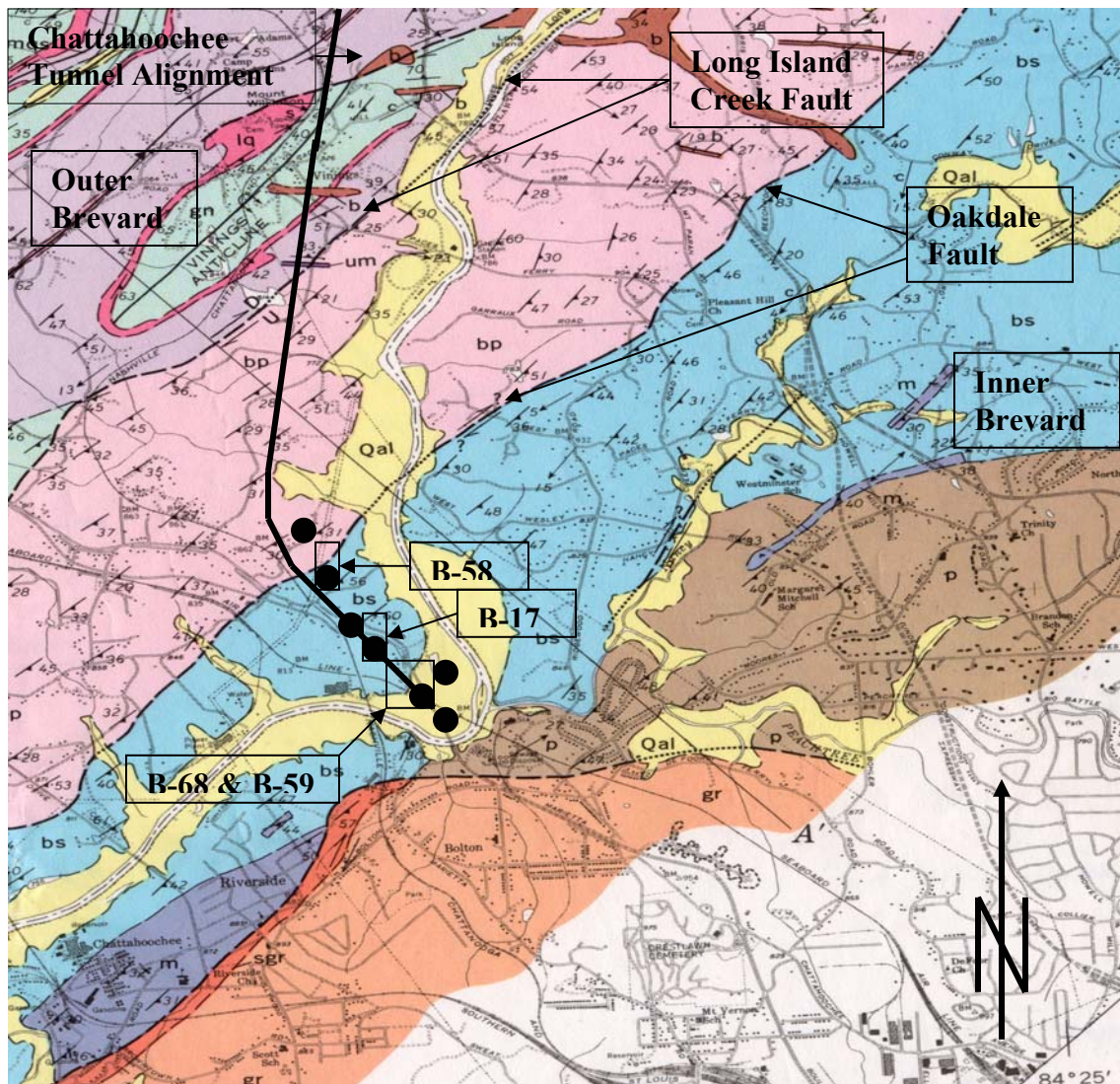


Figure 4.0. Map with locations of boreholes. Boxes around location circles indicate which boreholes (B-58, B-17, B-68, and B-59) were sampled for microprobe analysis. After Higgins (1966). Scale and symbols as in Figure 1.2.



All garnets are almandine rich (70-80 mol %) with minor pyrope and grossular components (Table 4.1). Both garnet types exhibit zoning with respect to MnO, MgO, and FeO (Table 4.1). Large garnet porphyroblasts have relatively high MnO values (3-5 wt % MnO) in their cores compared to the rims (0.6 – 1.0 wt % MnO). Smaller, unfractured garnet grains have MnO values of approximately 0.94 wt % MnO within their cores and rim values ranging from 0.22 to 0.55 wt % MnO (Figure 4.1). Larger garnet porphyroblasts have relatively low MgO values (1.5 wt % MgO) in their cores compared to the rims (2.5 wt % MgO) (Figure 4.2). Smaller, unfractured garnet grains have MgO values of approximately 2.3-2.4 wt % MgO within their cores and rim values ranging from 2.8 -3.0 wt % MgO. FeO also appears zoned within both morphological types of garnet. Larger garnet grains contain 31.0-32.0 wt % FeO in their cores compared to rim values of 35.0-37.0 wt % FeO. Smaller, unfractured garnet grains contain 30.0-32.0 wt % FeO within their cores and rim values ranging from 35.0-36.0 wt % FeO (Figure 4.3).

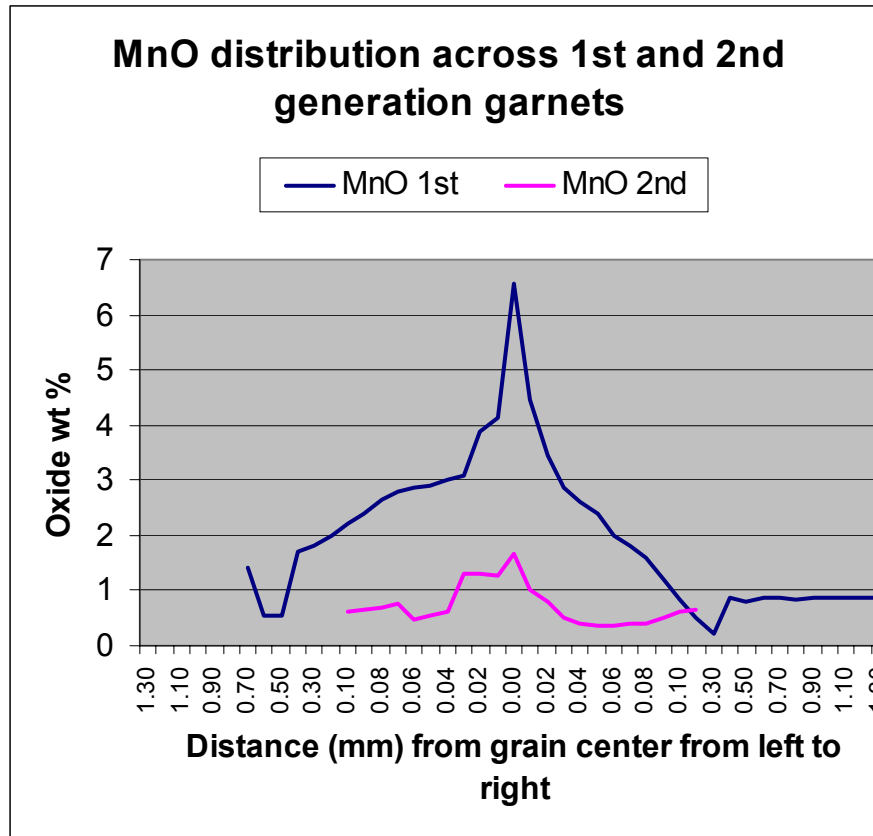


Figure 4.1. Graph plots MnO oxide wt % values against distance for 1<sup>st</sup> and 2<sup>nd</sup> generation garnet grain centers.

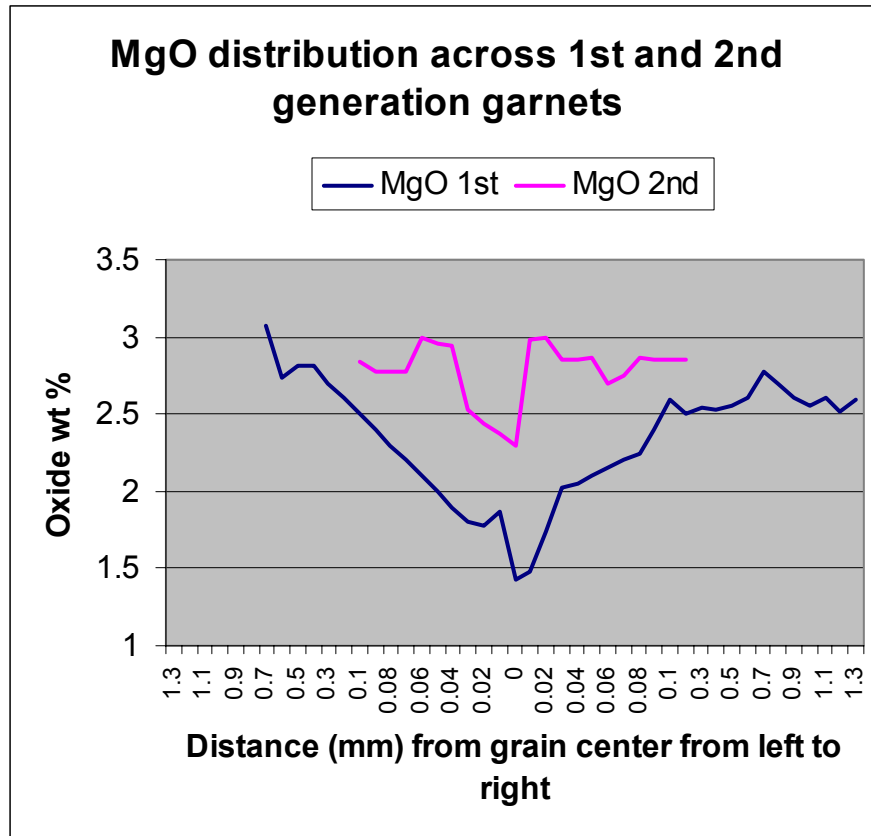


Figure 4.2. Graph plots MgO oxide wt % values against distance for 1<sup>st</sup> and 2<sup>nd</sup> generation garnet grain centers.

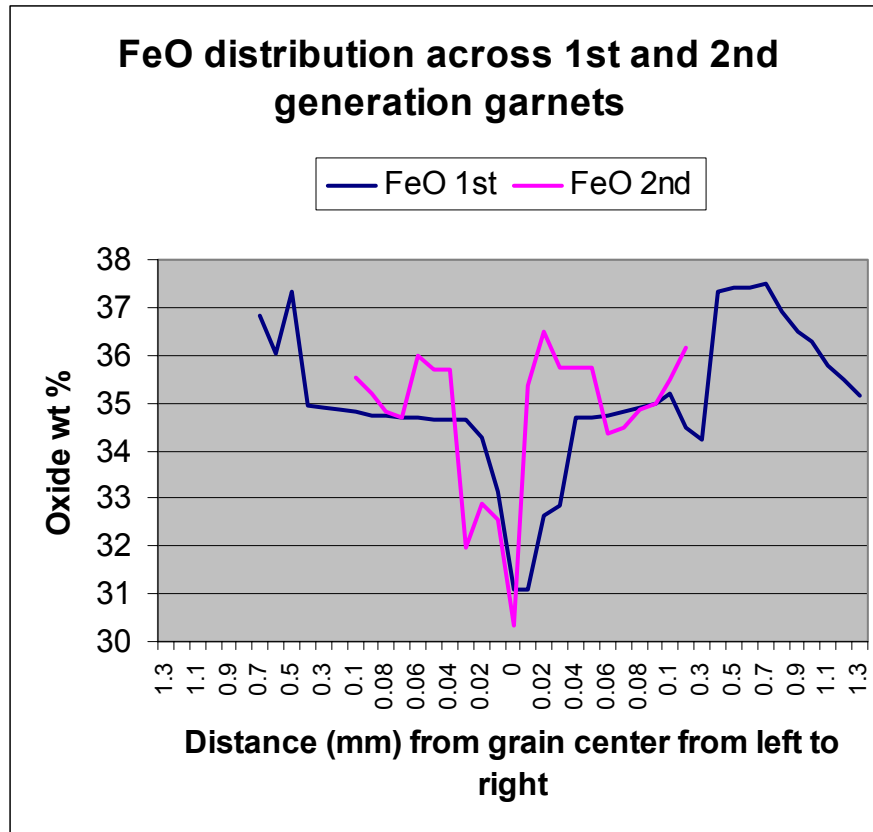


Figure 4.3. Graph plots FeO oxide wt % values against distance for 1<sup>st</sup> and 2<sup>nd</sup> generation garnet grain centers.

**Biotite** typically shows little or no variation compositionally and is compositionally intermediate between annite and phlogopite (Figure 4.4). Analyses revealed no chemical distinctions between biotite grains occurring as inclusions in either staurolite or garnet versus grains defining foliation.

**Staurolite** occurs as euhedral to subhedral porphyroblasts that commonly contain numerous inclusions. Staurolite grains were also analyzed in traverses to record any chemical variations. Core and rim values for  $\text{SiO}_2$ ,  $\text{FeO}$ , and  $\text{Al}_2\text{O}_3$ , were all comparable (Table 4.3). Hence, porphyroblasts are compositionally homogeneous with no apparent zoning.

**Muscovite** defines foliation and commonly wraps around garnet and staurolite porphyroblasts. The formula  $\text{K}_2\text{Al}_4[\text{Si}_6\text{Al}_2\text{O}_{20}](\text{OH}, \text{F})_4$  was used to determine site occupancies (Deere, Howie, and Zussman 1992). Muscovite analyses show little chemical variability except for  $\text{K}_2\text{O}$ , which ranged from 4.05 to 8.91 oxide weight % (Table 4.4).



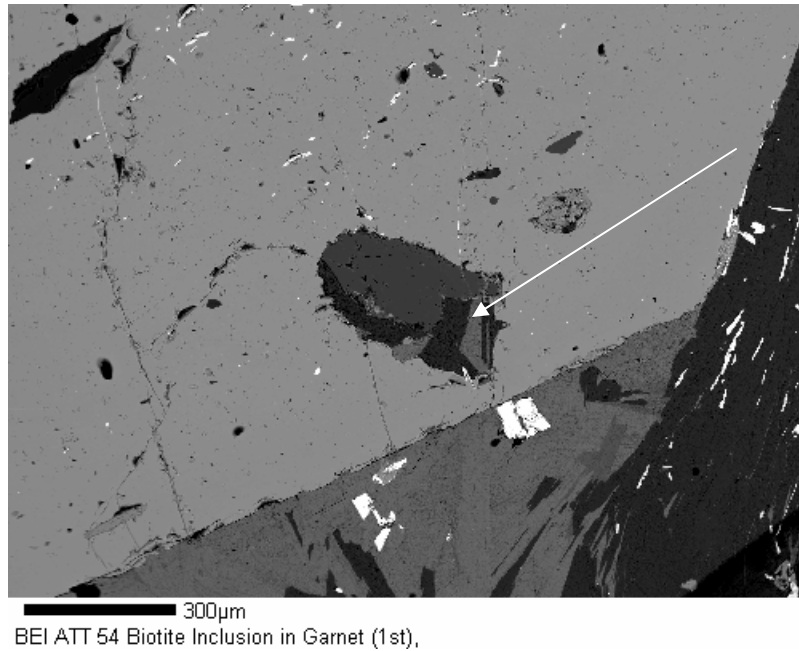


Figure 4.4. Backscattered electron image of garnet porphyroblast with biotite occurring as an inclusion towards the edge of the crystal. Arrow indicates biotite inclusion. From sample ATT-54; borehole B-58; 47.5 m bgs.

### **Psuedotachylyte Groundmass Composition**

The groundmass of the psuedotachylyte was analyzed with a broad electron beam and displays a composition rich in  $\text{SiO}_2$ ,  $\text{Al}_2\text{O}_3$ , and  $\text{K}_2\text{O}$ , and in one case,  $\text{FeO}$  and  $\text{MgO}$  (Table 4.5). Both analyzed points had minor amounts of  $\text{TiO}_2$ ,  $\text{CaO}$ , and  $\text{Na}_2\text{O}$ . One point had relatively high  $\text{BaO}$ . One of the analyses reflects a composition very close to that of microcline. The elevated values of Si, Al, and K within the psuedotachylyte may reflect the preferential melting of a potassium-rich mineral or minerals such as alkali feldspar or mica as a result of frictional sliding during a brittle deformation event (Passchier and Trouw 1996).

Table 4.0

Plagioclase compositions (wt%) from crystalline cores, Chattahoochee Tunnel Project

Sample	ATT-10	ATT-10	ATT-10	ATT-10	ATT-10	ATT-10	ATT-22	ATT-22	ATT-54	ATT-54
Depth *	56.3	56.3	56.3	56.3	56.3	56.3	39.4	39.4	47.5	47.5
Footnote				a	b					
N (avg)	3	4	4	2	3	7	2	5	1	1
SiO <sub>2</sub>	62.73	63.6	63.27	63.34	63.61	63.50	64.24	63.55	62.50	62.58
TiO <sub>2</sub>	BDL	BDL	BDL	BDL	BDL	BDL	BDL	BDL	BDL	BDL
Al <sub>2</sub> O <sub>3</sub>	23.88	23.61	23.63	23.33	23.01	23.49	23.25	23.42	24.95	24.59
MgO	BDL	BDL	BDL	BDL	BDL	BDL	BDL	BDL	BDL	BDL
FeO	BDL	BDL	0.24	BDL	BDL	BDL	BDL	BDL	0.19	0.23
MnO	BDL	BDL	BDL	BDL	BDL	BDL	BDL	BDL	BDL	BDL
CaO	4.99	4.67	3.91	4.81	4.36	4.71	4.89	4.80	5.96	6.10
K <sub>2</sub> O	0.21	0.18	0.71	0.16	0.17	0.31	0.08	0.14	0.08	0.09
Na <sub>2</sub> O	8.74	8.51	8.36	8.67	8.95	8.58	8.98	8.56	7.84	7.89
BaO	BDL	BDL	BDL	BDL	BDL	BDL	BDL	BDL	BDL	BDL
Total	100.65	100.69	100.27	100.48	100.17	100.77	101.58	100.55	101.62	101.55
cations normalized to 32 oxygens										
Si	11.05	11.16	11.16	11.15	11.22	11.15	11.19	11.17	10.91	10.94
Ti	0.00	0.00	0.00	0.00	0.00	0.00	0.00	0.00	0.00	0.00
Al	4.96	4.88	4.91	4.84	4.78	4.86	4.77	4.85	5.13	5.06
Mg	0.00	0.00	0.00	0.00	0.00	0.00	0.00	0.00	0.00	0.00
Fe	0.00	0.00	0.04	0.00	0.00	0.00	0.00	0.00	0.03	0.03
Mn	0.00	0.00	0.00	0.00	0.00	0.00	0.00	0.00	0.00	0.00
Ca	0.94	0.88	0.74	0.91	0.82	0.89	0.91	0.90	1.11	1.14
K	0.05	0.04	0.16	0.04	0.04	0.07	0.02	0.03	0.02	0.02
Na	2.98	2.89	2.86	2.96	3.06	2.92	3.03	2.92	2.65	2.67
Ba	0.00	0.00	0.00	0.00	0.00	0.00	0.00	0.00	0.00	0.00
sum cat	19.99	19.87	19.89	19.92	19.93	19.91	19.95	19.88	19.86	19.88
Ternary endmembers (molar)										
An	0.24	0.23	0.20	0.23	0.21	0.23	0.23	0.23	0.29	0.30
Ab	0.75	0.76	0.76	0.76	0.78	0.75	0.77	0.76	0.70	0.70
Or	0.01	0.01	0.04	0.01	0.01	0.02	0.00	0.01	0.00	0.00

## Footnotes

BDL= Below Detection Level

\* = Depth reported in m below ground surface

a= analysis from plagioclase grain core

b= analysis from plagioclase grain rim

Table 4.1  
Garnet Compositions (wt%) in Crystalline Cores, Chattahoochee Tunnel Project

Sample	ATT-54	ATT-54	ATT-54	ATT-22	ATT-22	ATT-22	ATT-37	ATT-37	ATT-37	ATT-37	ATT-37	ATT-37	ATT-37	ATT-37
Depth *	47.5	47.5	47.5	39.4	39.4	39.4	15.2	15.2	15.2	15.2	15.2	15.2	15.2	15.2
Footnote	a	b	c	a	c	b	a	a	B	a <sup>1</sup>	b <sup>1</sup>	b <sup>1</sup>	c <sup>1</sup>	c <sup>1</sup>
N (avg)	3	3	3	3	2	4	2	2	4	4	6	4	2	2
SiO <sub>2</sub>	36.55	36.76	36.39	36.13	36.23	36.37	36.02	35.87	36.28	36.72	36.81	36.64	36.86	36.93
TiO <sub>2</sub>	0.10	0.02	0.07	0.08	0.04	0.01	0.08	0.05	0.03	0.05	0.04	0.01	0.04	0.02
Al <sub>2</sub> O <sub>3</sub>	21.49	21.68	21.40	21.46	21.33	21.63	21.55	21.46	21.77	21.79	21.73	21.55	21.72	21.41
MgO	1.86	2.95	2.19	1.69	1.94	2.80	2.16	1.61	2.71	2.72	2.60	2.77	2.78	2.73
FeO	33.55	35.82	34.04	32.85	33.32	37.22	34.61	31.87	36.20	34.54	34.53	35.38	35.30	34.75
CaO	3.75	2.09	3.42	2.99	2.78	1.48	2.26	3.06	2.79	3.76	3.98	3.26	2.89	3.61
MnO	3.16	1.05	2.36	4.85	4.14	0.66	2.98	5.50	0.60	0.94	0.22	0.59	0.40	0.39
Cr <sub>2</sub> O <sub>3</sub>	BDL	0.01	0.02	0.03	BDL	0.01	0.03	0.01	0.01	0.01	0.02	0.02	0.08	0.02
Total	100.45	100.38	99.88	100.08	99.78	100.18	99.68	99.43	100.39	100.24	99.92	100.22	100.06	99.85
	Garnet endmembers (molar proportions)													
Uvar	0.00	0.00	0.00	0.00	0.00	0.00	0.00	0.00	0.00	0.00	0.00	0.00	0.01	0.00
Pyr	0.07	0.12	0.09	0.07	0.08	0.11	0.09	0.06	0.11	0.11	0.10	0.11	0.11	0.11
Spes	0.07	0.02	0.05	0.11	0.09	0.01	0.07	0.13	0.01	0.02	0.01	0.01	0.01	0.01
Gros	0.11	0.06	0.10	0.09	0.08	0.04	0.07	0.09	0.08	0.10	0.11	0.09	0.08	0.10
Alm	0.75	0.80	0.76	0.74	0.75	0.83	0.78	0.72	0.80	0.77	0.77	0.78	0.79	0.78

Footnotes

BDL= Below Detection Level

\* = Depth reported in m below ground surface

a=1st generation garnet core

b=1st generation garnet rim

c=1st generation garnet intermediate area

a<sup>1</sup>=2<sup>nd</sup> generation garnet core

b<sup>1</sup>=2<sup>nd</sup> generation garnet rim

c<sup>1</sup>=2<sup>nd</sup> generation garnet intermediate area

Table 4.2

## Biotite Compositions (wt%) in Crystalline Cores, Chattahoochee Tunnel Project

Sample	ATT-22	ATT-22	ATT-54	ATT-54	ATT-54	ATT-54	ATT-54	ATT-54	ATT37	ATT37
Depth *	39.44	39.44	47.55	47.55	47.55	47.55	47.55	47.55	15.24	15.24
Footnote	a	a	b	b	b	c <sup>1</sup>	c <sup>2</sup>	d	b	a
N (avg)	1	2	2	3	3	2	1	1	1	1
SiO <sub>2</sub>	34.66	33.93	35.95	35.29	35.02	34.72	34.68	35.87	47.68	35.60
TiO <sub>2</sub>	1.44	1.23	1.78	3.18	1.53	1.37	1.25	1.69	0.35	1.39
Al <sub>2</sub> O <sub>3</sub>	19.01	18.96	19.97	19.16	18.94	19.43	19.12	20.41	37.31	18.69
MgO	9.72	9.83	10.96	10.42	9.86	9.59	9.44	11.22	0.71	10.99
FeO	23.48	21.59	17.76	18.29	20.22	19.89	20.49	19.02	1.27	17.59
CaO	0.04	0.05	0.02	0.06	0.10	0.15	0.21	0.11	BDL	0.06
MnO	0.03	BDL	0.03	0.02	0.06	0.04	0.06	BDL	0.04	BDL
K <sub>2</sub> O	6.46	7.26	8.21	8.18	8.16	8.29	7.32	6.22	8.90	6.57
Na <sub>2</sub> O	0.28	0.27	0.29	0.29	0.23	0.19	0.17	0.24	1.23	0.37
F	0.41	0.49	0.35	0.33	0.34	0.34	0.28	0.34	BDL	0.34
Cl	0.02	0.10	0.02	0.01	0.01	0.01	0.01	0.01	0.02	0.32
Total	95.19	93.22	95.01	94.96	94.18	93.71	92.80	94.84	97.51	91.50
Mg #	0.42	0.45	0.52	0.50	0.47	0.46	0.45	0.51	0.50	0.53

## Footnotes

BDL= Below Detection Level

\*= depth reported in m below ground surface

a= fabric analysis

b= analysis within garnet embayment

c<sup>1</sup>= inclusion analysis within garnet (rim of biotite)c<sup>2</sup>= inclusion analysis within garnet (core of biotite)

d= inclusion analysis within staurolite



Table 4.3  
Staurolite Compositions (wt%) in Crystalline Cores, Chattahoochee Tunnel Project

Sample	ATT-22	ATT-22	ATT-22	ATT-22	ATT-22	ATT-22	ATT-22	ATT-22	ATT-22	ATT-22
Depth *	39.4	39.4	39.4	39.4	39.4	39.4	39.4	39.4	39.4	39.4
Footnote	b	a	a	b	b	A	b	b	a	b
SiO <sub>2</sub>	27.39	27.67	27.67	27.78	28.41	27.67	27.98	27.40	27.82	27.61
TiO <sub>2</sub>	0.61	0.41	0.56	0.43	0.52	0.64	0.44	0.47	0.46	0.48
Al <sub>2</sub> O <sub>3</sub>	53.76	53.85	52.96	54.06	53.57	53.37	53.38	53.93	53.65	52.75
MgO	1.35	1.43	1.38	1.36	1.54	1.39	1.42	1.38	1.53	1.38
FeO	12.05	12.64	12.74	12.61	13.27	12.27	12.99	12.80	12.52	12.42
CaO	BDL	BDL	BDL	BDL	BDL	BDL	BDL	BDL	BDL	BDL
MnO	BDL	BDL	BDL	BDL	BDL	BDL	BDL	BDL	BDL	BDL
K <sub>2</sub> O	BDL	BDL	BDL	BDL	BDL	0.03	BDL	BDL	BDL	BDL
Na <sub>2</sub> O	BDL	BDL	BDL	BDL	BDL	BDL	BDL	BDL	BDL	BDL
Total	95.20	96.07	95.35	96.33	97.33	95.41	96.23	95.97	95.99	94.72
cations normalized to 48 oxygens										
Si	8.07	8.10	8.17	8.11	8.23	8.15	8.19	8.04	8.15	8.20
Ti	0.13	0.09	0.13	0.10	0.11	0.14	0.10	0.10	0.10	0.11
Al	18.67	18.58	18.43	18.60	18.29	18.52	18.41	18.65	18.51	18.45
Mg	0.59	0.62	0.61	0.59	0.66	0.61	0.62	0.60	0.67	0.61
Fe	2.97	3.10	3.15	3.08	3.21	3.02	3.18	3.14	3.07	3.08
Ca	0.00	0.00	0.00	0.00	0.00	0.00	0.00	0.00	0.00	0.00
Mn	0.00	0.00	0.00	0.00	0.00	0.00	0.00	0.00	0.00	0.00
K	0.00	0.00	0.00	0.00	0.00	0.01	0.00	0.00	0.00	0.00
Na	0.00	0.00	0.00	0.00	0.00	0.00	0.00	0.00	0.00	0.00
sum cat	30.46	30.51	30.50	30.50	30.51	30.46	30.51	30.53	30.50	30.47

Footnotes

BDL= Below Detection Level

\*= depth reported in m below ground surface

a= analysis from staurolite grain core

b= analysis from staurolite grain rim

**Table 4.4**  
**Muscovite Compositions (wt%) in Crystalline Cores, Chattahoochee Tunnel**  
**Project**

Sample	ATT-22	ATT-54	ATT-54	ATT-54	ATT-37	ATT-37
Depth *	39.4	47.5	47.5	47.5	15.2	15.2
Footnote	a	a	A	a	a	a
SiO <sub>2</sub>	47.17	47.05	47.15	45.89	47.07	46.58
TiO <sub>2</sub>	0.29	0.62	0.42	0.43	0.39	0.31
Al <sub>2</sub> O <sub>3</sub>	37.71	35.62	35.5	35.58	37.82	37.75
MgO	0.77	0.7	0.73	0.59	0.48	0.61
FeO	1.13	2.94	2.73	2.3	0.96	0.96
CaO	0.05	BDL	0.04	BDL	BDL	0.04
MnO	BDL	BDL	BDL	BDL	BDL	BDL
K <sub>2</sub> O	8.09	8.91	8.33	7.84	8.01	8.07
Na <sub>2</sub> O	1.35	1.06	1.07	1.22	1.49	1.63
F	0.08	BDL	BDL	BDL	BDL	BDL
Cl	BDL	0.03	BDL	BDL	BDL	BDL
Total	96.65	96.94	96.05	93.88	96.26	95.96
cations normalized to 22 oxygens						
Si	6.09	6.15	6.19	6.14	6.1	6.07
Ti	0.03	0.06	0.04	0.04	0.04	0.03
Al	5.74	5.49	5.49	5.61	5.78	5.8
Mg	0.15	0.14	0.14	0.12	0.09	0.12
Fe	0.12	0.32	0.3	0.26	0.1	0.1
Ca	0.01	0	0.01	0	0	0.01
Mn	0.01	0	0.01	0	0	0
K	1.33	1.49	1.4	1.34	1.32	1.34
Na	0.34	0.27	0.27	0.32	0.37	0.41
F	0.02	0	0	0	0	0
Cl	0	0	0	0	0	0
sum cat	13.84	13.92	13.85	13.83	13.82	13.88
Mg #	0.549	0.298	0.322	0.313	0.47	0.531

**Footnotes**

BDL= below Detection Level

\*= depths are reported in m below ground surface

a= analysis from fabric

**Table 4.5**  
**Pseudotachylyte groundmass compositions (wt%) from crystalline cores, Chattahoochee Tunnel Project**

<b>Sample</b>	<b>ATT-10</b>	<b>ATT-10</b>
<b>Depth *</b>	<b>56.3</b>	<b>56.3</b>
<b>Footnote</b>	<b>d</b>	<b>d</b>
<b>N</b>	<b>1</b>	<b>1</b>
<b>SiO<sub>2</sub></b>	<b>63.87</b>	<b>60.92</b>
<b>TiO<sub>2</sub></b>	<b>0.83</b>	<b>0.61</b>
<b>Al<sub>2</sub>O<sub>3</sub></b>	<b>18.49</b>	<b>21.62</b>
<b>MgO</b>	<b>0.09</b>	<b>3.55</b>
<b>FeO</b>	<b>0.19</b>	<b>6.16</b>
<b>MnO</b>	<b>BDL</b>	<b>0.09</b>
<b>CaO</b>	<b>0.40</b>	<b>0.23</b>
<b>K<sub>2</sub>O</b>	<b>15.12</b>	<b>7.19</b>
<b>Na<sub>2</sub>O</b>	<b>0.16</b>	<b>0.10</b>
<b>BaO</b>	<b>0.34</b>	<b>0.04</b>
<b>Total</b>	<b>99.50</b>	<b>100.51</b>

**Footnotes**

**BDL= Below Detection Level**

**\* = Depth reported in m below ground surface**

## **METAMORPHISM AND DEFORMATION**

The rocks within the Brevard Fault Zone outside Atlanta, Ga., have experienced polyphase deformation and possible polyphase metamorphism suggested by petrographic, microtectonic, and mineralogic analyses. Due to un-oriented samples and the complexity of quartz mica schists and mica schists present; shear sense, types of displacement, or orientation of microstructures are not covered. However, the number of deformational events, both ductile and brittle, and style and grade of metamorphic events are discussed. Microtectonic analyses include an assessment of vein quartz recrystallization, an estimate of the temperature of intracrystalline deformation, an assessment of garnet morphologies, and chronologic placement of deformational and metamorphic events. Mineralogic analyses include an assessment of the significance of compositional differences between garnets with distinct morphologies and the groundmass composition of the psuedotachylyte.

### **Metamorphism**

The Brevard Fault Zone has experienced Barrovian style, middle amphibolite grade metamorphism ( $M_1$ ) as indicated by the relict assemblage of garnet-staurolite (Miyashiro, 1994; Blatt and Tracy, 1999).

Garnets associated with  $M_1$  are large (1.5 mm) subhedral porphyroblasts that contain numerous fractures and commonly exhibit sinusoidal inclusion trails of quartz and ilmenite suggesting grain rotation (Figure 5.1). Fracture and inclusion densities are

greatest within the cores of the porphyroblasts, while the rims contain significantly fewer of each. Staurolite occurs as medium sized (0.5-1.0 mm) porphyroblasts and also contains numerous quartz and ilmenite inclusion trails suggesting grain rotation.  $M_1$  garnet and staurolite are commonly embayed and display irregular grain boundaries. Minerals that appear in contact with  $M_1$  garnet or staurolite do not appear to be in equilibrium and exhibit features such as moth-eaten textures at grain contacts.

A second distinct metamorphic event,  $M_2$ , affected the BFZ following  $M_1$ .  $M_2$  is characterized by a peak assemblage of muscovite- biotite-garnet as is typical of Barrovian style, lower amphibolite grade. Garnets appear as small (0.2-0.4 mm) porphyroblasts that contain no inclusions or fractures (Figure 5.1). The long axes of  $M_2$  muscovite and biotite define the foliation.  $M_2$  garnet, biotite, and muscovite are in direct contact with no reaction textures and  $M_2$  garnets display clean grain boundaries and biotite crystals terminate at crystal faces of  $M_2$  garnets. Unlike the textures in  $M_1$  garnet and staurolite, these  $M_2$  textures suggest that this is the equilibrium metamorphic assemblage.

A third and final metamorphic event,  $M_3$ , affected the rocks of the Brevard fault zone. This event is a fluid enhanced metasomatic event. The minerals chlorite, calcite, and epidote characterize this episode. Chlorite and calcite appear within brittle fractures that cross-cut ductile deformation fabrics which contain the  $M_2$  mineral assemblage. Epidote occurs as small grains throughout the samples and cross-cut the fabric defined by the  $M_2$  minerals. The cross-cutting nature of these  $M_3$  minerals suggest that  $M_3$  occurred after a substantial amount of time had passed after  $M_2$  and that  $M_3$  is a distinct event and did not occur during the waning stages of  $M_2$ . Furthermore, the appearance of



epidote and calcite suggests that a fluid modified the bulk composition of the schists; consequently  $M_3$  is a metasomatic event and not simply a retrograde metamorphic event.

Several criteria following Barker (1990), Spry (1969), and (Passchier and Trouw 1998) were used to discriminate between a single distinct, but protracted, metamorphic event and two distinct prograde metamorphic events.

Two distinct types of garnets occur and are assigned to  $M_1$  and  $M_2$  events.  $M_1$  garnets are large (2.5 mm) and contain sinusoidal inclusion fabrics that are absent from  $M_2$  garnets.  $M_2$  garnets are significantly smaller in size (0.2-0.4 mm) than  $M_1$  garnets (0.3-2.5 mm) (Figures 5.0 and 5.1).

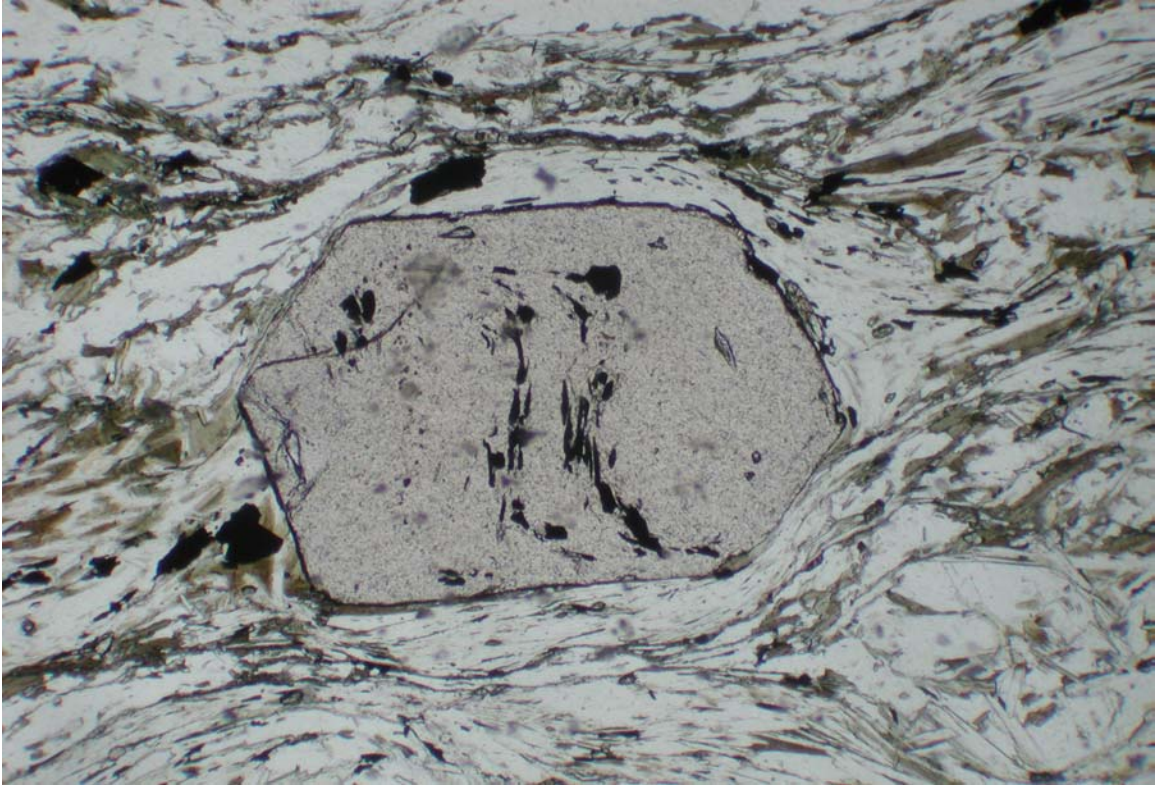


Figure 5.0.  $M_1$  garnet porphyroblast has  $M_2$  muscovite and  $M_2$  biotite wrapping around. Porphyroblast contains sinusoidal inclusion trails suggesting grain rotation. Uncrossed nicols. Field of view is 5.5 mm. Mica schist; sample ATT-25; borehole B-59; 53.3 m bgs.

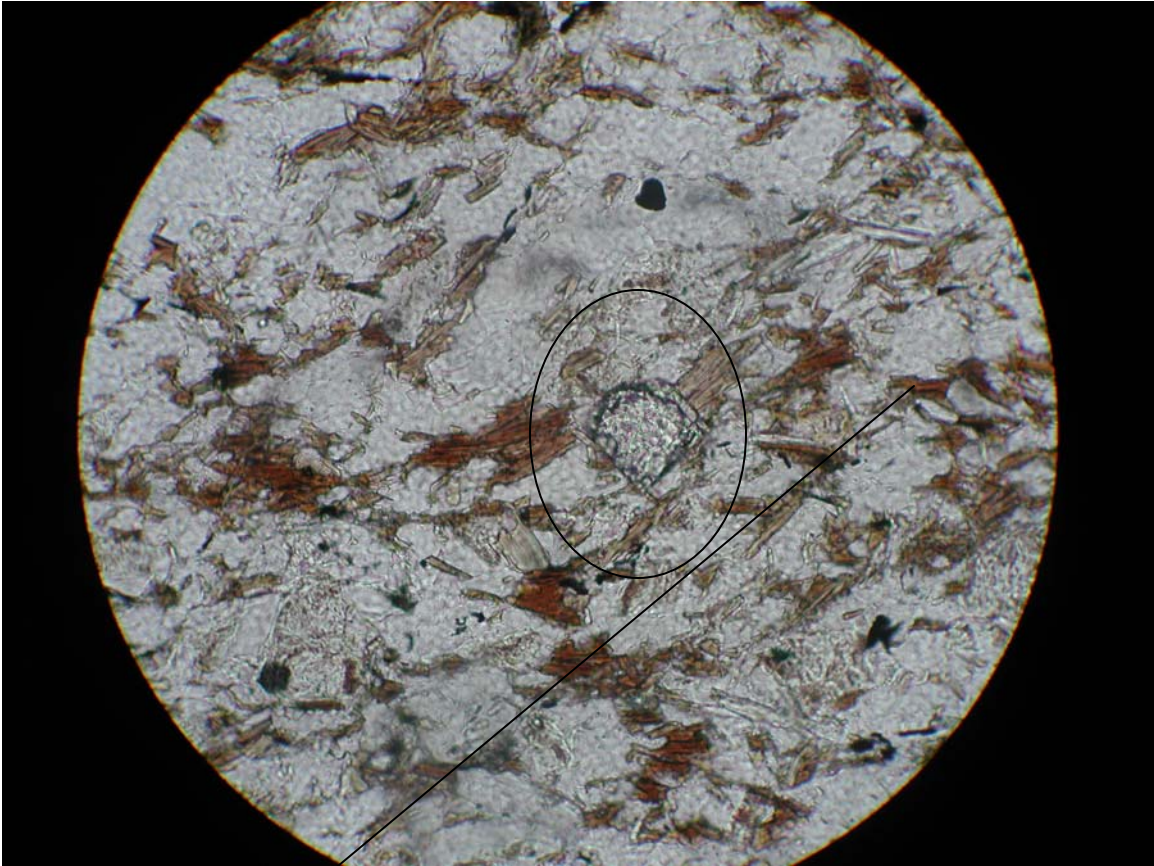


Figure 5.1. Circle is around  $M_2$  garnet porphyroblast that has  $M_2$  biotite terminating into the upper right crystal face. Line indicates  $S_2$  direction. Field of view is 1.0 mm. Schist; sample ATT-33; borehole B-69; 30.5 m bgs.

Barker (1990) noted the location of a cross-sectional cut of a garnet porphyroblast thin section can obscure or enhance the visibility of a sinusoidal inclusion pattern. For example, a center cut through a porphyroblast will result in a more pronounced S pattern of inclusions, whereas a rim cut of the same porphyroblast will result in a much less pronounced S pattern (Figure 5.2). Consequently, Barker suggested that less emphasis should be placed on smaller porphyroblasts in a thin section relative to the larger ones. In my samples, there are distinct differences between typical, small  $M_1$  garnets and small  $M_2$  garnets. Small, rim cut  $M_1$  garnets still display features such as irregular grain boundaries and inclusion trails which are characteristic of larger,  $M_1$  garnets, but these features are not as pronounced as Barker suggests and are absent in  $M_2$  garnets.

A second point to keep in mind is that during metamorphism and subsequent mineral growth, not all porphyroblasts nucleate at the same time, and those that nucleate later will be smaller. Therefore, these later porphyroblasts will preserve a fabric history (as shown by inclusions) which is representative of only the later parts of the tectono-metamorphic history (Barker 1990).

Barker's descriptions of observed S patterns are most important when attempting to ascertain the degree of garnet rotation, but do not allow identification of a distinct 2<sup>nd</sup> generation of garnet. However, if multiple garnet growth phases are present, the center of the early porphyroblasts will have a rotational fabric within the core which is absent near the rims. Rim cuts yield no rotational fabric with foliation slightly wrapping around at the crystal face. Garnets that formed during a second period of crystallization would lack an inclusional fabric present in earlier formed porphyroblasts. In my samples, garnets that I have identified as  $M_2$  garnets contain no inclusional fabrics, inclusions, or

fractures. The lack of these features is therefore consistent with multiple growth phases for garnet outlined by Barker (1990) (Figures 5.3 and 5.4)

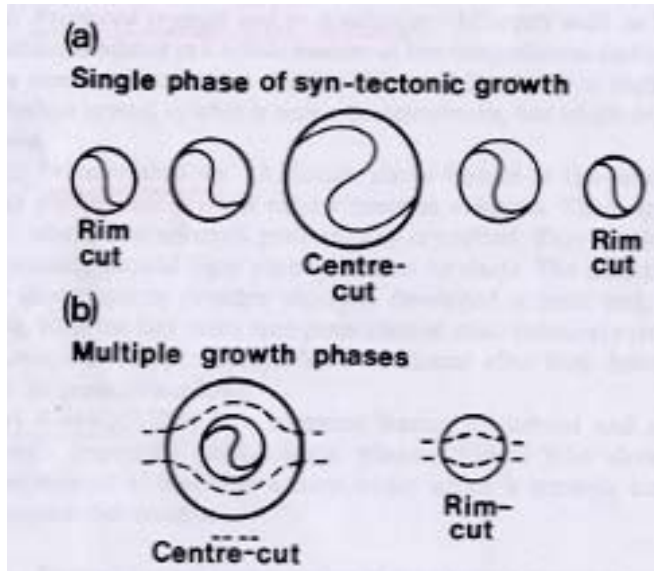


Figure 5.2. Drawing depicts differences between center and rim cuts of garnet porphyroblasts. Differences are in intensity of fabric rotation within porphyroblasts. From Barker 1990.



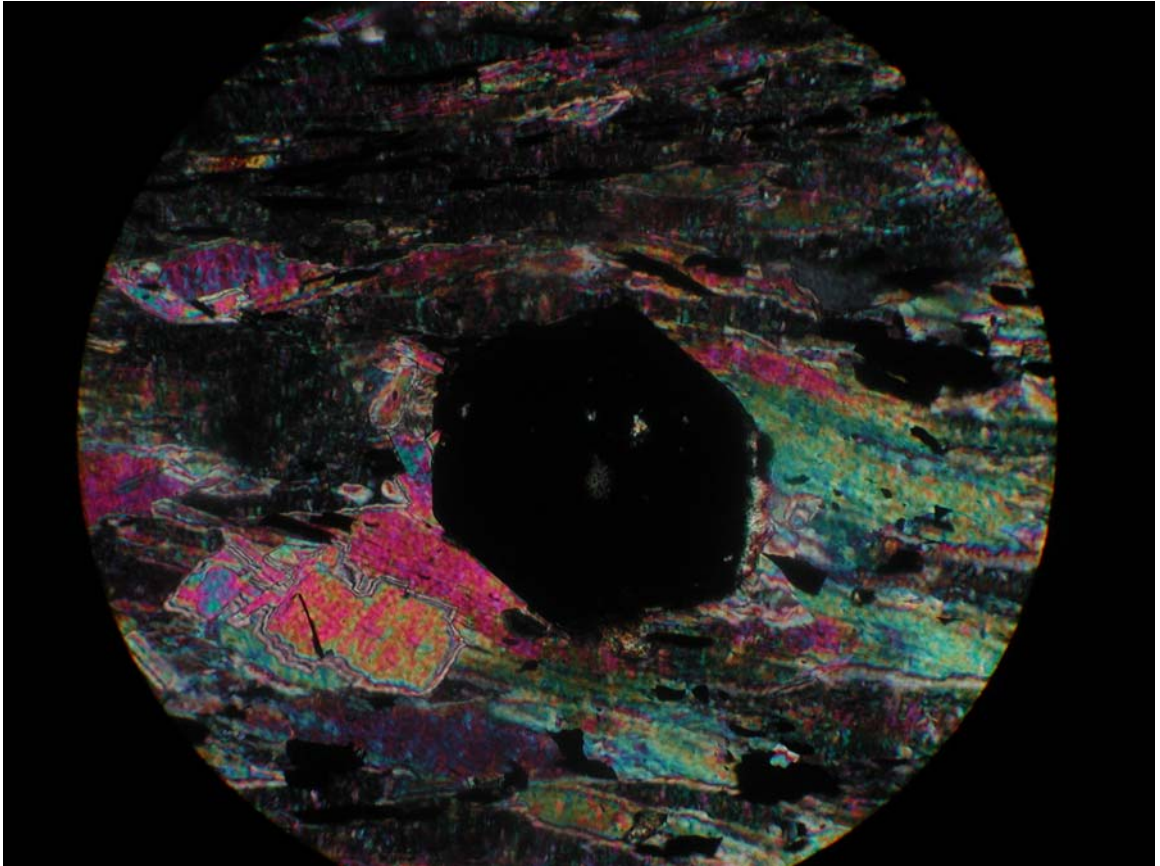


Figure 5.3.  $M_2$  garnet porphyroblast containing no inclusion fabric or fractures. Muscovite terminates into the crystal face. Crossed nicols. Field of view is 1.0 mm. Mica schist; sample ATT-48; borehole B-37; 45.7 m bgs.

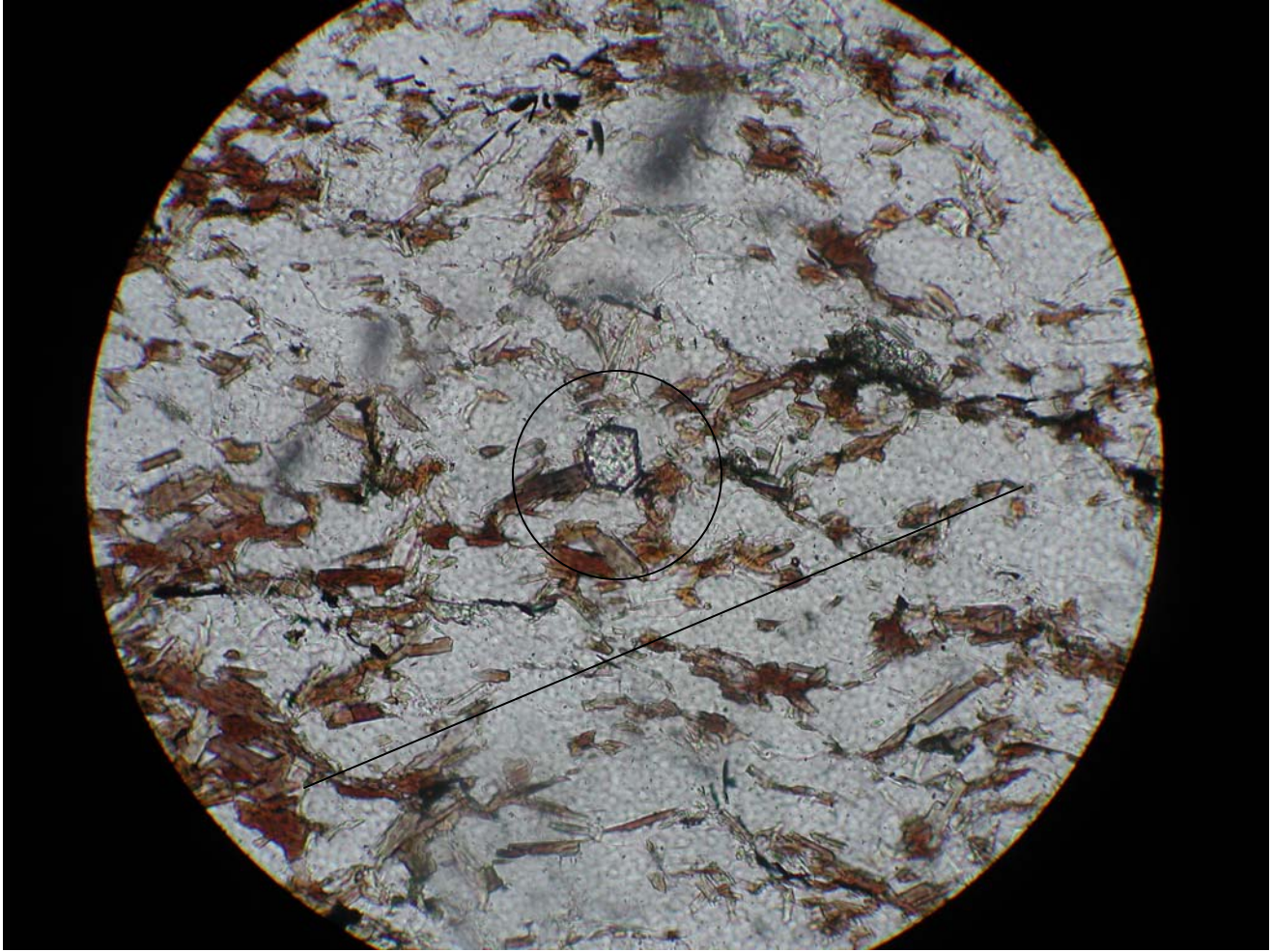


Figure 5.4. Circle is around M<sub>2</sub> garnet that has M<sub>2</sub> biotite terminating into the left-hand side crystal face. Line indicates S<sub>2</sub> direction. Uncrossed nicols. Field of view is 1.0 mm. Quartz mica schist; sample ATT-29; borehole B-69; 25 m bgs.

Garnet compositional zoning also bears on the distinction between  $M_1$  and  $M_2$  garnets. Within  $M_1$  garnets, porphyroblast cores have 3-5 wt % MnO while rims have 0.6 – 1.0 wt % MnO. Within  $M_2$  garnets, values of approximately 0.9-1.0 wt % MnO occur in the porphyroblast core while rim values range from 0.2 to 0.6 wt % MnO (Table 4.1). In addition,  $M_1$  garnet cores have 1.5 wt % MgO while rims have 2.5 wt % MgO. Within  $M_2$  garnets, porphyroblast cores have 2.3 to 2.4 wt % MgO while rim values range from 2.8 to 3.0 wt % MgO (Table 4.1). Hence, both MnO and MgO concentrations in the rims of the  $M_1$  garnets and the cores of the  $M_2$  garnets overlap.  $M_1$  garnet inclusion and fracture densities are greatest within the cores while the rims contain fewer of inclusions and fractures. It is possible that only the cores of  $M_1$  garnets formed during the  $M_1$  event and that the rims of  $M_1$  garnets crystallized coevally with  $M_2$  garnets. According to Barker, it is common for porphyroblast cores to be rich in inclusions and the rims to be largely devoid of inclusions. Such textural relations can be explained in terms of rapid growth causing numerous inclusions followed by a slower growth rate and therefore fewer included crystals (Barker 1990). However, in my samples evidence supports two distinct periods of garnet crystallization. For example,  $M_1$  garnet and staurolite are commonly embayed and display irregular grain boundaries. Minerals that appear in contact do not appear to be in equilibrium with  $M_1$  garnet or staurolite.  $M_2$  garnet, biotite, and muscovite are in direct contact with no reaction textures.  $M_2$  garnets display clean grain boundaries and biotite crystals terminate at crystal faces of  $M_2$  garnets (Figures 5.5 and 5.6).

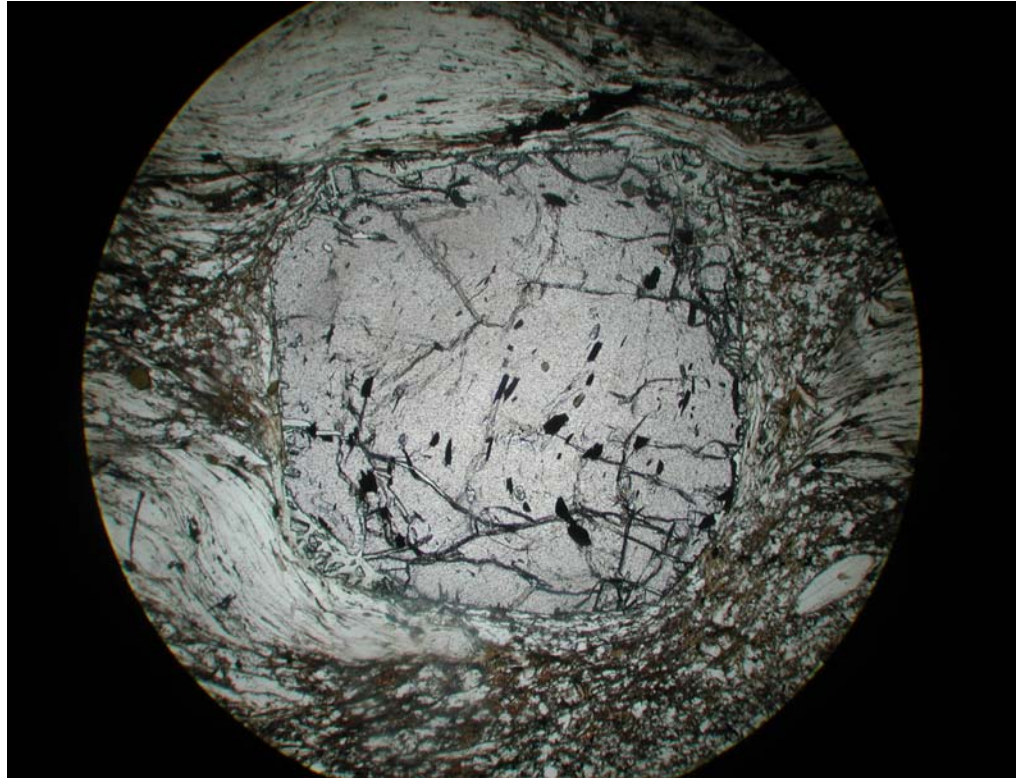


Figure 5.5.  $M_1$  garnet porphyroblast with irregular grain boundaries and sinusoidal inclusional fabric with muscovite and biotite wrapping around grain. Uncrossed nicols. Field of view is 5.5 mm. Mica schist; sample ATT-19; borehole B-68; 53.4 m bgs.



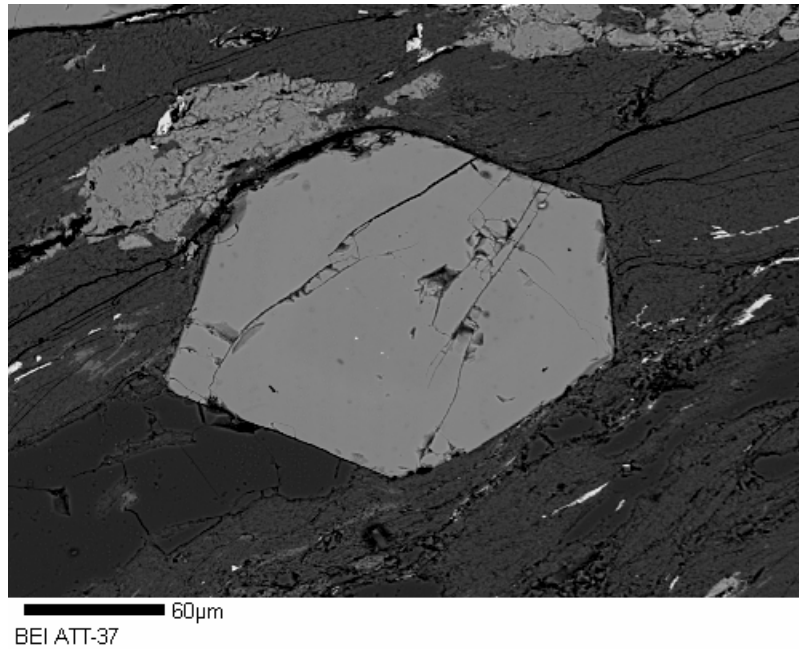


Figure 5.6. Back-scattered electron image of a  $M_2$  garnet porphyroblast with muscovite (dark phase on right and upper left hand sides of garnet) terminating at the crystal face. Mica schist; sample ATT-37; borehole B-17; 15.2 m bgs.

Spry (1969) described recrystallization of muscovite in terms of syn-tectonic crystallization and post-tectonic growth. Evidence for syntectonic crystallization will tend to be destroyed by post-tectonic growth because early-formed crystals with high lattice energy due to lattice strain tend to be replaced by lower energy, unstrained crystals. In Spry's model, mica formed continuously and the early-formed crystals were bent, whereas crystals forming relatively late were less affected by the folding. In the BFZ rocks, this appears commonly (Figure 5.9 and Figure 5.10). Muscovite recrystallized in response to intracrystalline strain into unstrained grains that are oriented parallel to later stress orientations.



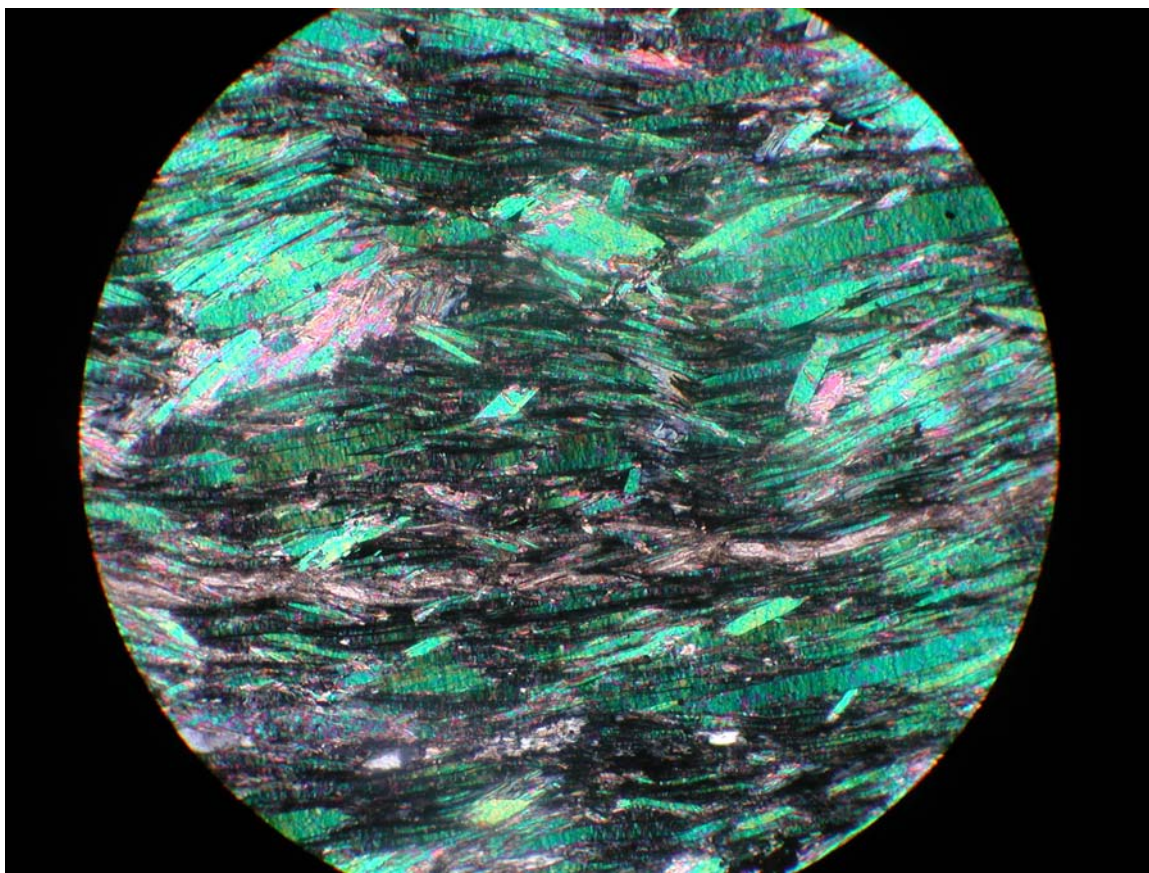


Figure 5.9.  $M_2$  muscovite has recrystallized in a different orientation cross-cutting the fabric (line) defined by strained  $M_2$  muscovite. Line with arrow is aligned parallel to long axes of recrystallized  $M_2$  muscovite. Crossed nicols. Field of view is 2.0 mm. Mica schist; sample ATT-36; borehole B-70; 30.5 m bgs.

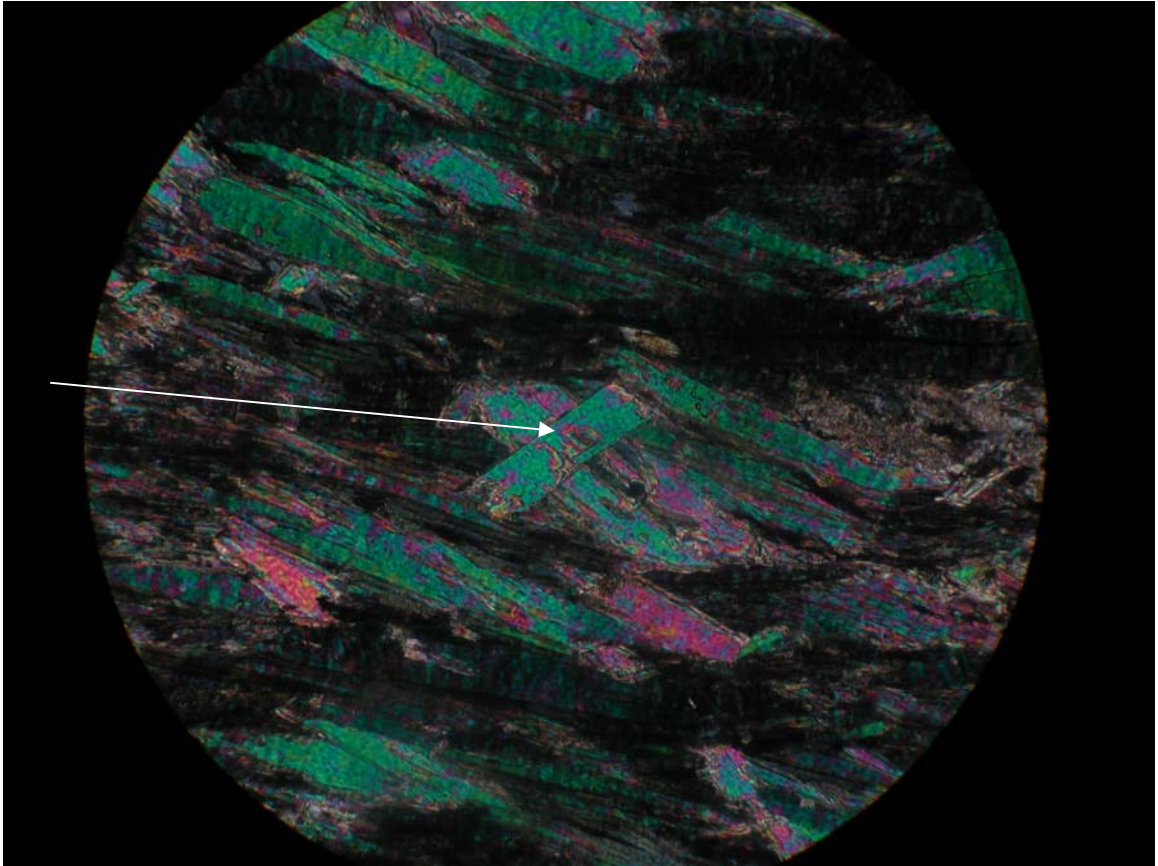


Figure 5.10. Arrow points to  $M_2$  muscovite that has recrystallized in on orientation cross-cutting  $M_2$  muscovite. Recrystallized  $M_2$  muscovite appears unstrained and undeformed. Crossed nicols. Field of view is 1.0 mm. Mica schist; sample ATT-36; borehole B-70; 30.5 m bgs.

## Deformation

Multiple episodes of ductile and brittle deformation have affected the rocks of the BFZ. The first deformational event,  $D_1$ , produced a foliation,  $S_1$ , which may only be evidenced by inclusion trails within  $M_1$  garnet and staurolite. Inclusion trails within garnet and staurolite appear to intersect the foliation close to  $90^\circ$  and are possibly not related.

Following  $D_1$ ,  $D_2$  occurred producing an  $S_2$  foliation.  $S_2$  is a continuous foliation or continuous schistosity (Passchier & Trouw 1998), and is present throughout the BFZ in both quartz mica schists and mica schists. After  $D_2$ , a fluid containing boron circulated through the Brevard Zone rocks and caused the nucleation and growth of tourmaline. Tourmaline occurs as small (0.4 mm diameter) porphyroblasts that commonly cross-cut the  $S_2$  defining muscovite and biotite. Local concentrations of tourmaline have been folded indicating growth prior to later ductile deformation (Figure 5.11).

Following  $D_2$ , a third deformational event,  $D_3$ , occurred.  $D_3$  deformed the rocks of the BFZ in a ductile fashion and produced  $F_3$  folds, and a  $S_3$  foliation defined by sheared muscovites.  $F_3$  folds are tight to close and similar, (Figure 5.12), and their axial traces intersect the  $S_2$  foliation at an acute angle of approximately  $10-15^\circ$ .

Both  $M_2$  muscovite and quartz veins have been folded by these  $F_3$  folds and these folds are recognized within both Brevard lithologies. Sheared  $M_2$  muscovite defines the  $S_3$  foliation, (Figure 5.13), which occurs only in mica schists.

Following  $D_3$ , a fourth deformational event,  $D_4$ , produced  $F_4$  folds which are open to gentle and similar (Figure 5.14). Axial trace orientations are different from those of

F<sub>3</sub> folds by approximately 20-30°, and thus F<sub>4</sub> fold axes intersect the S<sub>2</sub> foliation at angles of 30-45°. F<sub>4</sub> folds gently affect all preexisting features such as vein quartz and M<sub>2</sub> muscovite and biotite and are normally confined to the mylonitic schist unit.

Following D<sub>4</sub>, a fifth deformational event, D<sub>5</sub>, occurred. D<sub>5</sub> is brittle in nature and thus, a significant period of time had elapsed since D<sub>4</sub>. D<sub>5</sub> produced brittle fracturing and psuedotachylyte. Both psuedotachylyte and brittle fractures are oriented at acute angles of 15-50° to S<sub>2</sub>.



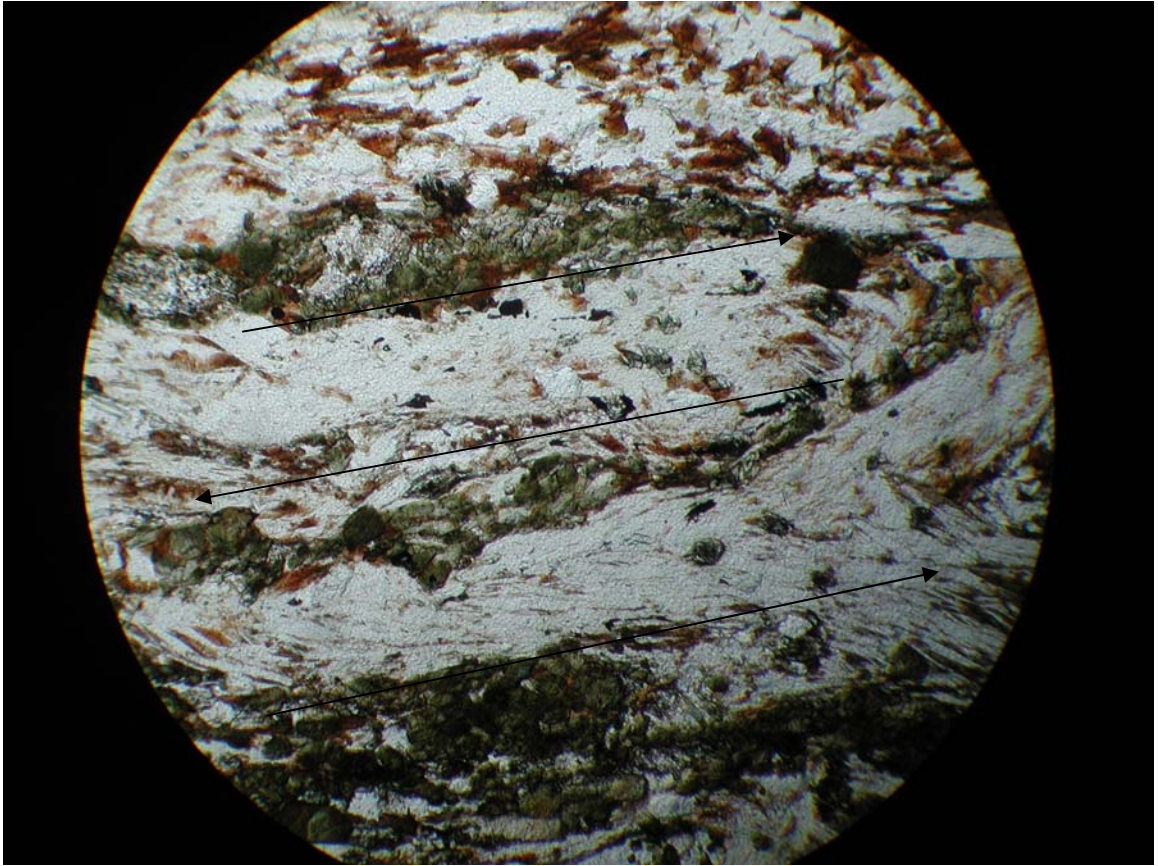


Figure 5.11. Band of tourmaline (arrows) that has been tightly folded. Uncrossed nicols. Field of view is 5.5 mm. Mica schist; sample ATT-43; borehole B-17; 28.7 m bgs.

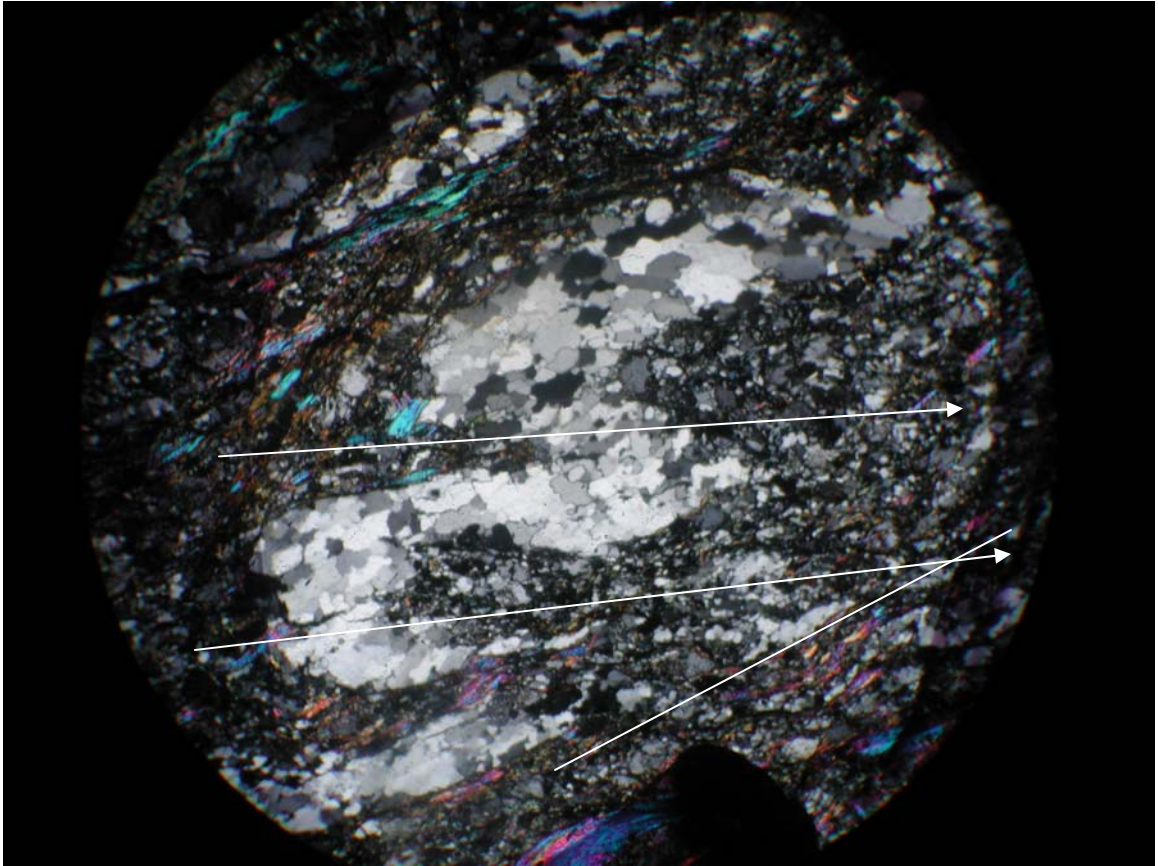


Figure 5.12. Quartz vein folded by  $F_3$  event. Line indicates  $S_2$  and line with arrow indicates axial trace of  $F_3$  fold. Crossed nicols. Field of view is 5.5 mm. Mica schist; sample ATT-34; borehole B-70; 15.2 m bgs.



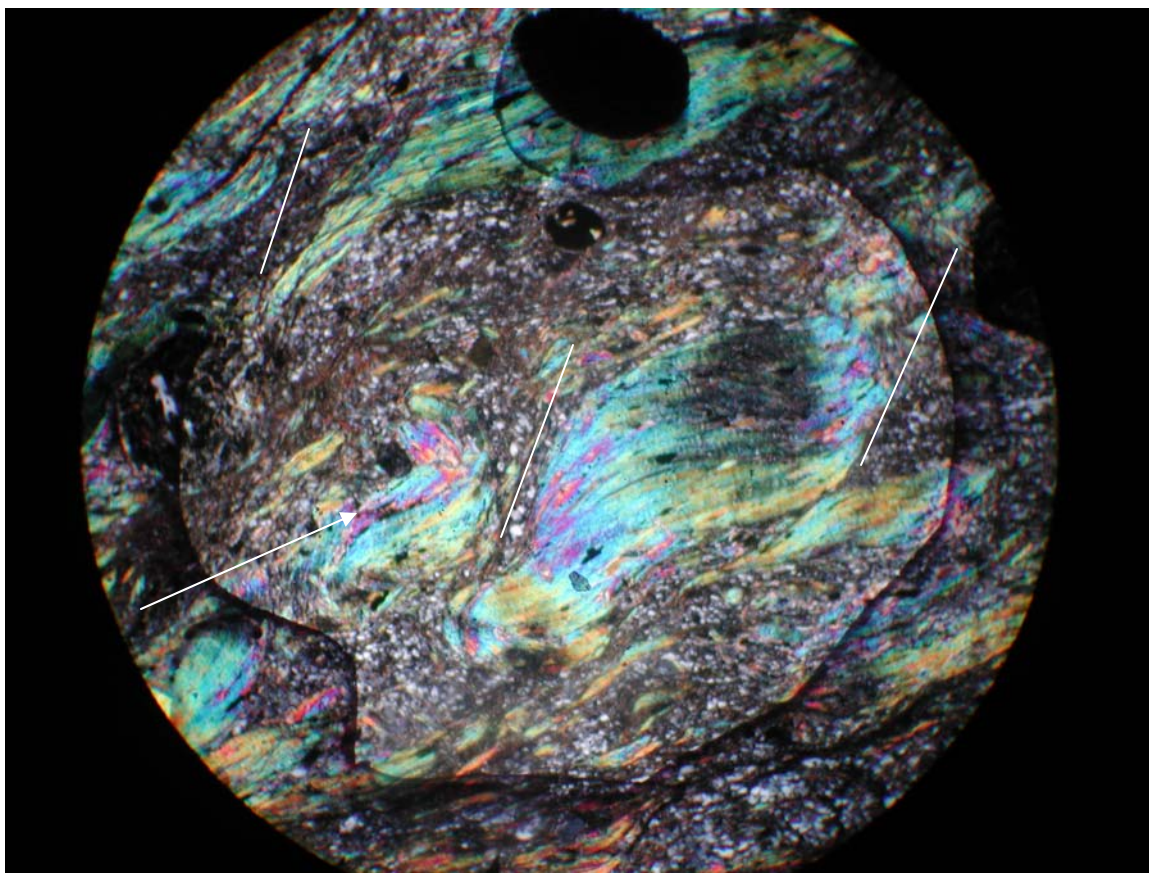


Figure 5.13. Sheared muscovite defines a secondary foliation,  $S_3$ . Line shows the approximate orientation of  $S_3$ . Arrow is aligned parallel to  $S_2$  foliation. Crossed nicols. Field of view is 2.0 mm. Mica schist; sample ATT-18; borehole B-68; 45.8 m bgs.

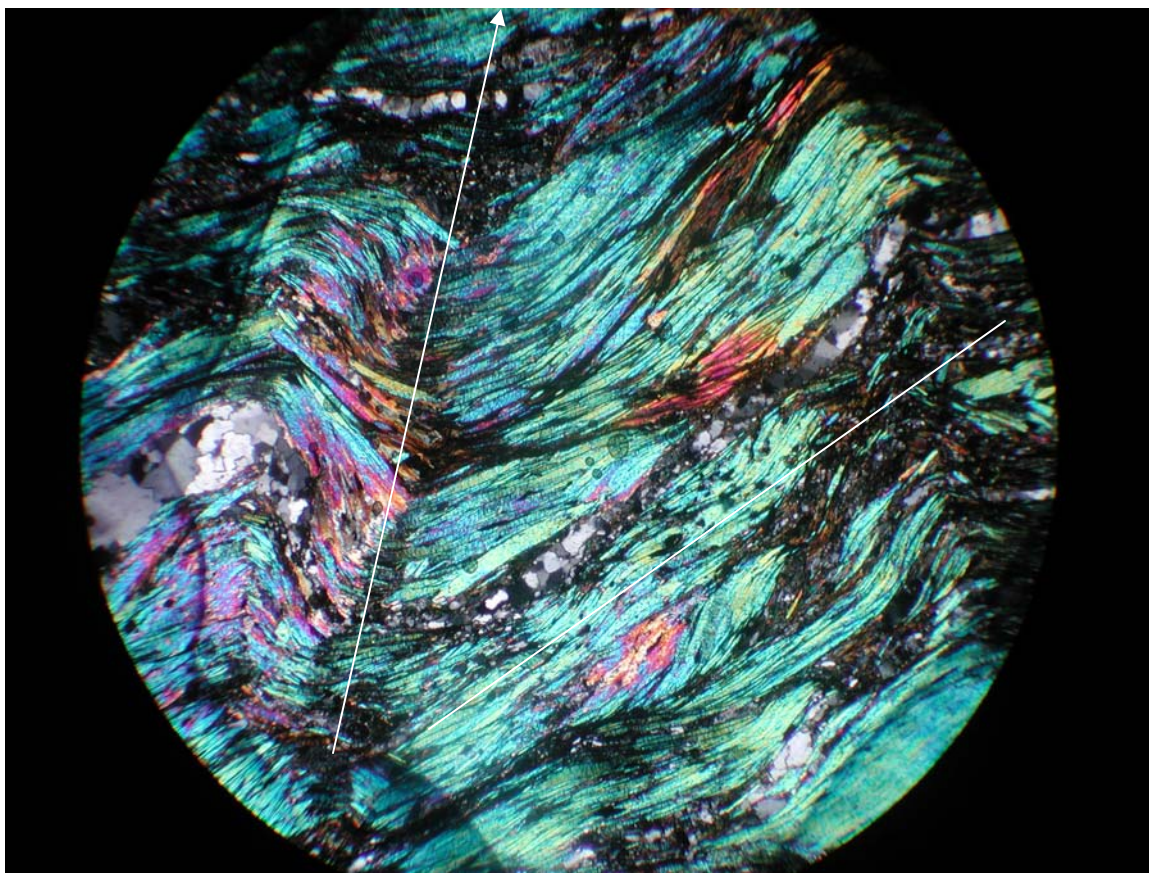


Figure 5.14.  $M_2$  muscovite folded by  $F_4$  event. Line indicates  $S_2$  and line with arrow indicates  $F_4$  axial trace. Crossed nicols. Field of view is 5.5 mm. Mica schist; sample ATT-34, borehole B-70; 15.2 m bgs.

## **Metamorphism and Deformation Correlation**

Microtectonic, petrographic, and geochemical analysis allow for correlation between metamorphic and deformational events.  $M_1$  is coeval with  $D_1$  and is only represented by relict garnet and staurolite. The grain boundaries of  $M_1$  garnet and staurolite are very irregular do not appear to be in equilibrium with the surrounding fabric.

Discerning whether garnets are pre- or syn- tectonic can be difficult due to the fact that similar structures can be found in both cases (Barker 1990). A common feature that is absent from pre-tectonic crystals but present in syn-tectonic crystals is an aligned inclusional fabric. The BFZ rocks have undergone several episodes of deformation so that the  $S_2$  foliation has been folded. The  $S_1$  foliation became included as the porphyroblast grew and the rotated inclusional fabric formed.  $M_1$  garnet and staurolite exclusively contain sinusoidal inclusion fabrics that intersect the foliation at an angle close to  $90^\circ$  and possibly are not related to the surrounding foliation. If they were related, these inclusional fabrics would wrap into the foliation, and this is not the case. These two minerals are interpreted to represent a relict assemblage and coeval with  $D_1$  deformation.

$M_2$  and  $D_2$  occurred coevally.  $M_2$  biotite appears as small (0.1 to 0.4 mm) grains that define the  $S_s$  foliation (Figure 5.16).  $M_2$  muscovites also define the  $S_2$  foliation and terminate into the crystal faces of  $M_2$  garnet.  $M_2$  minerals do not display moth-eaten textures or relict cores that would suggest a state of disequilibrium and thus reflect an equilibrium assemblage.

Multiple lines of evidence suggest that  $D_3$  occurred before  $D_4$ . Recrystallized muscovite are small (0.2 mm) grains that have their long axes aligned parallel to  $F_3$  axial trace orientations, both proximate and distal to  $F_3$  folds. Quartz neoblasts within larger quartz veins have been recrystallized into an orientation consistent with  $F_3$  axial traces (Figures 5.16 and 5.17).



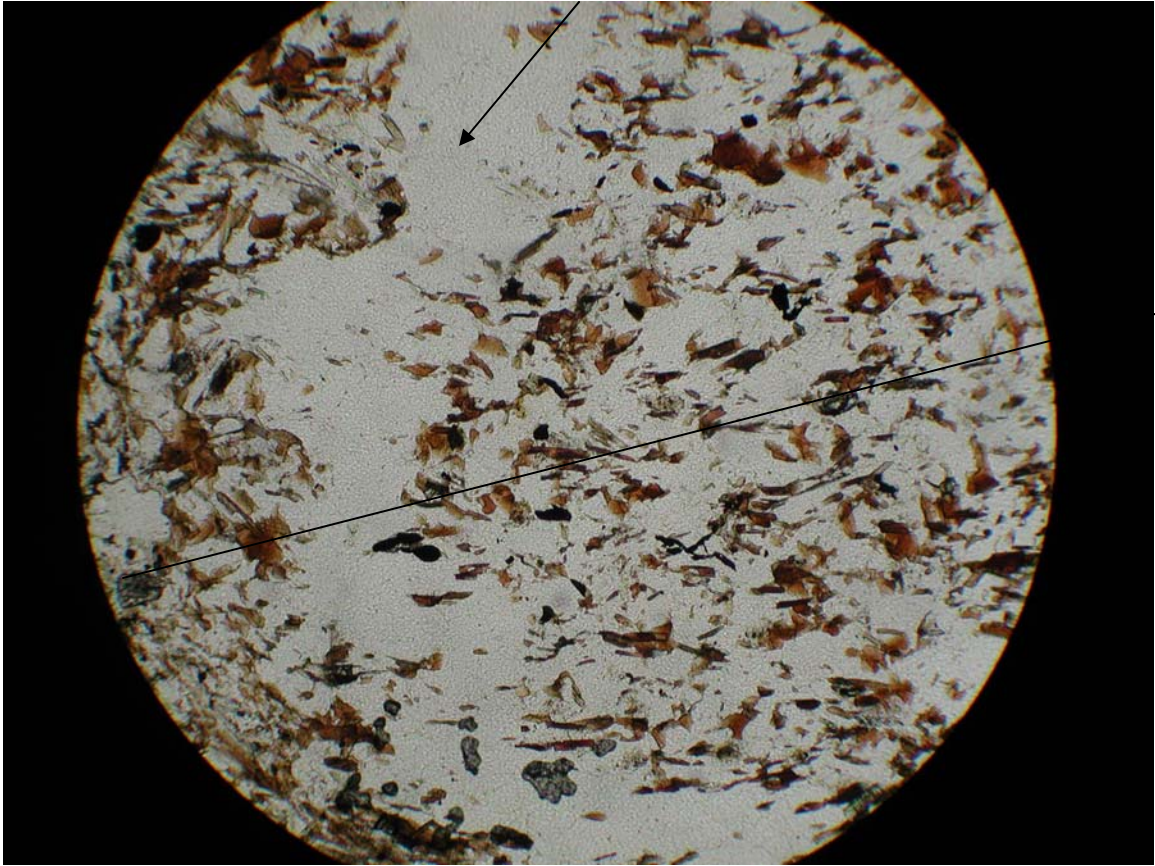


Figure 5.15. A quartz vein has been tightly folded (arrow). Biotite within  $F_3$  fold appears undeformed and has long axes oriented in an axial planar fashion (line). Axial trace is oriented from bottom left to upper right. Uncrossed nicols. Field of view is 2.0mm. Mica schist; sample ATT-43; borehole B-17; 28.7 m bgs.

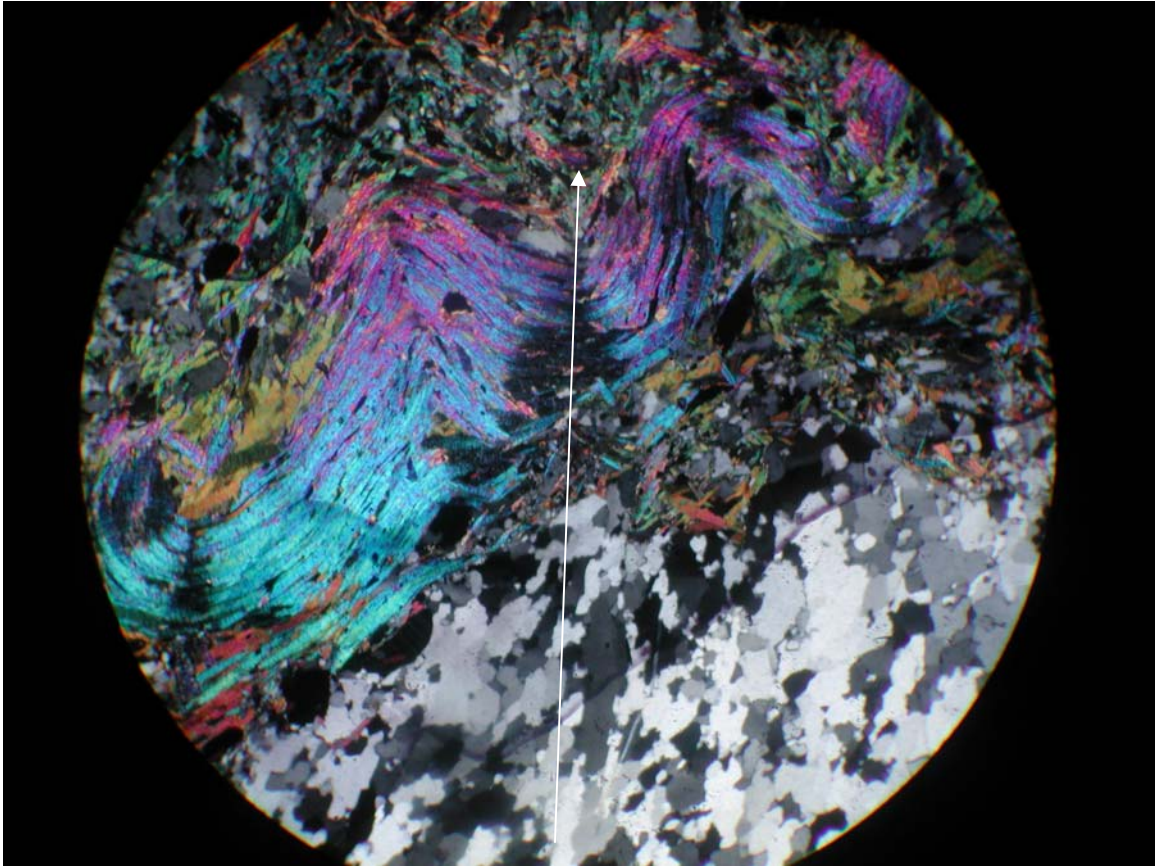


Figure 5.16. Line is oriented parallel to long axes quartz neoblasts and the axial trace of a  $F_3$  fold. Crossed nicols. Field of view is 5.5 mm. Mica schist; sample ATT-50, borehole B-37; 61.0 m bgs.



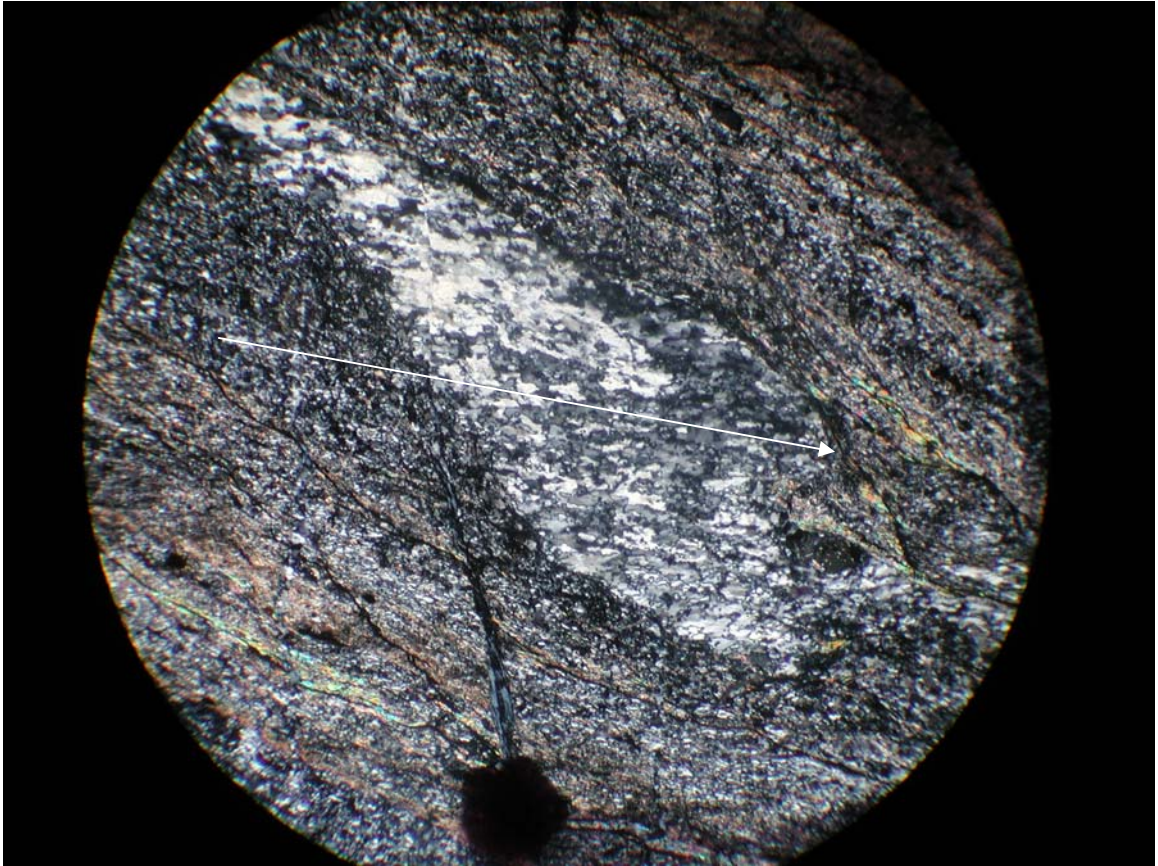


Figure 5.17. Quartz neoblasts are aligned parallel to axial trace of a  $F_3$  fold (line with arrow) located outside the photomicrograph. Crossed nicols. Field of view is 5.5 mm. Quartz mica schist; sample ATT-13; borehole B-18; 30.5 m bgs.

These observations indicate that while growth of  $M_2$  minerals occurred, stress related to  $D_2$  resulted in  $M_2$  minerals aligning themselves parallel to a penetrative deformational fabric, in the form of  $S_2$  foliations.

Passchier and Trouw (1998) describe the deformation behavior of quartz as difficult due to the complex role that water plays during deformation. The presence of water in the crystal lattice possibly influences the strength of quartz and the mechanism by which dislocation slip occurs. The authors described deformation structures as temperature increased for quartz factoring in water within the system. At low grade conditions (300-400°C), dislocation glide and creep become important. Characteristic structures are “sweeping” undulose extinction and deformation lamellae. At medium to high grade conditions (400-700° C), characteristic structures are relatively strongly flattened porphyroclasts and numerous recovery and recrystallization structures such as the presence of highly irregular grain boundaries, a gradual transition of aggregates of subgrains to aggregates of new grains with approximately the same size, and by subgrain boundaries which pass laterally into grain boundaries. Both of these textures represent subgrain rotation recrystallization and grain boundary migration recrystallization (Passchier and Trouw 1998). These structures are consistent with those observed  $F_3$  structures found in quartz veins in the BFZ rocks and, thus, suggest temperatures between 400-700°C during the formation of  $F_3$  folds.

There is a lack of evidence that would suggest that  $M_2$  occurred coevally with  $D_4$ .  $F_3$  folds affect  $M_2$  micas and vein quartz only. Recrystallized muscovite is significantly smaller (0.2 mm) than  $M_2$  muscovite (0.5-1.5 mm) and is consistently aligned with  $F_3$  axial traces. Strained  $M_2$  muscovite, with a larger grain size, allows  $F_3$  folding to be

observed, but due to smaller grain sizes of recrystallized muscovite and the gentle nature of  $F_4$  folds,  $F_4$  folds are not observed in small, individual grains of  $M_2$  muscovite.  $F_4$  folds are recognized only from the form of quartz veins, not the orientation of quartz neoblasts. Quartz is not recrystallized into an axial planar orientation parallel to axes of  $F_4$  folds, but is parallel to  $F_3$  folds. Similarly, long axes of  $M_2$  biotite is not oriented parallel to the axial trace of  $F_4$  folds, but to the axial trace of  $F_3$  folds only. If  $D_4$  occurred before  $D_3$ , then observed  $F_4$  structures would be absent, due to later lower amphibolite grade metamorphism, which, would have overprinted  $D_4$  structures.

These observations suggest that  $D_4$  followed  $D_3$ . Temperatures were elevated for ductile deformation to occur, i.e. bending, and thus were between 300 and 400 °C for quartz and above 250° for biotite (Passchier and Trouw 1998). If temperatures were below these values, then  $F_4$  folds would be seen through kinks or fractures, and this is not the case.  $D_4$  occurred while temperature was still high enough for  $F_4$  folds to form primarily through bending of  $M_2$  muscovite and vein quartz, but not high enough for quartz recrystallization or development of preferred mineral orientations.

$M_3$  occurred after  $D_2$  tectonism related to growth of  $M_2$  minerals. Epidote grains cross-cut all ductile fabrics present (Figure 5.18). Chlorite occurs primarily within brittle fractures rather than as a fabric constituent (Figure 5.19). Calcite also only occurs within brittle fractures. Epidote occurs throughout the samples and cross-cuts all ductile fabrics. The style of occurrence suggests that these minerals reflect a distinct  $M_3$ , a fluid enhanced metasomatic event in which fluids modified the bulk composition of quartz mica schists and mica schists resulting in a metasomatic event and not retrograde metamorphism.

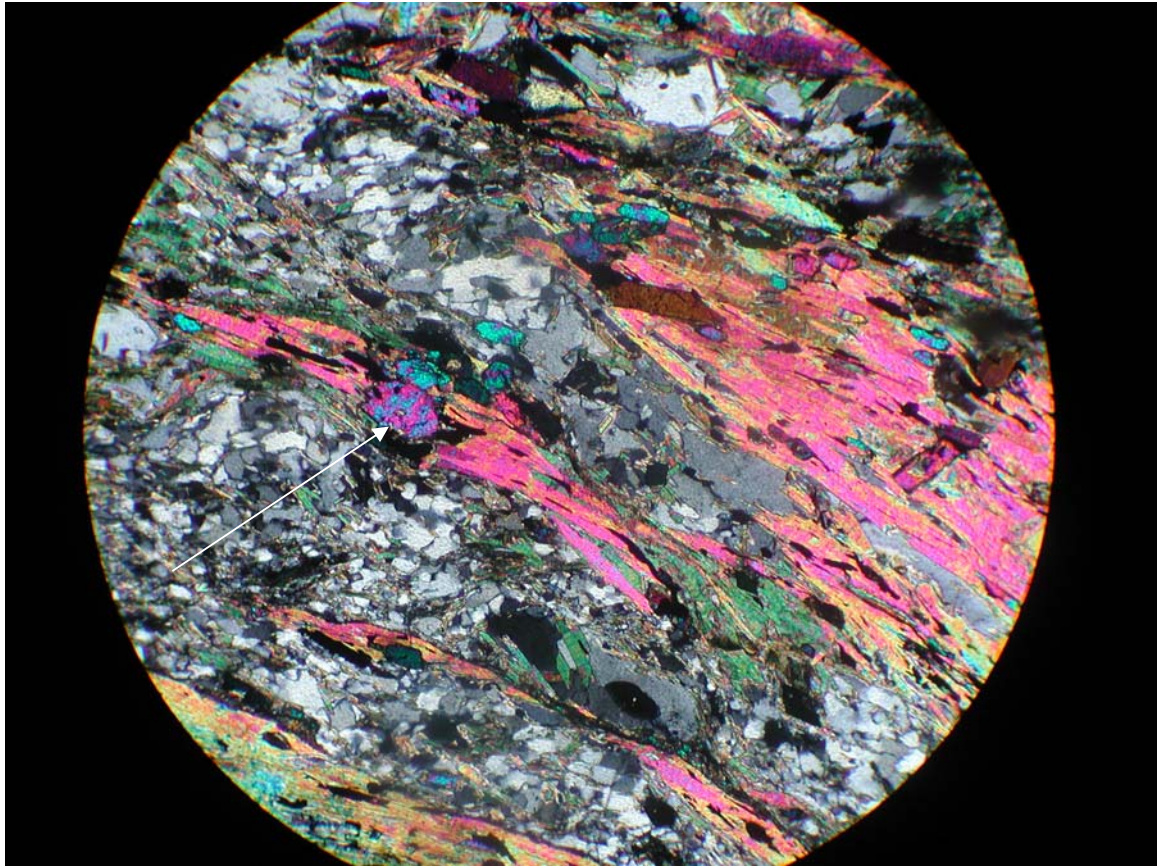


Figure 5.18. Arrow points to epidote grain that cross-cuts  $M_2$  muscovite. Crossed nicols. Field of view is 2.0 mm. quartz mica schist; sample ATT-47; borehole B-37; 38.0 m bgs.



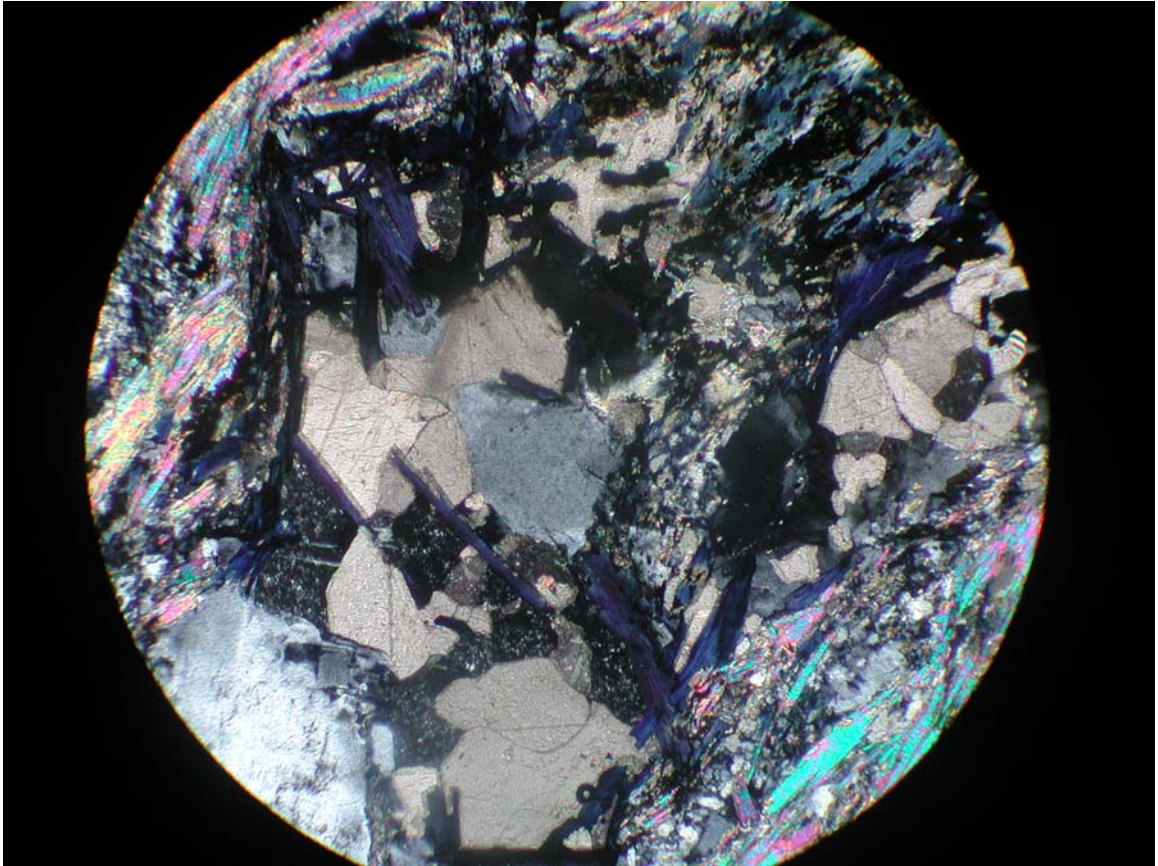


Figure 5.19. Chlorite occurs with random orientation and with calcite within a brittle fracture. Crossed nicols. Field of view is 5.5 mm. Mica schist; sample ATT-36; borehole B-70; 30.5 m bgs.

## DISCUSSION

The rocks constituting the Brevard Fault Zone outside of Atlanta, Georgia, have experienced a long history of metamorphism and deformation. Rocks within my thesis area coincide with the mylonitic button schist and mylonitic biotite gneiss units described by Kath and Crawford (2001), button schists of Higgins (1966), and garnet mica schists of Medlin and Crawford (1973).

Many geologists have looked at the sheared granites and gneisses within or adjacent to the BFZ to attempt to assign ages to events that formed deformational fabrics observed in these rocks. Vauchez (1987) investigated the deformational history of the BFZ using the Palmetto & Ben Hill Granites, located east of Atlanta, Ga., which have crystallization ages of 325 Ma, and found that these granites were sheared only once, which he postulated to have occurred at ~ 310 Ma. Hence, this deformation would correspond to the Alleghanian orogeny. Vauchez did not explore the possibility that there were earlier deformation events that occurred before emplacement of these granites. Sinha et al. (1988) conducted Rb-Sr whole rock analyses and U-Pb analyses on zircons and monazites from the Henderson gneiss in North Carolina. The Henderson gneiss is cut by the Brevard Fault Zone and is strongly deformed. They found Rb-Sr ages (~273 Ma) from retrograded zones within the gneiss and zircon U-Pb ages of ~450 Ma. Consequently, they suggested a prograde metamorphic/ deformation (i.e. Taconic) event at 450 Ma, which produced metamorphic mineral growth and the mylonitic fabric. The 273 Ma age for the most retrograded samples reflects a second event. Higgins et al.



(1997) investigated the age of the Austell gneiss, which lies to the northwest of the Brevard Zone outside of Atlanta, Georgia, and is cut by the Brevard. Crystallization ages of 430 Ma for zircon were determined using the U-Pb system. Both Sinha et al. (1988) and Higgins et al. (1997) correlate their Ordovician ages to ductile deformation within the Brevard Fault Zone. The 450-430 Ma (i.e. Taconic) dates obtained by the aforementioned authors may correlate with the prograde event evidenced by the  $M_1$  assemblages and  $D_1$  fabrics within my study area. The second age provided by Sinha et al. (1988) may correlate assemblages to  $M_3$  within my thesis study area.

### **Metamorphism**

The most intense metamorphic event,  $M_1$ , affecting the lithologies of the BFZ near Atlanta, reached middle amphibolite facies conditions. The coexistence of relict staurolite-garnet is consistent with this metamorphic grade. These results support existing data from Higgins (1966), Roper and Dunn (1973), Roper and Justice (1973), Medlin and Crawford (1973), Hatcher (1978), and Sinha et al. (1988) which showed amphibolite grade metamorphism in the BFZ. Higgins (1966) and Medlin and Crawford (1973) have reported kyanite within my thesis area, but this mineral was not observed in my samples.

A second, lower amphibolite, metamorphic event,  $M_2$ , overprinted the primary metamorphic minerals. The assemblage biotite-garnet-muscovite characterizes this event. Roper and Justice (1973) and Roper and Dunn (1973) also found mineral textures indicative of garnet and biotite growth associated with a second metamorphic event. This metamorphic event is somewhat higher grade than the greenschist facies overprint suggested by Medlin and Crawford (1973), Hatcher (1974, 1978), and Lewis (1980).

A third metamorphic event,  $M_3$ , metasomatic in nature, possibly occurred much later. The phases chlorite, calcite, and epidote typify this event. These minerals are not oriented, and occur as grains or in fractures which crosscut ductile deformational fabrics. My  $M_3$  event may be correlative with a retrograde event which followed peak metamorphism and is based upon the replacement of garnet with chlorite elsewhere in the BFZ (Crawford and Medlin 1973; Higgins 1966; Lewis 1980; Hatcher 1974).

### **Deformation**

The main events thought to have affected the southern Appalachians are the Taconic (510-460 Ma), Acadian (410-360 Ma), and Alleghanian (325-265 Ma) orogenies (Hatcher 1988; Goldberg and Dallmeyer 1997; Roper and Justice 1973). Textural indicators of deformation should be correlative with these orogenies and has been extensively documented within the Brevard fault zone in this work as well as others (Reed and Bryant 1964; Hatcher 1974; Roper and Justice 1973; Higgins 1966; Medlin and Crawford 1973; Higgins et. al. 1988; Vauchez 1987). I interpret  $D_1$  to represent the earliest deformational event that lead to the formation of the  $S_1$  foliation. This foliation is preserved only in the inclusion trails of relict garnet and staurolite. This  $D_1$  event is inferred to correspond to the Taconic orogeny. The Taconic orogeny is the first, important Paleozoic orogeny to affect the southern Appalachians and attributing the earliest metamorphic and deformational events in the BFZ rocks is consistent with current ideas concerning southeastern geology (Hatcher 1989; Rodgers 1982). The presence of a second, distinct amphibolite grade mineral assemblage and associated crosscutting textural features suggest that the minerals that define the  $S_2$  foliation must be younger than early Acadian.

Several authors, as well as myself, have inferred separate folding events ( $D_3$  and  $D_4$  here) within the BFZ (Crawford and Medlin 1973; Roper and Dunn 1973; Roper and Justice 1973; Hatcher 1970). The  $D_3$  deformation within my thesis area produced close to tight folding, and a  $S_3$  foliation defined by sheared muscovites. Roper and Dunn (1971) observed a similar style of folding and deduced that these similar folds were produced during  $D_2$ , which they attributed to the Taconic orogeny. I think that these similar folds are significantly younger than  $D_2$  because the folds and  $S_3$  foliations deform the  $S_2$  foliation. Moreover,  $M_2$  minerals, which I suggest formed during a second thermal peak, define  $D_2$  fabrics. Hence, these  $D_2$  fabrics are interpreted to be younger than  $D_1$  and to correspond to the Acadian orogeny.

Goldberg and Dallmeyer (1997) reported on the chronology of Paleozoic metamorphism and deformation within the Blue Ridge thrust complex in Tennessee and North Carolina. Using Rb-Sr and Sm-Nd systems in garnet and hornblende, crystal growth was documented during the Ordovician (490-440 Ma) and the Devonian (415-355 Ma). The authors also noted two, texturally distinct type of garnet crystals. Smaller, euhedral garnets yielded Devonian ages and were interpreted to have formed during the Acadian orogeny. Their study area is bound on the southeast by the BFZ and thus their work supports my interpretation of distinct Taconic and Acadian metamorphic events within this study.

$D_4$  produced open-gentle folds that affect both  $M_1$  and  $M_2$  mineral assemblages. If  $D_3$  is Acadian, then  $D_4$  folds must correspond to later events in the last orogeny, the Alleghanian, to affect the BFZ. Brittle deformation,  $D_5$ , produced psuedotachylyte and brittle fractures that cross cut all metamorphic and ductile fabrics defined by  $M_1$  and  $M_2$

minerals. This interpreted to be related to brittle faulting during the waning stages of the Alleghanian orogeny (Hatcher 1999, Higgins 1966, Secor et. al. 1986) (Figure 6.0 and Table 6.0).

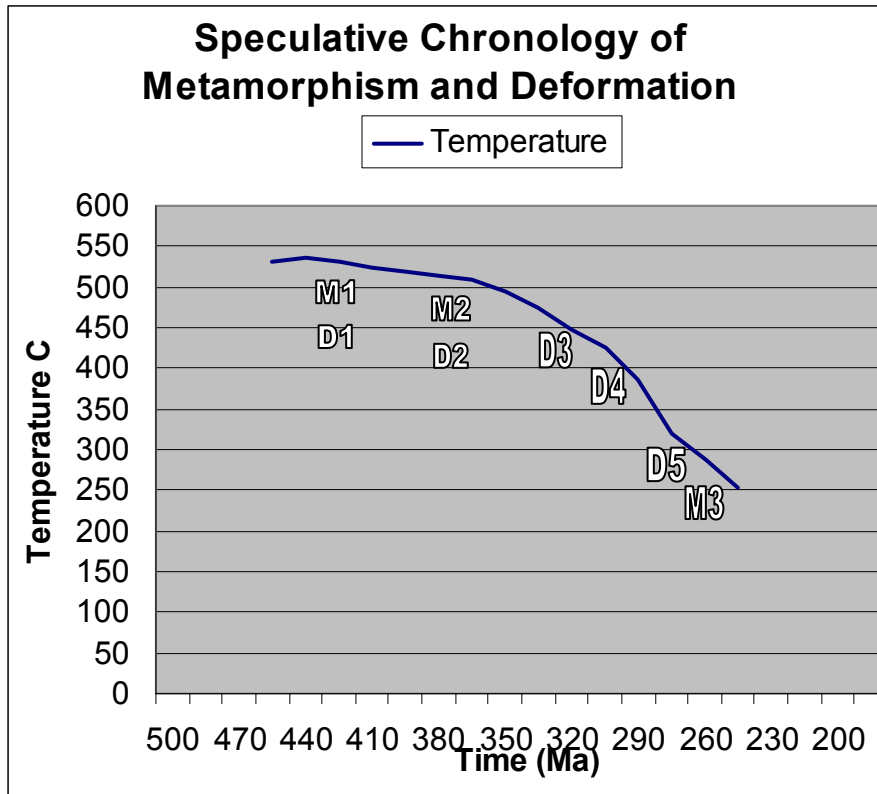


Figure 6.0. Graph shows inferred metamorphic and deformational events tentatively correlated with time and approximate temperature. Temperature constraints are from mineral assemblages. The earliest age constraints are from Higgins (1997) age of 450-430 Ma determined for the crystallization of the Austell gneiss which is cut by the Brevard Fault Zone. The only other age constraint is that of Sinha et. al. (1988) for the retrograde event affecting the Henderson augen gneiss at 273 Ma which is cut by the Brevard Fault zone.  $M_1$  and  $D_1$  correspond to the Taconic orogeny.  $M_2$  and  $D_2$  correspond to the Acadian orogeny.  $D_3$  is placed after  $D_2$ , early in the Alleghanian orogeny.  $D_4$  follows  $D_3$  later in the Alleghanian, where temperature would still be sufficient to deform muscovite and quartz through ductile processes.  $D_5$  is placed at temperatures associated with brittle deformation and below those required for ductile processes to operate.  $M_3$  is placed after  $D_4$ , but before the beginning of the Triassic period. Movement on the Brevard is limited by the occurrence of cross-cutting Triassic age dikes that cross-cut the Brevard Fault Zone (Higgins 1966).

**Table  
6.0**

**Metamorphic event and  
assemblage**

**Deformational  
event**

**Texture**

**M<sub>1</sub> Middle Amphibolite  
grade  
relict staurolite-  
garnet**

**D<sub>1</sub>**

**S<sub>1</sub> foliation within relict  
porphyroblasts**

**M<sub>2</sub> Lower Amphibolite  
grade  
garnet-biotite-  
muscovite**

**D<sub>2</sub>**

**S<sub>2</sub> foliation**

**D<sub>3</sub>**

**F<sub>3</sub> folds; close to tight and  
similar**

**S<sub>3</sub> foliation**

**D<sub>4</sub>**

**F<sub>4</sub> folds; open to close and  
similar**

**D<sub>5</sub>**

**Brittle fracturing and  
psuedotachylytes**

**M<sub>3</sub> Fluid-enhanced metasomatic  
event  
epidote-chlorite-  
calcite**



## CONCLUSION

The quartz mica schists and mica schists that constitute the inner Brevard fault zone, outside of Atlanta, Georgia, have experienced polyphase metamorphism and deformation. Evidence obtained from petrographic, mineralogic, and microtextural analyses indicate that three distinct metamorphic events ( $M_1$ - $M_3$ ) and five distinct deformational events ( $D_1$ - $D_5$ ) occurred within the Brevard fault zone.  $M_1$  is Barrovian style, middle amphibolite grade metamorphism as indicated by the relict coexistence of staurolite-garnet.  $D_1$  occurred coevally with  $M_1$  and produced an  $S_1$  foliation only suggested by inclusion trails within  $M_1$  minerals that do not appear to be related to the primary foliation. The age of this event is interpreted to be consistent with the suggestions of Higgins (1988) and Sinha et al. (1988) for a 450-430 Ma event affecting the BFZ and corresponds to the Taconic orogeny.  $M_2$  is also a Barrovian style, lower amphibolite grade metamorphic event indicated by renewed growth of biotite-garnet-muscovite.  $D_2$  occurred synchronously with  $M_2$  and produced an  $S_2$  foliation.  $M_2$  mica grains have recrystallized into an orientation parallel to the axial traces of  $F_3$  folds. Quartz has been recrystallized into an axial planar orientation consistent with the axial traces of  $F_3$  folds.  $D_3$  also produced a  $S_3$  foliation within mica schists.  $M_2$  and  $D_2$  are interpreted to coincide with the Acadian orogeny.  $D_3$  followed  $D_2$  and produced  $F_3$  folds.  $F_3$  folds affect  $M_1$  and  $M_2$  minerals and possess axial trace orientations that differ from  $F_4$  folds by approximately 20-30°. The Alleghanian orogeny is correlated with  $D_4$  but no new metamorphic minerals are associated with this event.  $D_5$  produced brittle fracturing

interpreted to be the same as the 273 Ma retrograde event found by Sinha et. al (1988) within the Brevard fault zone rocks of North Carolina. Epidote, calcite, and chlorite formed during  $M_3$  and occur within brittle fractures that crosscut all ductile fabrics.  $D_5$  produced brittle fracturing and psuedotachylyte

Barker, A. J., 1990, **Introduction to Metamorphic Textures and Microstructures.**

Glasgow: Blackie; New York: Chapman and Hall, 162 p.

Blatt, Harvey, and Tracy, Robert, 1999, **Petrology: Igneous, Sedimentary, and**

**Metamorphic.** W. H. Freeman and Company, 529 p.

Bobyarchick, Andy R., 1999, The History of Investigation of the Brevard Fault Zone

and Evolving Concepts in Tectonics. *Southeastern Geology*, v 38, no. 3, p.

223-238.

Bobyarchick, Andy R., 1993, An Alternative Interpretation of Strike-Slip Shear Sense in

the Brevard Fault Zone. *Geological Society of America Abstracts with*

*Programs*, p 4.

Dallmeyer, R. D., 1988, Late Paleozoic tectonothermal evolution of the western

Piedmont and eastern Blue Ridge, Georgia: Controls on the chronology of terrane

accretion and transport in the southern Appalachian orogen. *Geological Society*

*of America Bulletin*, v. 100, p. 702-713.

Deer, W.A., Howie, R. A., Zussman, J., 1992, **The Rock Forming Minerals**, 2nd

edition, Longman, Burnt Mill, England 696 pp.

Edelman, Stephen H., Liu, Angang, and Hatcher, Robert D., Jr., 1987, The Brevard Fault

Zone in South Carolina and Adjacent Areas: An Alleghanian Orogen Scale

Dextral Shear Zone Reactivated as a Thrust Fault. *Journal of Geology*, v. 95, p.

793-806.

- Evans, Carol, and Mosher, Sharon, 1986, Microstructures and Sense of Shear in the Brevard Fault Zone, Southern Appalachians. Geological Society of America Abstracts with Programs, p 596
- Garner, Terence, Luneburg, Catalina, Schmocker, Martin, and Lebit, Hermann, 2001, Structures and Microstructures Along the Brevard Fault Zone, GSA Annual meeting, session no. 61, booth #32.
- Goldberg, S. A., and Dallmeyer, R. D., 1997, Chronology of Paleozoic Metamorphism and Deformation in the Blue Ridge Thrust Complex, North Carolina and Tennessee. American Journal of Science, Vol. 297, p. 488-526.
- Hames, Willis B., and Cheney, J. T., 1997, On the loss of  $^{40}\text{Ar}$  from muscovite during polymetamorphism, *Geochimica et Cosmochimica*, V. 61, No. 18, pp. 3863-3872.
- Hatcher, Robert D., Jr., 1970, Stratigraphy of the Brevard Fault Zone and Poor Mountain Area, Northwestern South Carolina. Geological Society of America Bulletin, V. 81, p. 933-940.
- Hatcher, Robert D., Jr., 1978, Tectonics of the Western Piedmont and Blue Ridge, Southern Appalachians: Review and Speculation. American Journal of Science, v. 278, p. 276-304.
- Hatcher, Robert D., Jr., 1988, The Brevard Fault Zone: Facts that Constrain a Multiphase Multidirectional Movement History. Geological Society of America Abstracts with Programs, v. 20 n. 4, p. 269.
- Hatcher, Robert D., Jr., 1989, "Tectonic Synthesis of the U.S. Appalachians", **The Appalachian-Ouachita Orogen in the United States**: Boulder, Colorado, Geological Society of America, The Geology of North America, v. F-2

- Hatcher, Robert D., Jr., 1999, Geotraverse Across Part of the Acadian Orogen in the Southern Appalachians
- Hatcher, Robert D., Jr., and Odom, A. L., 1980, Timing of Thrusting in the Southern Appalachians, USA: Model for Orogeny? *Journal of Geological Society, London*, v. 137, p. 321-327.
- Higgins, Michael W., 1966, Geology of the Brevard Lineament near Atlanta, Georgia: Georgia Department of Mines, Mining and Geology, Geol. Survey Bulletin 77.
- Higgins, Michael W., Robert L. Atkins, Thomas J. Crawford, Ralph F. Crawford, Rebekah Brooks, and Robert B. Cook, 1988, The Structure, Stratigraphy, and Tectonostratigraphy and Evolution of the Southernmost Part of the Appalachian Orogen. United States Geological Survey Professional Paper 1475.
- Higgins, Michael W., Arth, Joseph G., Wooden, Joseph L., Crawford, Thomas, Thomas J., Stern, Thomas W., and Crawford, Ralph F., 1997, Age and Origin of the Austell Gneiss, Western Georgia Piedmont-Blue Ridge, and its Bearing on the Ages of Orogenic Events in the Southern Appalachians. *Geological Society of America Memoir* 191, p. 181-192.
- Higgins, Michael W., Crawford, Thomas J., Atkins, Robert L., and Crawford, Ralph F., 1999, Geologic Map of the Atlanta 30" x 60" Quadrangle, Georgia. Open File Report 98-2445.
- Kath, Randy L., and Crawford, Thomas J., 2001, Detailed Geologic Mapping Along the Chattahoochee Tunnel, Cobb County, Georgia, *Georgia Geological Society Guidebook*, V. 21, p. 23-38.

- Kline, Stephen W., 1980, Sandy Springs Sequence Rocks Southeast of the Brevard Zone Near Atlanta, Georgia, and Their Bearing on the Zone; Geological Society of America Abstracts with Programs, v. 12, no. 4, pg 181.
- Lewis, Sharon E., 1980, An Examination of the Northwestern Terminus of the Brevard Fault Zone and Relationships with the Stony Ridge Fault Zone, the Sauratown Mountains Anticlinorium, The Smith River Allocthon and the Inner Piedmont. Carolina Geological Society, Guidebook for 1980 Annual Meeting, p 49-55.
- Liu, Angang, Edelman, Steven H., Hatcher, Robert D., Jr., and Hopson, Janet L., 1987, Timing of Major Thrusting Episodes in the Southern Appalachian Internides, Brevard Fault Zone and Adjacent Areas. Geological Society of America Abstracts with Programs, p. 748.
- Liu, Angang, and Hatcher, Robert D., Jr., 1988, Great Circle Distribution of the Intersection Lineations in S-C Mylonites: Observations from the Brevard Fault Zone and Chauga Belt. Geological Society of America Abstracts with Programs, p A214.
- Marshak, Stephen, and Mitra, Guatum, 1988, **Basic Methods of Structural Geology**. Englewood Cliffs, New Jersey, Prentice Hall College Division. 446 p.
- Medlin, Jack H., and Crawford, Thomas J., 1973, Stratigraphy and Structure Along the Brevard Fault Zone in Western Georgia and Eastern Alabama. American Journal of Science, Cooper vol. 273- A, p. 89-104.
- Miyashiro, Akiho, 1994, **Metamorphic Petrology**. New York, Oxford University Press. 404 p.



- Norwick, Stephen A., 2001, Difference Between Elemental Concentrations in Pseudotachylyte, Contact White Natural Glass and Parent Rhyolite Tuff from the Healdsburg - Rodgers Creek Fault Zone, Taylor Mountain, Sonoma County, California, GSA Annual meeting, Session no. 61, paper no. 61-0.
- Odom, A. Leroy, and Fullagar, Paul D., 1973, Geochronologic and Tectonic Relationships Between the Inner Piedmont, Brevard Zone, and Blue Ridge Belts, North Carolina. *American Journal of Science*, Cooper vol. 273-A, p. 133-149.
- Passchier, C. W., and Trouw, R. A. J., 1996, **Microtectonics**, Springer: Berlin, 289 p.
- Reed, John C., Jr., and Bryant, Bruce, 1964, Evidence for Strike-Slip Faulting Along the Brevard Zone in North Carolina. *Geological Society of America Bulletin* v. 75, p. 1177-1196.
- Rodgers, J., 1982, "The Life History of a Mountain Range-The Appalachians", **Mountain Building Processes**, Academic Press, Harcourt Brace Jovanovich, p. 229-241.
- Roper, Paul J., and Dunn, David E., 1973, Superposed Deformation and Polymetamorphism, Brevard Zone, South Carolina, *Geological Society of America Bulletin*, v. 84, p. 3373-3386.
- Roper, Paul J., and Justice, Philip S., 1973, Polytectonic Evolution of the Brevard Zone. *American Journal of Science*, Cooper vol. 273-A, p. 105-132.
- Secor, Donald T. Jr., Snoke, Arthur W., and Dallmeyer, R. David, 1986, Character of the Alleghanian orogeny in the Southern Appalachians: Part III. Regional Tectonic Relations. *Geological Society of America Bulletin*, v 97, p. 1345-1353.

- Sinha, A. Krishna, Hewitt, David A., and Rimstidt, J. Donald, 1988, Metamorphic Petrology and Strontium Isotope Geochemistry Associated with the Development of Mylonites: An Example from the Brevard Fault Zone, North Carolina. *American Journal of Science*, v 288-A, p. 115-147.
- Spry, Alan H., 1969, **Metamorphic Textures**, Oxford, New York, Pergamon Press, 350 p.
- Sterner, Ray, Shaded Satellite Relief Map of Georgia.  
[www.fermi.jhuapl.edu/states/maps\\_bw/ga\\_bw.gif](http://www.fermi.jhuapl.edu/states/maps_bw/ga_bw.gif)
- Vaucher, Alain, 1987, Brevard Fault Zone, Southern Appalachians: A Medium-Angle, Dextral, Alleghanian Shear Zone. *Geology*, v. 15, p. 669-672.
- Vaucher, A., Kessler, S. F., Le'corche', J.-P., and Villeneuve, M., 1987, Southward Extrusion Tectonics During the Carboniferous Africa- North America Collision. *Tectonophysics*, v. 142, p. 317-322.
- Vaucher, Alain, 1988, Polygenetic evolution and longitudinal transport within the Henderson mylonitic gneiss, North Carolina (southern Appalachian Piedmont). *Geology*, v. 16, p. 1011-1014.